MOST Project - 4
UNCLASSIFIED
85177
003634
ADA035002

NRL Memorandum Report 1400

(9) Interim rept. no. 4;

PROJECT ARTEMIS.
High Power Acoustic Source.

FOURTH INTERIM REPORT ON ACOUSTIC PERFORMANCE.

(Unclassified Title)

(10) R. H. Ferris

SOUND DIVISION

(11) 12 Mar 63

(12) 131 p.

(14) NRL-MR-1400

March 12, 1962 1963

DISTRIBUTION STATEMENT A
Approved for public release;
Distribution Unlimited

DDC
RECEIVED
DEC 2 1978
A

640124-0042

U. S. NAVAL RESEARCH LABORATORY
Washington, D.C.

1400

CONFIDENTIAL

DOWNGRADED AT 3-YEAR INTERVALS
DECLASSIFIED AFTER 12 YEARS

Further distribution of this report or of any abstract or quotation therefrom may be made only with the approval of the Director, Naval Research Laboratory, Washington, D.C., or of the activity sponsoring the research reported therein, as appropriate.

25/1950

UNCLASSIFIED

NRL MEMORANDUM REPORT 1400
ERRATUM

PROJECT ARTEMIS

High Power Acoustic Source

Fourth Interim Report
Acoustic Performance

by R. H. Ferris

This report should be dated March 12, 1963

U.S. Naval Research Laboratory
Washington, D.C.

UNCLASSIFIED

81477

[redacted]

CONTENTS

Distribution	ii
Abstract	iii
Problem Authorization	iii
Problem Status	iii
Introduction	1
Experimental Procedure	5
Chesapeake Bay Tests	5
Lake Pend Oreille Tests	7
Results	8
Directivity	8
Efficiency	9
Acoustic Loading	10
Impedance	11
Element Displacement Characteristics	11
Outer Mass Displacements	11
Spring Deflections	15
Conclusions	21

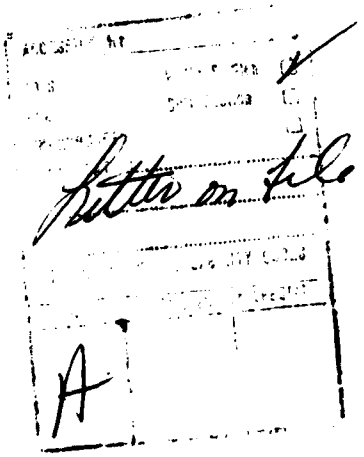

[redacted]

UNCLASSIFIED

UNCLASSIFIED

CONFIDENTIAL

DISTRIBUTION

CNO	
Op-001	1
Op-03EG	2
Op-07	1
Op-31	1
Op-70	1
Op-714D	1
ONR	
Code 467	11
NEL	2
NAVUWTRSOUNDREFLAB	1
NAVUWTRSOUNDLAB	2
Arthur D. Little, Inc., Acorn Park Cambridge 40, Massachusetts	1
Hudson Laboratories, Columbia University 145 Palisade Street, Dobbs Ferry, New York	
Dr. R. A. Frosch	10
Massa Division, Cohu Electronics, Inc. 5 Fottler Road, Hingham, Massachusetts	1
Mr. Frank Massa	

CONFIDENTIAL

UNCLASSIFIED

UNCLASSIFIED

CONFIDENTIAL

ABSTRACT

U. S. Naval Research Laboratory Confidential Memorandum Reports 1205, 1214 and 1273 presented the results of initial tests with the ARTEMIS source. In those tests, it was learned that the permissible operating power level is severely restricted by abnormally large transducer deflections which can cause mechanical destruction of the transducer elements. The large deflections were attributed to interaction of the small elements in the large multielement array.

This report describes two additional series of tests which were intended to evaluate the effectiveness of three techniques for reducing the effects of acoustic interaction on transducer element velocity distribution. These techniques included (1) element electrical connections, (2) tuning at each element, and (3) mechanical assembly of groups of elements to form larger elements.

Evidence is presented which leads to the conclusion that the permissible operating power level can be substantially increased. Additional information is introduced concerning the manner in which nonrectilinear vibrational modes in the transducer element contribute to the power limitation.

PROBLEM AUTHORIZATION

ONR RS 046
NRL problem 55S02-11

PROBLEM STATUS

This is an interim report on one phase of the project. Work is continuing.

CONFIDENTIAL

UNCLASSIFIED

INTRODUCTION

Initial tests of the ARTEMIS source transducer revealed a non-uniform distribution of transducer element displacement amplitude and phase over the face of the multielement array. Thus, the maximum safe input power was limited to that level which is consistent with safe operation for those elements having the highest displacement amplitudes. Furthermore, it was shown that the transducer spring deflection was not necessarily proportional to the displacement of the radiating face and that the displacement and phase of both the inner and outer masses must be measured in order to determine the extent of spring deflection. Fatigue of the transducer element springs is the limiting factor in the power handling capacity of these elements. The results of initial tests on the ARTEMIS source are reported in U. S. Naval Research Laboratory Memorandum Reports 1205, 1214 and 1273.

This report describes a series of tests which were designed to investigate the effectiveness of three techniques for reducing the effects of acoustic interaction on the velocity distribution among elements in the ARTEMIS array. The first method consisted of bonding a group of elements into a subassembly to effectively increase the size of the unit element. This should have the effect of increasing the self-acoustic loading of the unit element and thus reduce the relative contribution of the interaction loading. The second approach was to utilize a parallel electrical connection of transducer elements as opposed to the series-parallel configuration of the original array. The parallel connection permits a current distribution in which the current through an element is inversely proportional to the element impedance; thus an element with high impedance due to low loading caused by the interaction field would receive a lower drive current than the element with low impedance resulting from high loading. The third technique used parallel connected elements which were individually tuned by means of series capacitors to reduce the susceptibility to variations in loading.

The first tests series was conducted during the month of May 1962 in the Cape Charles area of the Chesapeake Bay in a water depth of 90 feet. Operations were performed aboard the USS HUNTING (EAG 398), a laboratory research vessel, the experimental array being submerged through a well amidships. The experimental array for this test series consisted of nominally one wavelength square array of 144 Massa model TR-11C and TR-11B variable reluctance transducer elements forming

a plane projecting surface approximately 12 feet by 12 feet. Subassemblies of transducer elements were fabricated by mechanically bonding the sides of several elements together to make a single larger radiating element. There were three such subassemblies, one of 36 elements in a six by six configuration and two of 12 elements in three by four configurations. These were mounted in a modified Massa model MT-2 array frame, the remaining spaces in the frame being filled by 12 individual transducer elements. The array frame containing the bonded subassemblies was mounted side by side with another MT-2 array frame containing 72 individual elements. The 36 element bonded subassembly constitutes the lower left quadrant of the array. The two 12 element subassemblies are mounted immediately above the 36 element group and the remainder of the array is composed of individual transducer elements. Figure 1 is a photograph of the two array frames during fabrication before being joined together. Figure 2 is a rear view of the completed array in place on the USS HUNTING.

Each transducer element is 11-1/8 inches square on the radiating face and 11-3/4 inches deep. They are normally covered with 1/8 inch of rubber bonded to all sides. In forming the 36 element subassembly, the rubber covering was removed and the adjacent bare metal surfaces bonded together. The entire assembly was then painted. The nine elements each in the upper right-hand and lower left-hand quadrants of the 36 element assembly were modified by the addition of accelerometers attached to the inner masses. Each of the 18 elements was provided with two internal accelerometers, one on the top and one on the bottom edge of the inner mass. In addition, each of the 36 elements in the subassembly was modified by the addition of a stainless steel slug inserted in the lower face on the cable entrance end of each transducer. This slug was centered below an existing slug in the center of each transducer face and, like the existing slug, was provided with a tapped hole to which a Massa model AC-106 accelerometer could be attached. Thus, provision was made for monitoring the displacement at two points on the outer mass of each of the 36 elements and at two points on the inner mass of each of 18 elements

One of the twelve element subassemblies was fabricated by bonding the bare metal elements into a configuration three elements wide by four elements high. Each of the twelve elements in the subassembly was modified to include two internal accelerometers and provisions for two external accelerometers in the manner as in 18 of the elements in the 36 element subassembly.

The second twelve element group was fabricated by bonding rubber covered elements into a configuration three elements wide by four elements high. A rubber to rubber bond was made over the complete area of adjoining faces. Each of these elements was provided with tapped holes for two external accelerometers but no internal accelerometers were installed.

Twelve unmodified transducer elements were installed in the top two rows of the array frame containing the consolidated subassemblies. The unmodified elements contain no internal accelerometers. They have one tapped hole in the center of the back face of each element into which an accelerometer can be attached.

The second array frame contained 69 unmodified and three modified transducer elements. Elements were arranged in twelve rows with six elements in each row. The three modified elements, each with two internal accelerometers and provisions for two external accelerometers, were installed in the three left-hand positions of the sixth row from the top.

Twelve gas filled pressure release tubes were installed on the rear side of each array frame, one tube behind each row of six elements. These tubes suppress acoustic radiation from the rear face of the transducer array. While these flattened tubes are mounted approximately three-quarters of an inch behind the elements in the ARTEMIS source, in this experimental array they were placed approximately eight inches back in order to provide space for the attachment of accelerometers to the rear faces of the transducer elements.

The array frame containing the consolidated subassemblies was designated "module one" and the other 72 element frame, "module two". Individual element positions are referred to by a series of numbers such as 2-6-3 where the first number indicates the module, the second the row and the third the column. Row numbers start at the top and column numbers at the left. Figure 3 illustrates a front view of the element and subassembly locations. Elements in those positions marked with a diagonal line contain internal accelerometers.

Electrical power was supplied to the transducer array through five trunk cables, one for the 36 element subassembly, one for each of the 12 element groups, and one for the 72 element module. These cables

provided for parallel connection of groups of six elements in series. A row of six elements constituted a series group except in the case of the two consolidated twelve element subassemblies where the upper and lower halves constituted series groups. In addition to the five trunk cables, a set of 36 cables was provided which could be used to connect individually to elements in a group, thus permitting parallel connection of 36 transducers, the remainder of the array being connected in series-parallel through the required number of trunk cables.

Two watertight junction boxes were installed on the array frames, one at each side. All accelerometer cables terminated in these junction boxes where their outputs were sequentially sampled and amplified for transmission to data recording instrumentation in a laboratory space on the ship. In addition to accelerometers, fourteen current sensors were available to sample the alternating currents into series groups of transducer elements. In all, 132 channels of data were sequentially sampled, including two calibration channels.

The second test series was conducted during the month of July 1962 at the U. S. Navy Electronics Laboratory Pend Oreille Calibration Station at Bayview, Idaho. Two experimental arrays, each approximately one-half wavelength square, were investigated. One array was the 36 element consolidated subassembly used in the Chesapeake Bay tests, whereas the other consisted of 36 unconsolidated elements. Thus, two square arrays of equal size were formed, one with 36 consolidated elements (figure 4) and one with 36 unconsolidated elements (figure 5). The unconsolidated array consisted of 18 unmodified TR-11B elements and 18 elements modified by the addition of internal accelerometers and pairs of tapped holes for external accelerometers as described for the consolidated array. The elements with internal accelerometers were arranged in the same configuration in the unconsolidated array as in the consolidated array. Figures 4 and 5 illustrate the front and back views of the consolidated and unconsolidated arrays respectively. Since these two arrays were not tested simultaneously, one instrumentation junction box served for both arrays, being installed first on one array and then on the other. It provided for 81 data channels including one for calibration. As in the Chesapeake Bay tests, flattened, resonant, gas filled, stainless steel tubes were installed approximately eight inches behind each row of elements to suppress acoustic radiation to the rear. The 36 elements in each array were connected in parallel to the alternating driving current by means of transformers and 36 extension cables.

EXPERIMENTAL PROCEDURE

Chesapeake Bay Tests

In the tests conducted in the Chesapeake Bay with the 144 element array, a comparison was made among the conditions of series-parallel and parallel operation with both consolidated and unconsolidated array sectors, and with both tuned and untuned operation in the parallel configuration. For the first set of tests, the 36 element consolidated subassembly was operated in series-parallel, parallel untuned, and parallel with individual element tuning. In this set the majority of the accelerometers were positioned on the 36 element consolidated quadrant, and the remainder of the array was operated in the series-parallel mode. The external accelerometers were then repositioned to the lower half of module number two and the tests repeated on this group of unconsolidated elements. The third quadrant tested included the two 12-element consolidated subassemblies and the twelve individual elements in module number one. Finally, the upper half of module number two was investigated. Figure 6 illustrates the power and metering circuits, exclusive of the sensor sampling system, used in these tests. Each of the five transducer groups (i.e., the 36 element consolidated subassembly, the two 12 element consolidated subassemblies, the 12 individual elements in module one, and all of the elements in module two) had individual metering circuits for power and current. Since the five groups were parallel connected, common voltage metering was used. Additionally, a voltmeter, ammeter and wattmeter metered the total power to the five groups. All of these meters were of the portable standard type.

In each test involving parallel operation, the transducer elements in one array quadrant were connected in parallel electrically. This was accomplished through six transformer assemblies shown in block form in figure 6 and in detail in figure 7. Each transformer assembly accommodated six transducer elements and transformed the impedance of six parallel connected elements to that of six series connected elements. This arrangement permitted the 36 parallel connected elements to be driven from the same amplifier which drove the remainder of the series-parallel connected array and also enabled a series-parallel connection for the polarizing current. Each transformer assembly contained the necessary blocking capacitors to permit application of the dc polarizing power. A precision wattmeter and ammeter metered the power to the

input of the six transformer assemblies and a set of six two-percent panel meters measured the currents to the individual transformers. A motor generator was connected to provide ten amperes of polarizing current to each of the transducer elements. However, since the groups of elements were parallel connected to the direct current, the actual current to each group was dependent upon cable resistance. As a result, elements in the group connected to the transformer assembly through separate cables to each transducer, received somewhat less polarizing current than elements in the other groups. It is estimated that the elements in this group were polarized with seven amperes while the remaining elements received eleven amperes each. In the experiments in which the transformer connected elements were individually tuned, a five microfarad capacitor was inserted in series with the common lead of each element as shown in figure 7.

A block diagram of the sensor sampling instrumentation is shown in figure 8. Junction box number one (JB1) contained a 50 position stepping switch and a 40 decibel preamplifier providing 49 data channels and one calibration channel. The stepping switch was remotely controlled to sample the channels sequentially. One bank of contacts selected voltages from a voltage divider to identify the channel being sampled. Junction box number two contained two 50 position stepping switches providing 99 data channels of which 80 were used. Signal amplitudes were converted to digital form by the process of demodulation, followed by voltage to frequency conversion and digitizing with a conventional digital frequency meter. The phase of each accelerometer signal was measured relative to the oscillator signal to the power amplifier. The phase was measured digitally by counting the number of clock pulses occurring between the positive going axis crossings of the oscillator signal and the accelerometer signal. The clock frequency was adjusted such that the output count read directly in degrees of phase. The channel identification voltage was digitized by means of the voltage to frequency converter and frequency meter.

To start a sequence of data acquisition, the stepping switches were returned to their number one positions. Each switch in turn was then caused to step through all of its positions. As each phase and amplitude measurement was completed, the data was automatically printed along with a channel identification number and the operating frequency. The operating frequency was set in manually on a set of decade switches.

The input quantities of vdtage, current and power were manually recorded at each frequency. The current into the total array was held constant at six amperes. In each experiment the frequency was varied from 350 to 450 cycles per second in five cycle steps except from 390 to 430 cycles per second where it was varied in 2-1/2 cycle steps. In all experiments the array was submerged to a depth of 45 feet to its acoustic center.

Lake Pend Oreille Tests

The two 36 element arrays were tested one at a time at a depth of 90 feet with all elements connected electrically in parallel. This connection used the transformer assemblies diagrammed in figure 7. A diagram of the power circuits used in these tests is shown in figure 9. Three ten-microfarad tuning capacitors were connected in series with the common lead to each transducer element. A switching arrangement permitted the option of connecting either two or three of these capacitors in series or of shorting out the entire group. Thus, three choices of direct connection, five microfarads, or 3-1/3 microfarads were available for transducer tuning. When the direct connection was used, a five microfarad group tuning capacitor was connected in series with the transformer primaries to group-tune the array. When either the 3-1/3 or five microfarad individual tuning capacitors were used, the group tuning capacitor was shorted out.

The instruments used to measure current, voltage and power were of the portable standard type. Currents to each transformer primary were monitored with two percent panel meters. An interlock circuit shorted the signal input to the power amplifier in the event of failure of the direct polarizing current.

The same automatic data acquisition was used in the Lake Pend Oreille tests as was used in the Chesapeake Bay tests with the exception that only one underwater junction box was required to accommodate the reduced number of data channels.

The consolidated array was tested first with group tuning and next with the elements individually tuned with series connected five microfarad capacitors. Three tests were conducted with the unconsolidated array, one with group tuning and one each with individual 3-1/3 and five microfarad tuning capacitors. In each of the five tests the input current,

voltage and power were manually recorded while the accelerometer data were automatically printed at five cycles per second frequency increments from 350 to 450 cycles per second except for frequencies between 380 and 420 cycles per second where the increments were reduced to 2-1/2 cycles per second. The direct polarizing current was maintained at 60 amperes to each array or nominally ten amperes per element. The alternating current was held constant at five amperes as the frequency was varied. In addition, a linearity check was performed for each transducer configuration. This consisted of incrementally increasing the current from 2-1/2 to 12-1/2 amperes in 2-1/2 ampere steps at a frequency of 410 cycles per second. All data were sampled at each current increment. At the conclusion of the other tests, the unconsolidated array with group tuning was driven at 18.8 amperes.

Directivity patterns were measured at frequencies of 350, 380, 400, 410, 420, and 450 cycles per second for each transducer configuration. Each beam pattern was measured using 0.1 amperes alternating current and the patterns at 410 cycles per second were repeated with 10.0 amperes. The low level current response was measured from 100 to 1200 cycles per second on both the acoustic axis and the reciprocal acoustic axis with the receiving hydrophone at a range of ten meters. Thereafter, the response on the acoustic axis was monitored for all operations.

RESULTS

In the following discussion of results, the data from the Lake Pend Oreille and Chesapeake Bay experiments have been combined and are presented in functional categories.

Directivity

Directivity patterns were measured in the horizontal plane at frequencies of 350, 380, 400, 410, 420 and 450 cycles per second for each of the five experiments performed with the 36 element arrays at Lake Pend Oreille. Figures 10 through 16 illustrate the patterns obtained when the projector and receiving hydrophone were submerged to a depth of 90 feet with a ten meter separation. It can be observed that the patterns are not completely symmetrical at some frequencies. The dissymmetry might be accounted for by the presence of an air-filled junction box on

the right-hand side of the array structure. The patterns at each frequency were obtained with a current of 0.1 amperes of signal current and ten amperes polarizing current into the projector. In each experiment the pattern was repeated at 410 cycles per second with ten amperes signal current. The patterns obtained at the higher currents are not significantly different from those taken at 0.1 amperes.

The directivity indices which were used in the computations of projected acoustic power were obtained from the 0.1 ampere directivity patterns. Power summations were made at ten degree increments from five to 175 and from 185 to 355 degrees. The results from the two halves of each pattern were then averaged. Computed directivity indices for the five experiments are plotted in figure 17. The values computed from 0.1 ampere patterns are circled, whereas those computed from 10.0 ampere patterns are marked with an "X". Values of directivity indices at frequencies other than those at which patterns were obtained, were interpolated from a smooth curve as shown in figure 17. It is recognized that computations of directivity indices, from patterns taken in the horizontal plane only, probably yield somewhat erroneous results. This is particularly true for the consolidated array where there is evidence that the radiating face had a velocity distribution symmetrical about a vertical axis.

Efficiency

The calculated electroacoustic efficiencies are plotted in figure 18 for the five array configurations and operating conditions as indicated on the curves. The driving current was held constant at five amperes for all frequencies. Figure 19 illustrates the linearity of the efficiency with respect to the operating power level. The frequency was held constant at 410 cycles per second while the driving current was increased from 2.5 to 10.0 amperes for each experiment. After the completion of lower power level tests, each array was driven at 12.5 amperes and the unconsolidated array with group tuning was driven at higher current levels as indicated. The efficiency of the unconsolidated, group tuned array operating at a frequency of 410 cycles per second with a driving current of five amperes is indicated as 56 percent in figure 17 whereas it is shown as 70 percent in figure 18. This apparent discrepancy might be explained as a temperature effect. The linearity test for the unconsolidated array was performed shortly after submergence whereas the

frequency response and high power data were obtained after a prolonged period of submergence. With each array, the frequency response tests were performed at a time between the ten ampere and 12.5 ampere linearity tests. The consolidated, individually tuned array exhibited a somewhat reduced efficiency in the frequency response tests but was restored to a value in excess of 60 percent when the array was driven at 12.5 amperes. The reason for the reduction in efficiency occurring between the linearity and frequency response tests for the unconsolidated array is not understood at this time, although temperature effects are considered a possible cause.

Acoustic Loading

Since the nonuniform velocity distribution over the face of the projector is attributed largely to acoustic interaction effects, a knowledge of the acoustic loading experienced by each transducer element at each frequency within the operating band would add to an understanding of the problem. Unfortunately, the necessary parameters are not readily measurable with existing instrumentation. However, a value can be computed from the measured transducer velocity and radiated acoustic power which is related to the over-all or average transducer loading. Computations have been made in which the measured acoustic power is compared with the theoretical power which would be radiated by a piston of the same dimensions operating into a unity ρc load and having a uniform velocity equal to the root-mean-square velocity of the transducer face. At each frequency, a root-mean-square velocity was computed from the measured velocities of the radiating faces of the 36 elements. An acoustic power was computed for a uniformly vibrating piston having this velocity value and an acoustic load equal to ρcA, where "A" is equal to the radiating area. The "loading ratio" is here defined as the ratio of the actual acoustic power to this computed value. The loading ratios computed from the data of each of the five experiments conducted at Lake Pend Oreille are plotted in figure 20. The dashed line in each plot represents a loading ratio of one half. It can be seen that the ratio for the consolidated, group tuned configuration is relatively high for all frequencies above 390 cycles per second. Referring to figure 18, it also can be seen that the efficiency is high under these same conditions. Further on in this report it is pointed out that the transducer spring deflections for a given radiated power are optimum for this configuration at certain frequencies near 400 cycles per second.

Figure 21 illustrates the power dependence of loading ratio. In general, the loading ratio remains constant as the driving current is increased from 2.5 to 12.5 amperes. As was noted in the discussion of efficiency, the unconsolidated array apparently suffered some degradation of performance after the current had initially been increased from 2.5 to 10 amperes.

Impedance

Vector impedance locus diagrams for each transducer configuration are illustrated in figures 22, 23, and 24. Only the series parallel impedances for the 12 element groups are shown since impedance measurements of the individual groups were not obtained when these groups were connected to the paralleling transformers. In figure 23, the unconsolidated group impedance is illustrated for a 72 element group in the series-parallel connection, resulting in lower impedance values when compared with 36 element groups. The module containing 72 unconsolidated elements was divided electrically into two groups only when the paralleling transformers were used. When individual tuning capacitors were used in the tests with the 144 element array, the group tuning capacitor was also left in the circuit. This does not affect the operation of the transducer in any way except in the measured impedance. When the impedance of the 36 element, unconsolidated, group tuned configuration was measured, the meter returns were shifted to the load side of the tuning capacitor and hence the plot shown at the right center of figure 23 is modified accordingly.

Element Displacement Characteristics

Outer Mass Displacements

Velocity variations over the face of an array which are due to acoustic interaction effects can be expected to have a symmetry related to the electrical and mechanical geometry of the array configuration. Figures 25 through 38 illustrate the distributions of the displacement amplitudes of the radiating faces for the array configurations tested.

All of the amplitude distribution plots were constructed by computing the mean value of displacements for each array configuration and each frequency. The individually measured values of displacement amplitudes were then divided into four amplitude levels; those greater than ten percent above average, those having values between average and ten

percent above average, those between average and ten percent below average, and those having all lower values. The shading code shown in figures 25 through 30 is applicable to all amplitude distribution plots.

Figures 25 through 30 contain distribution plots for the 36 element consolidated array at 20 cycle per second frequency increments from 350 to 450 cycles per second. The three plots on the upper half of each page illustrate the distributions obtained when the consolidated array formed one quadrant of the 144 element array tested in the Chesapeake Bay. The electrical connections indicated under each plot refer only to the 36 element group while the remaining three-fourths of the array was series-parallel connected. The two plots at the bottom of each page were obtained from the data of the Lake Pend Oreille tests in which this 36 element group comprised the entire array. A similar presentation is made for the 36 element unconsolidated group in figures 31 through 36. One additional plot is shown on each page since two values of individual tuning capacitors were used for the unconsolidated group in the Pend Oreille tests. Distributions for the two 12 element consolidated groups are shown in figure 37 and 38. The distributions for three different frequencies are shown on each page. These data were obtained with parallel connection to the quadrant of the array containing the two 12 element groups and 12 individual elements in two rows directly above the 12 element groups. The remainer of the array was connected in series parallel.

Many of the plots show a nearly random distribution. However, certain trends are evident. The 36 element consolidated group displays a distribution which tends to be symmetrical about a vertical axis. This might be accounted for by the mechanical construction of this subassembly since aluminum stiffening channels are bolted along the vertical center line of both the front and back faces. Aluminum angles are also bolted along the top and bottom horizontal edges. Symmetry about a vertical axis is very noticeable in those tests in which the consolidated group was operated independently. When operated as a quadrant of a larger array, the acoustic interactions and boundary conditions presented by the remainder of the array apparently overshadow the effects of vertical stiffening. The predominant characteristic of the 36 element unconsolidated group, when operating independently, is a tendency toward higher amplitudes along the four edges than in the central region.

The average of outer mass displacements for each of the subassemblies is plotted as a function of frequency in figures 39 through 55. Maximum and minimum values of displacement amplitude are also plotted for the purpose of indicating the range of values encountered. The group configuration and type of electrical connection are indicated on each plot.

In view of the fact that the objective of this research is to develop means for increasing the projected acoustic power without exceeding the mechanical limitations of the transducer elements, it is considered desirable to normalize the transducer element displacement data to a reference power level in order to facilitate interpretation of results for the various test conditions. The reference level used in this report is one kilowatt acoustic power for the data obtained with the 36 element arrays at Lake Pend Oreille. No facilities for monitoring the acoustic output of the 144 element array were available for the tests in the Chesapeake Bay. Consequently, element displacement data for these tests are normalized to one kilowatt of electrical input power to the 36 element quadrant of the array being investigated in each experiment. The twelve-element groups were, therefore, normalized to one-third of a kilowatt. In the case of parallel element connection, the power input to individual 12 element subassemblies was not measured directly. For the purpose of normalization, the input power to each 12 element group was assumed to be one-third of the power to the 36 element parallel connected group.

The parallel connection, as compared to the series parallel, considerably reduces the extent of displacement variation in every case. Figures 39 and 40, 42 and 43, 45 and 46, and 48 and 49 illustrate the improvement for the four configurations tested in the λ by λ array. There is a tendency, however, for the displacement variations to increase at frequencies higher than 430 cycles per second when the parallel, group tuned connection is used with the exception of the 12 element consolidated group with rubber covering. The use of five microfarad individual tuning capacitors eliminated the increased variation at high frequencies but, in the case of the 36 element consolidated group, it introduced large variations at frequencies near the mechanical resonance. As can be seen in figures 51 through 55, less variation was experienced with the group tuned connection than with individual tuning when the 36 element groups were operated individually.

Since it is the element having the most abnormal behavior which limits the permissible operating power, it is the maximum rather than the average values which are more significant insofar as power handling capability is concerned. Absence of exceptionally high displacement

values is an indication of good performance. However, outer mass displacements do not, in themselves, constitute a limitation on power since this is determined by spring deflection which is influenced jointly by inner and outer mass displacements. In order to facilitate a direct comparison of the maximum outer mass displacement amplitudes encountered among the various element configurations, composite plots of these values are illustrated in figures 56 through 60. Figures 56, 58 and 59 enable a direct comparison of the effects of mechanical consolidation of the elements, whereas figures 57 and 60 illustrate the changes brought about by the different electrical configurations. From figures 56 and 57 it can be seen that the parallel connection is more favorable than the series-parallel connection for both 36 element groups in the 144 element array with the exception that the parallel group tuned combination yields high values at the upper end of the frequency band. Individual tuning eliminates the rise at high frequencies in both cases. However, the consolidated groups then take on high values at frequencies near mechanical resonance. The optimum combination, insofar as outer mass displacement is concerned, appears to be the unconsolidated group with parallel connection and individual tuning.

In the case of the 36 element groups operated by themselves, it can be seen from figure 60 that the parallel group tuned connection yields the most favorable results. Figure 59 indicates that with the parallel group tuned connection, there is but little difference in the performance of the consolidated and unconsolidated configurations. The consolidated array has some advantage in the mid-frequency range.

The 12 element groups can be directly compared only for the series-parallel connection. The electrical power input was not measured for the individual groups when the paralleling transformers were used to connect 36 elements in parallel; hence, normalization to a constant input power was done on the assumption that the power was equally divided among the three 12 element groups. Since this assumption is probably only approximately valid, a comparison of absolute magnitudes should not be made among the groups. For the series-parallel connection, the rubber covered consolidated group displays the more favorable performance, particularly at the upper end of the frequency band.

Figures 61 through 64 are randomly selected examples of the manner in which the outer mass displacement of individual elements vary as a

function of frequency. The diagram in each figure illustrates element positions in the array. In general, the elements display a less erratic variation with frequency for the parallel connection as opposed to the series parallel. In figure 62, the displacement amplitudes of two adjacent elements are plotted. Withthe series-parallel connection these elements exhibit radically different frequency characteristics even though they are driven by the same current.

The array impedance is a function of operating power level due to the nonlinearity of the transducer elements. Because of this, there is not a completely linear relationship between the displacement of the radiating face and the driving current. The average outer mass displacement is plotted as a function of driving current in figure 65 for the 36 element arrays. The dashed portions of the curves represent time lapses during which the frequency response measurements, at a constant current of five amperes, were made. Although the ratio of average outer mass displacement to driving current decreases with increasing current, the efficiency remains essentially constant, with the exception of the reduction in efficiency occurring between ten and 12.5 amperes for the unconsolidated group tuned configuration, as can be seen in figure 19. It has been shown that the square of the displacement is linearly related to acoustic power for all cases except as noted above.

Spring Deflections

The upper limit of power at which the subject transducer elements can be safely operated is determined by transducer spring deflection. The springs break as a result of fatigue when operated for prolonged periods at deflections greater than a certain maximum value. Since spring deflection amplitudes vary from element to element, and even from spring to spring within an element, the maximum safe power level is determined by the spring having the maximum deflection. The spring deflection is a function of the displacement amplitudes of the inner and outer masses and the phase angle between them. Displacement phases and amplitudes of the inner masses were measured at two locations in each of those elements instrumented with internal accelerometers. One accelerometer is positioned at the upper edge and one at the lower edge of the internal mass. The springs are located on the sides of the element with two sets in front and two at the rear on each side as shown in figure 66. In the operating position the cable entrance is at the top of the rear radiating face. The element shown is the TR-11B type. The

model TR-11C has a modified spring and side plate design. One accelerometer was attached to the outer mass at the center of the radiating face of each element. If it is assumed that the outer mass is completely rigid and experiences rectilinear motion only, then the upper accelerometer on the inner mass together with the outer mass accelerometer provides a measure of the deflection of the uppermost springs, and the lower inner mass accelerometer output combined with the output of the outer mass accelerometer is a measure of the deflection of the bottom springs. The amplitude of spring deflection is given by

$$\sqrt{a^2 + b^2 + 2\,ab\cos\theta}$$

where "a" is the outer mass displacement amplitude, "b" is one of the inner mass displacement amplitudes, and θ is the phase angle between the inner and outer mass displacement.

Figures 67 through 80 illustrate the averages of the spring deflections computed from these sets of accelerometer outputs for the various transducer configurations. The shaded area in each of the illustrations is bounded by the maximum and minimum values of deflection amplitude. The data concerning the 144 element (λ by λ) array, for which no acoustic measurements were obtained, have been normalized to one kilowatt electrical input power by multiplying each calculated spring deflection by the ratio

$$\sqrt{\frac{1000}{P_e}}$$

where P_e is the measured electrical input power to the 36 element quadrant of the array being investigated. Since the efficiency, for each of the various electrical and mechanical configurations, is not necessarily the same, direct comparison of deflection amplitudes among the configurations must be made with reservations. However, the spread of the data as indicated by the width of the shaded area is a valid index of the performance. The parallel connected, group tuned, unconsolidated group exhibits a relatively small spread of deflection amplitudes when compared with all other configurations. Estimated comparisons of the performance among all of the configurations will subsequently be made on the basis of the maximum deflection amplitudes illustrated in these plots and assumed values of efficiency. The data from the Lake Pend

Oreille tests with the 36 element arrays have been normalized to one kilowatt of acoustic power. Therefore, direct comparisons can be made among figures 76 through 80. In all of the tests, the consolidated configurations exhibited exceptionally large values of deflection over a small range of frequencies below resonance.

In order to facilitate a direct comparison of the maximum spring deflections encountered among the various element configurations, composite plots of these values are illustrated in figures 81 through 85. Figures 81 through 83 enable a direct comparison of the effects of mechanical consolidation of the elements whereas figures 84 and 85 illustrate the changes brought about by the different electrical configurations.

The effects produced by the relative amplitudes of maximum spring deflection as shown in these plots will be discussed in the section dealing with power capability.

The manner in which spring deflection varies as a function of input current is illustrated in figures 86 through 90. These curves show the average values together with shaded areas representing the range of values for the five experiments conducted with the 36 element arrays at a frequency of 410 cycles per second. All values of deflection have been normalized to one kilowatt of acoustic power. Both the average deflection per unit acoustic power and the spread of values remains nearly constant for all operating power levels. The dashed lines on these curves represent the interval during which the frequency response data was taken. The data points at five amperes which are marked with crosses were obtained from the frequency response data at 410 cycles per second.

In order to compare the power capability of the various configurations, curves have been prepared showing the computed radiated acoustic power per element for an allowable spring deflection of ten mils peak to peak. The choice of ten mils as the value for the maximum permissible spring deflection is based upon the recommendation of the manufacturer plus experimental verification that this is a safe operating value. It is possible that a larger value could be used, particularly for the type of spring utilized in the model TR-11C transducer, but this has not been verified to date. In the curves prepared from the data of the Lake Pend Oreille tests, the power was computed as 1/36

of the projected acoustic power of the 36 element arrays after being normalized to an allowable maximum spring deflection of ten mils peak to peak. Normalization was accomplished by multiplying the acoustic power by

$$\left(\frac{10}{\text{maximum spring deflection}}\right)^2$$

The maximum spring deflections used in the computations are those shown in figures 81 through 85.

In the absence of acoustic power data for the Chesapeake Bay tests, the acoustic power was computed on the basis of the electrical input power and assumed efficiencies. The values of efficiencies employed were the same as those measured for the consolidated and unconsolidated arrays at Lake Pend Oreille. Since it was necessary to assume values of efficiency for the data concerning the one wavelength square array, conclusions drawn from the allowable acoustic power computations for this array must be accepted with reservations. The curves of extrapolated power per element are illustrated in figures 91 through 95.

In figure 91 the series-parallel electrical connection is directly compared with the parallel connections for the consolidated and unconsolidated 36 element groups in the 144 element array. A marked advantage of the parallel connection is indicated for the unconsolidated group at all frequencies. In the consolidated group, the parallel connection is advantageous only at the low end of the frequency band. A direct comparison among the different mechanical configurations is made in figures 92 and 93 for the various electrical connections in the 144 element array. The 12 element consolidated group is represented only for the series-parallel connection since the power input to this group was not separately measured when it was connected to the paralleling transformers. No curves are available for the rubber-covered consolidated group as no elements in that group were equipped with internal accelerometers. The unconsolidated group demonstrated decidedly better performance in the parallel connection. Figures 94 and 95 illustrate the performance obtained with the 36 element arrays at Lake Pend Oreille. The effects of electrical tuning are compared in figure 94 and the mechanical configurations are compared in figure 95. Individual tuning produced very little effect on the power handling capability. The consolidated array exceeded the performance of the unconsolidated array

in the mid-frequency region but was greatly inferior at low frequencies centered about 370 cycles per second. The best over-all performance was obtained with the unconsolidated array with parallel connection.

On the basis of these curves, an attempt can be made to predict the source level of the full-scale ARTEMIS array of 1440 elements. The broad assumption must be made that the projected power can be linearly extrapolated to the larger array. This does not take into account the differences in interaction effects and acoustic loading as the size of the array is increased. On the basis of this assumption and an assumed directivity index of 20 decibels for the 1440 element array, the source level would be 123.6 decibels above the indicated power per element as illustrated in figures 91 through 95.

Ideally, both the inner and outer masses of the transducer elements are rigid structures and should have pure rectilinear motion with no flexural or rotary components. That this is actually not the case in practice can be seen by examining the outputs of the four accelerometers attached to especially instrumented elements. If the motion were rectilinear, the two accelerometers attached one at the top and one at the bottom edges of the inner mass would have equal output amplitudes and phases. Similarly, the accelerometers attached at the center and at the lower edge of the rear radiating face of the outer mass would have identical outputs. As previously stated, a measure of the transducer spring deflection can be obtained by appropriately combining the measured output of the accelerometer attached to the center of the radiating face of the outer mass with the output of either of the internal accelerometers. The two values of spring displacement obtained for each element in this manner are compared in figures 96 through 100. Figures 96 and 97 apply to the half wavelength square consolidated array and figures 98 through 100 refer to the half wavelength square unconsolidated array. The average difference between the deflections of the top and bottom springs is presented as a percentage of the average spring deflection of the array. The shaded area represents the range of values encountered. It can be seen that large peaks occur for both the consolidated and unconsolidated arrays. Referring to figure 95 which illustrates the acoustic power capability, it is evident that a correspondence exists between reduced power handling capability and excessive values of nonrectilinear components of motion. The consolidated array exhibits very large values of spring deflection difference at frequencies in the region of 370 cycles per second which coincides with reduced power

handling capability. The unconsolidated array displays peak spring deflection differences to some extent in the same frequency region and a larger peak in the neighborhood of 400 cycles per second. Again referring to figure 95, it can be seen that the consolidated array exceeds the unconsolidated array in power handling capability at frequencies near 400 cycles per second. There is not complete correspondence between power capacity and the degree of nonrectilinear motion since uniformity in the rectilinear component of motion among the individual elements of the array is also instrumental in determining power handling capability. There is no doubt that rotary or flexural modes in the transducer elements tend to degrade the array performance.

An examination of the data indicates that the computed nonuniform spring deflections within an element are caused primarily by differences in the amplitude of motion at two points on the inner mass, rather than by phase variations and that large percentage differences of spring deflection correspond to numerically large displacement amplitude differences for the inner mass. The difference in spring deflections within the elements is approximately linearly related to the absolute magnitude of spring deflection. In figure 101 the average spring deflection difference is plotted versus average spring deflection fromthe data obtained with the half wavelength square array as the driving current was varied from 2.5 to 12.5 amperes for the consolidated array and from 2.5 to 18.8 amperes for the unconsolidated array. Although the curves are nearly linear in both cases, it can be seen that the spring deflection difference in the unconsolidated array is approximately double that experienced in the consolidated array.

Analysis of the data from pairs of accelerometers mounted on the outer masses of certain elements indicates that the outer masses are also subject to nonrectilinear components of motion but to a lesser extent than the inner masses and with less pronounced frequency dependence. Figures 102 and 103 illustrate the differences of displacement between pairs of accelerometers on outer masses expressed as a percentage of the average outer mass displacement of the array. These data were taken from the tests of the one wavelength square array since this information is not available for the half wavelength square arrays. No comparable data on outer mass displacement differences is available for the unconsolidated array.

While it is true that the displacement data between pairs of accelerometers were not measured simultaneously due to the use of a sequential data

sampling system, the time variation of displacement amplitude has been shown to be insufficient to account for the measured differences. Examination of data from experimental runs which had been repeated revealed that displacement data was repeatable with an average accuracy of 2.5 percent and in no case which was examined did it exceed four percent.

The mechanism of the observed flexural or rotary modes of vibration are not well understood. Instrumentation included in the tests herein reported, while sufficient to detect the presence of a nonrectilinear mode, was inadequate to determine its form.

CONCLUSIONS

The test series conducted in the Chesapeake Bay with a one wavelength square array consisting of 144 close-packed transducer elements demonstrated that a parallel connection of elements enhanced the array performance when compared with the series-parallel connection of the form presently in use in the ARTEMIS source. Improvement was evidenced primarily by a more uniform velocity distribution of the radiating surface and, subject to an assumed electroacoustic efficiency, an enhanced power handling capability of between four and nine decibels, depending upon frequency, for the array configuration used in this test.

In this test series an attempt was made to obtain a comparison of the merits of two methods of mechanically consolidating elements into groups. Two 12 element groups were fabricated, one with adjacent bare metal surfaces bonded together and the other with the bonding performed between rubber-covered surfaces. Although the rubber-covered group displayed a somewhat more favorable performance, results were inconclusive due to a difference of the position of these groups in the array and to limitations on the electrical instrumentation. A 36 element consolidated group was also included in this array in order to compare its performance with that of an equivalent unconsolidated group. Again the same limitations as expressed for the 12 element groups prevented a conclusive comparison.

A second test series conducted at the Naval Electronics Laboratory's acoustic calibration station at Lake Pend Oreille, Idaho, enabled a more rigorous collation of the performance of a consolidated versus an

unconsolidated array. Here, two one-half wavelength square arrays were employed, in one of which the individual elements were rigidly bonded together. The results of this test demonstrated that the performance of the two arrays was approximately equivalent except at frequencies near 370 and 400 cycles per second. At 370 cycles per second the elements of the consolidated array experience very large spring deflections relative to the deflections at other frequencies for the same acoustic power. The power handling capacity is reduced by approximately six decibels in this region. In the vicinity of 400 cycles per second the consolidated array exhibits approximately a two decibel advantage over the unconsolidated array. A further study was made of the advantages of electrically tuning the individual elements of the arrays. It was found that this type of tuning did not enhance the performance of the array for those values of reactances which were employed, for operation over the entire frequency band.

The most satisfactory performance over the frequency band from 350 to 450 cycles per second is adjudged to be obtained with the unconsolidated array having the parallel, group tuned connection.

Vibrational modes of a flexural or rotary nature were observed in the transducer elements, particularly in the internal masses. These were found to contribute to the spring deflections, thus reducing the permissible acoustic power output.

The following list summarizes the conclusions obtained from the test results presented in this report.

1. Series-parallel versus parallel connection of elements:

The parallel connection resulted in a more uniform velocity distribution of the radiating surface and an enhanced power handling capability.

2. Consolidated versus unconsolidated elements:

The unconsolidated array exhibited the more satisfactory over-all performance although the consolidated array was slightly superior at certain frequencies.

3. Individual versus group tuning of elements:

No marked advantage of individual tuning of the elements was observed.

4. Spurious vibration modes:

Vibrational modes of a flexural or rotary nature were observed which contributed to the limitation of allowable power level.

Fig. 1 - Front view of the two array frames during fabrication which were jointed to form the 144 element test array

Fig. 2 - Rear view of 144 element test array mounted on the USS HUNTING

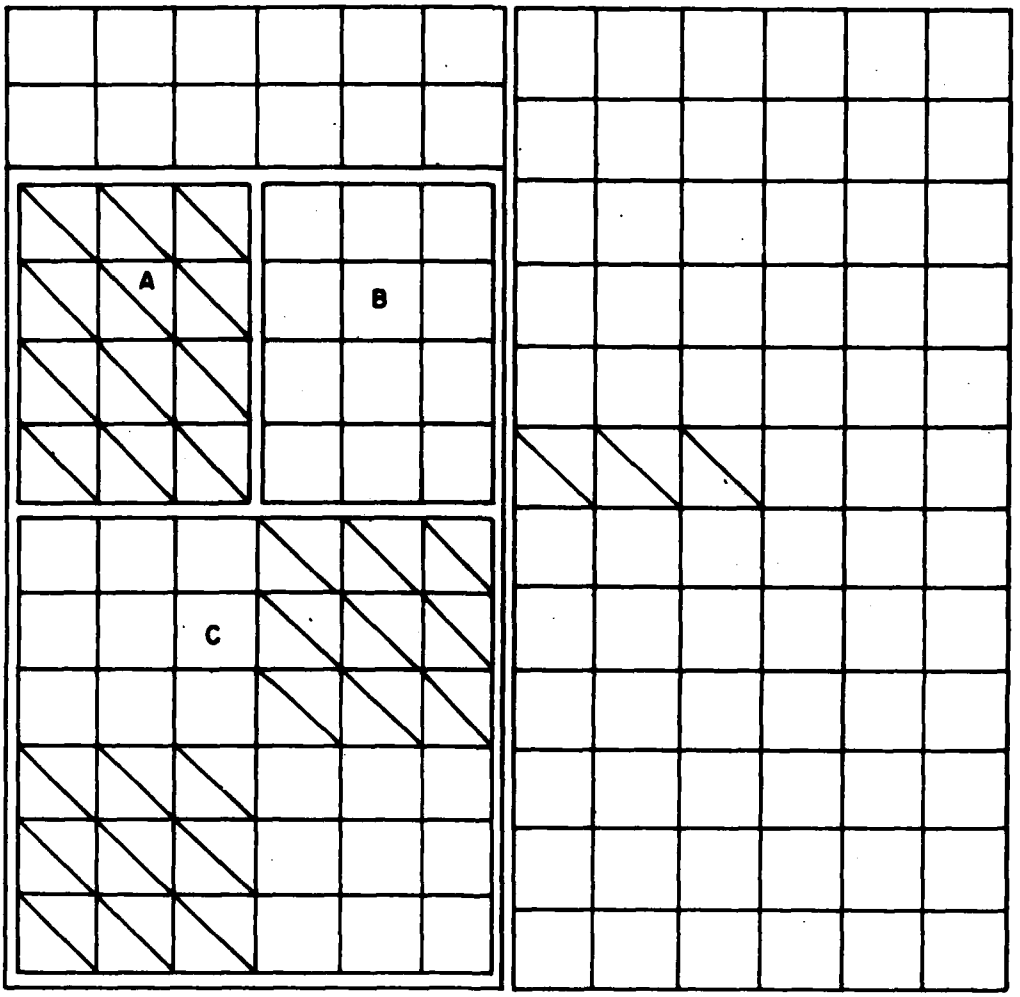

— — ELEMENTS WITH ACCELEROMETERS ON THE INTERNAL MASS

A — — 12 ELEMENT CONSOLIDATED BARE GROUP
B — — 12 ELEMENT CONSOLIDATED RUBBER-COVERED GROUP
C — — 36 ELEMENT CONSOLIDATED GROUP

Fig. 3 - Subassembly locations in the 144 element array

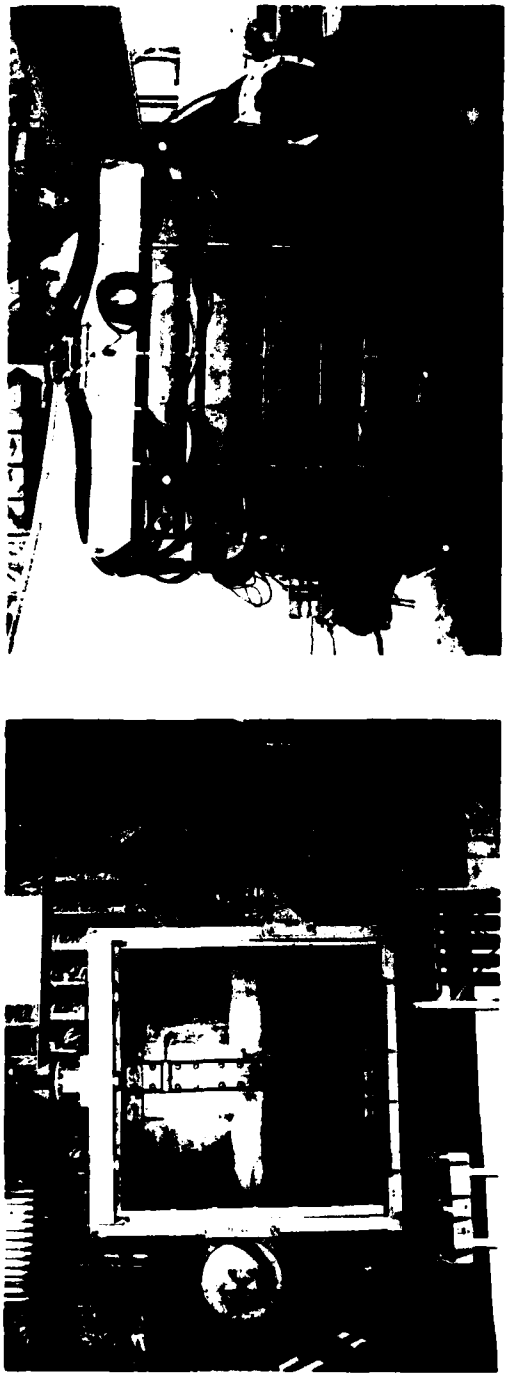

Fig. 4 - Front (left) and back (right) views of 36 element consolidated array

Fig. 5 - Front (left) and back (right) views of 36 element unconsolidated array

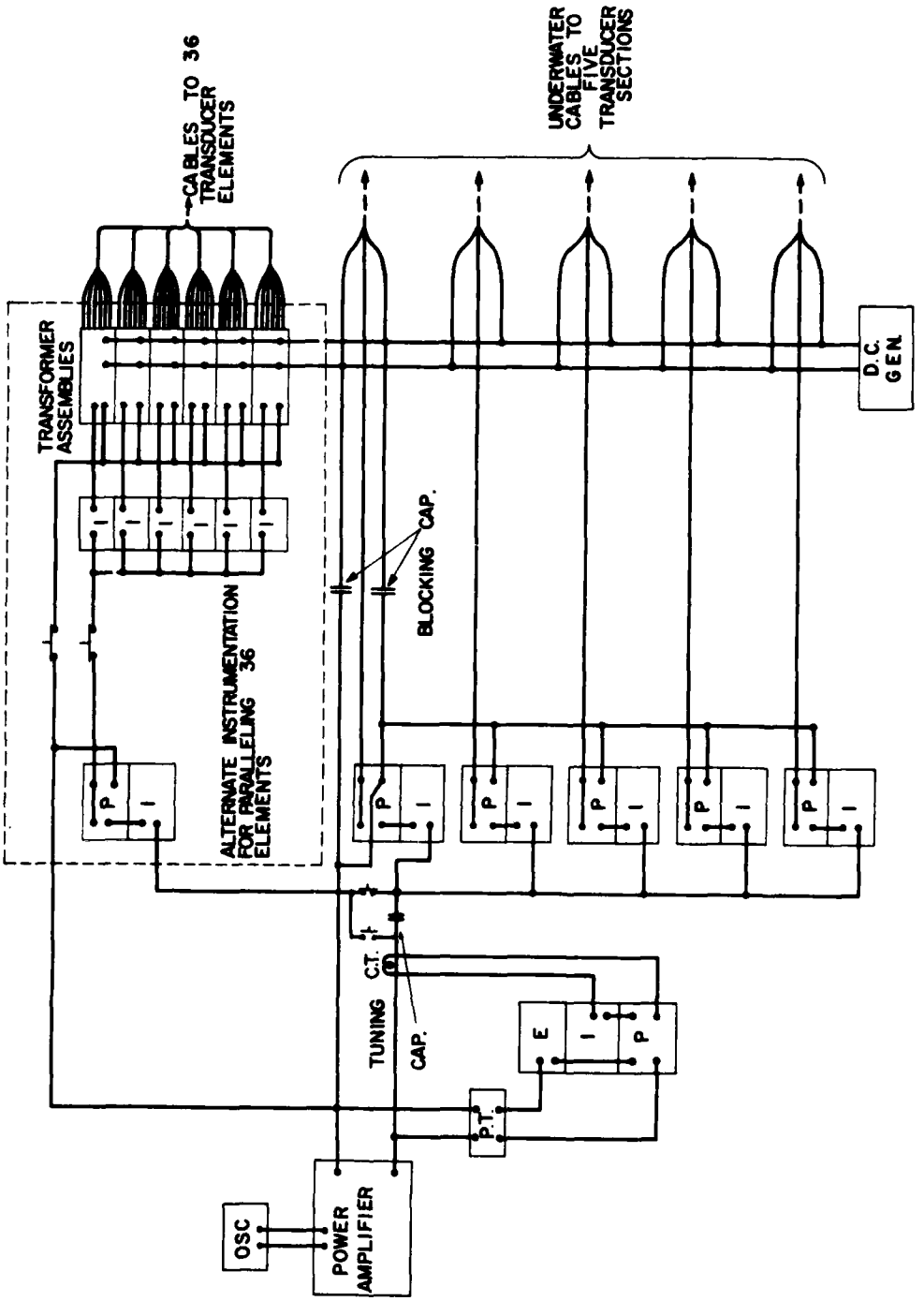

POWER AND METERING CIRCUITS

Fig. 6 - Power and metering circuit for test of 144 element array

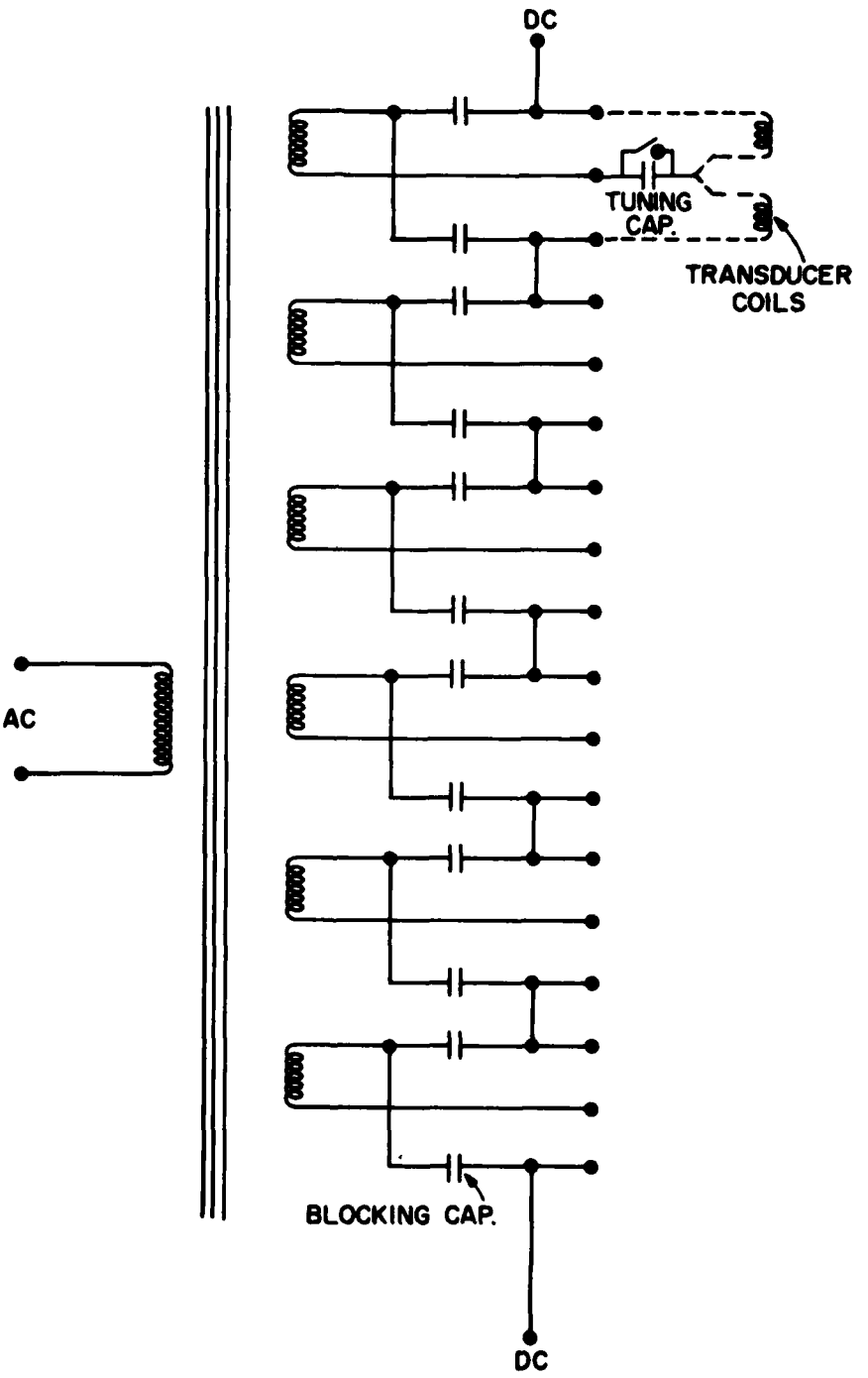

Fig. 7 - Paralleling transformer assembly

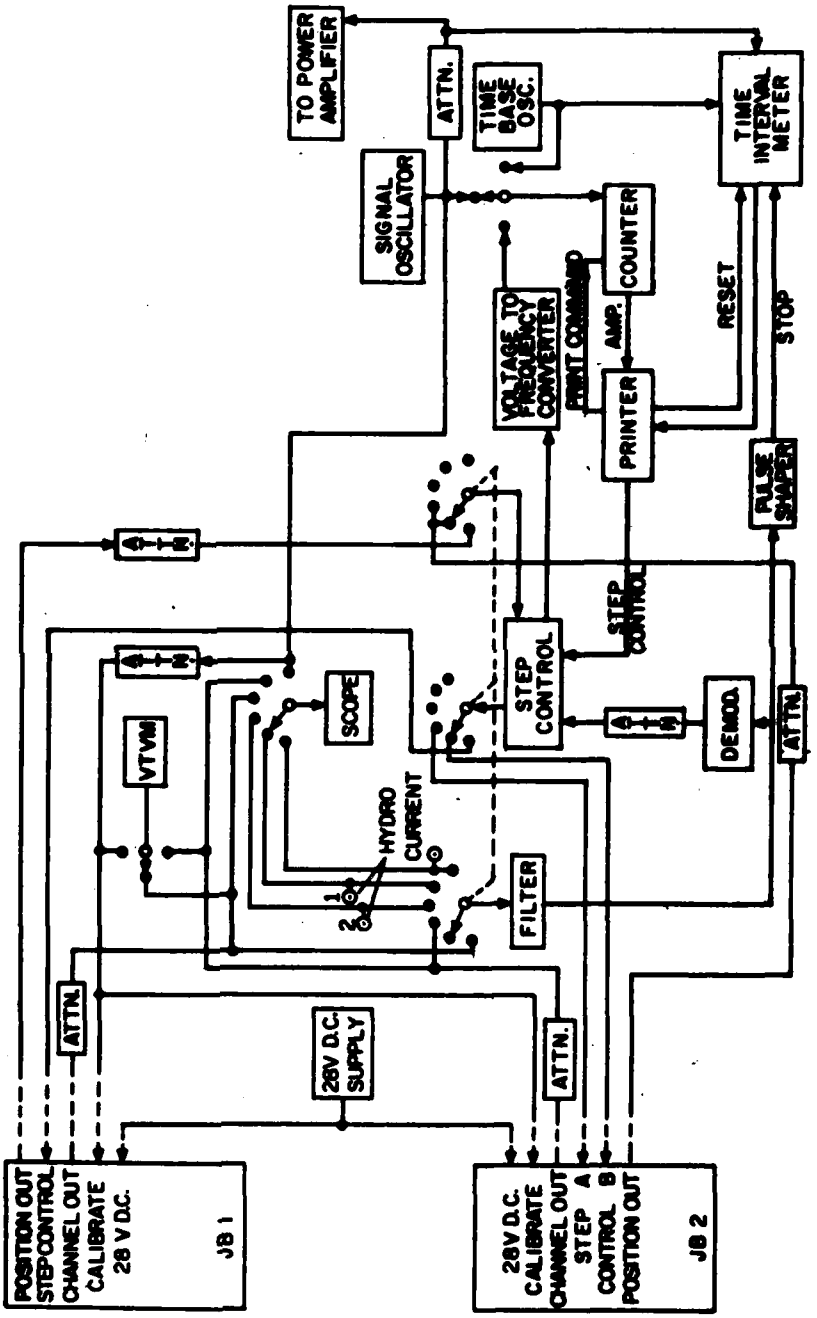

Fig. 8 - Automatic sensor sampling and read-out instrumentation

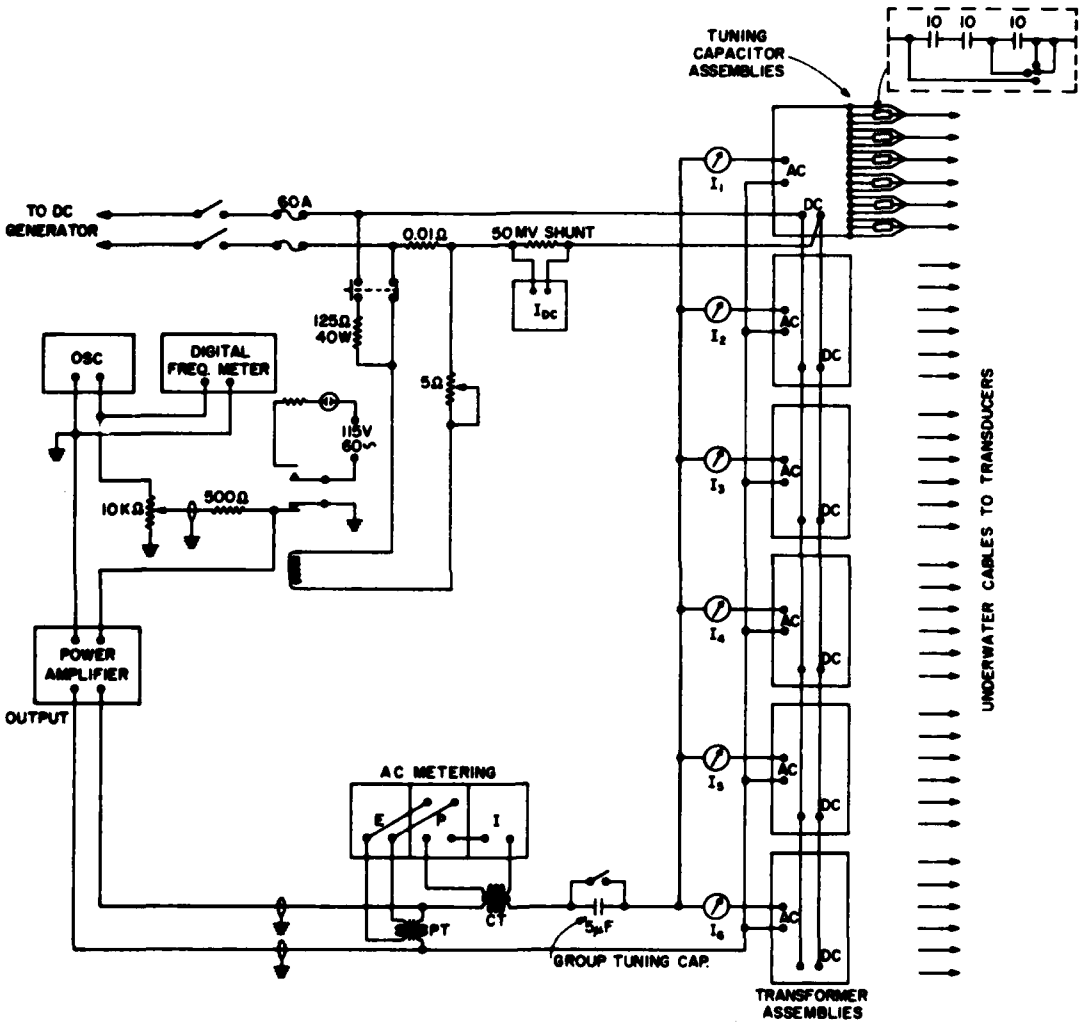

Fig. 9 - Power and metering circuit used in tests of 36 element array

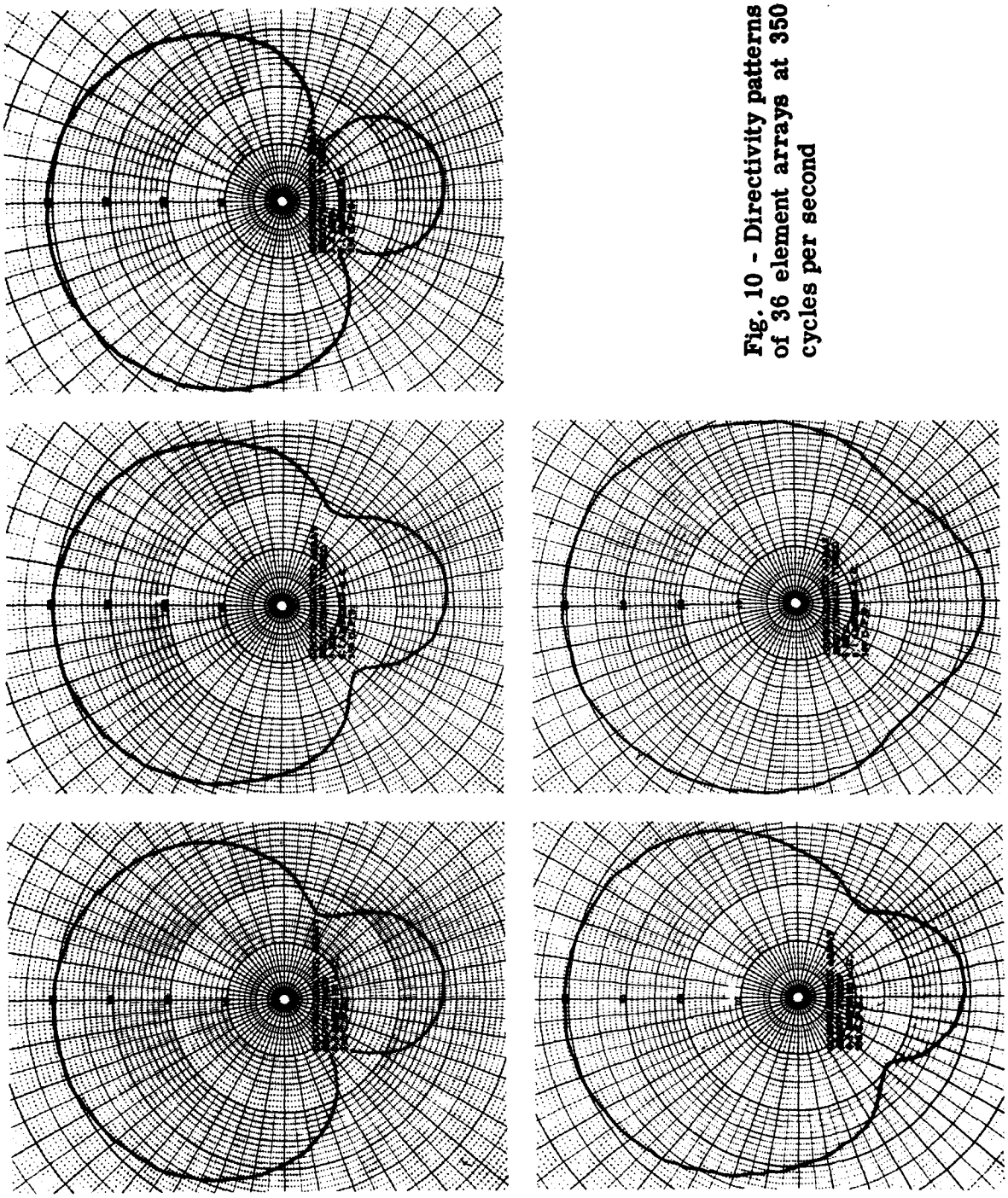

Fig. 10 - Directivity patterns of 36 element arrays at 350 cycles per second

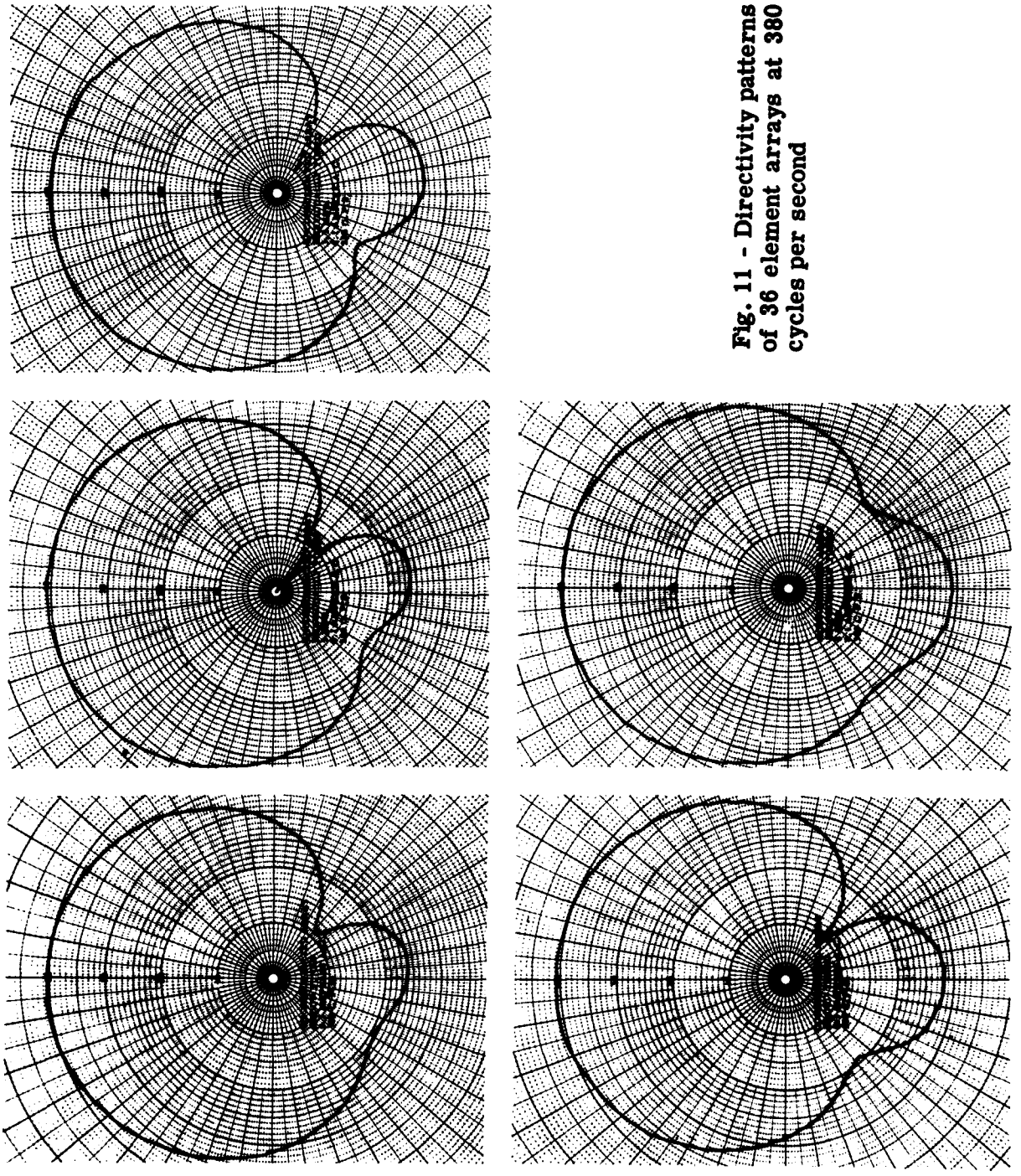

Fig. 11 - Directivity patterns of 36 element arrays at 380 cycles per second

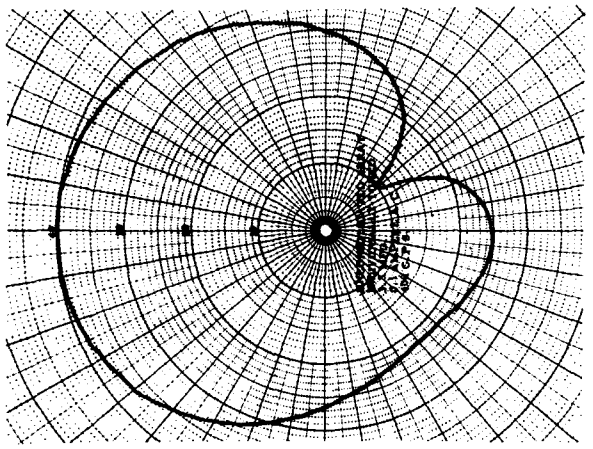

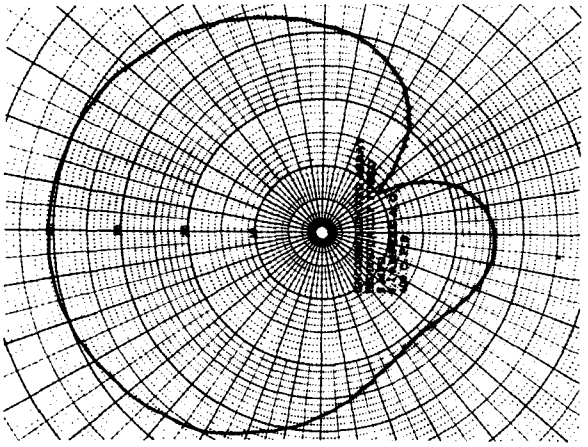

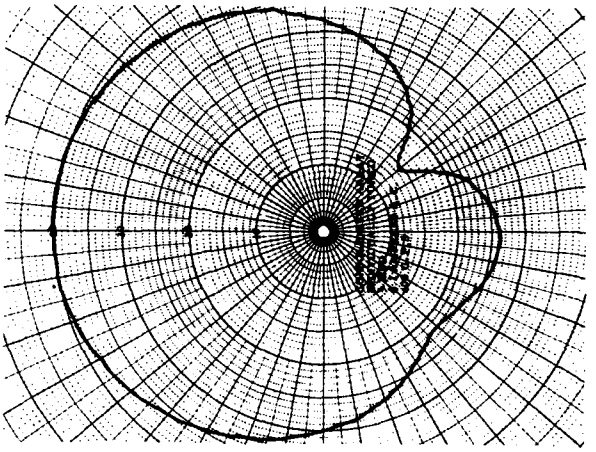

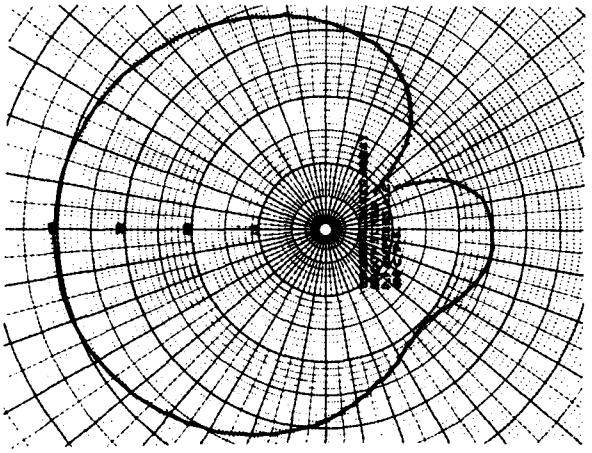

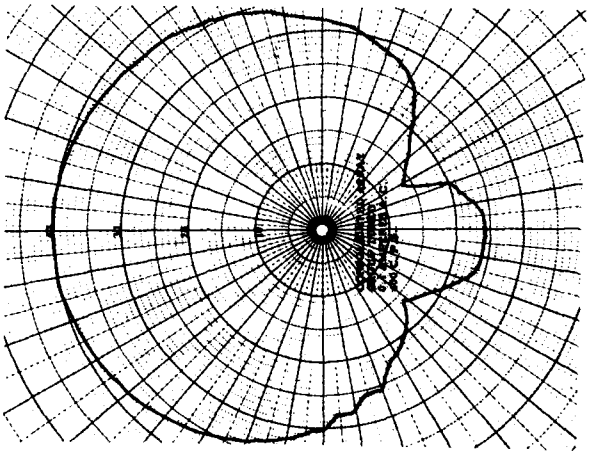

Fig. 12 - Directivity patterns of 36 element arrays at 400 cycles per second

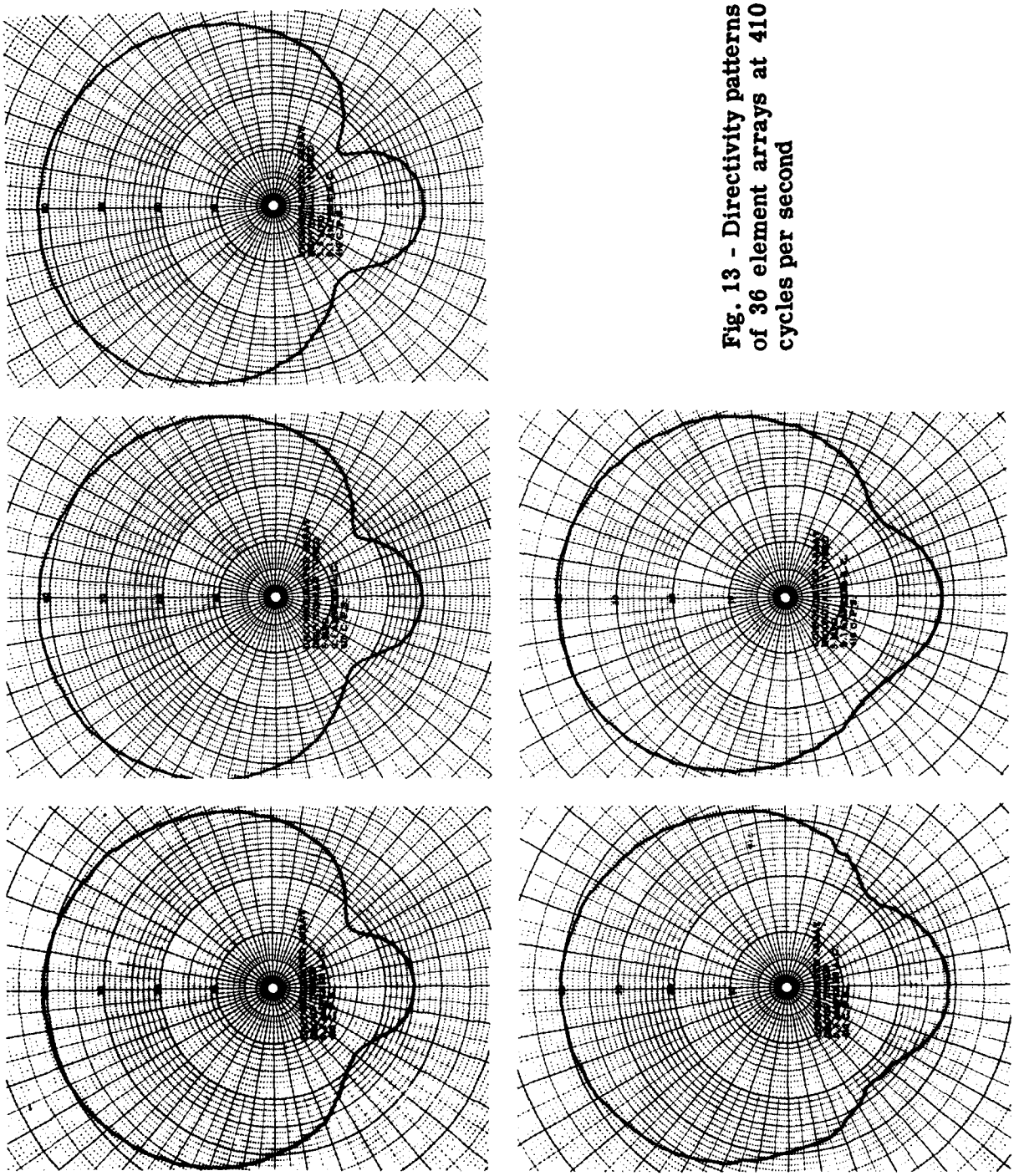

Fig. 13 - Directivity patterns of 36 element arrays at 410 cycles per second

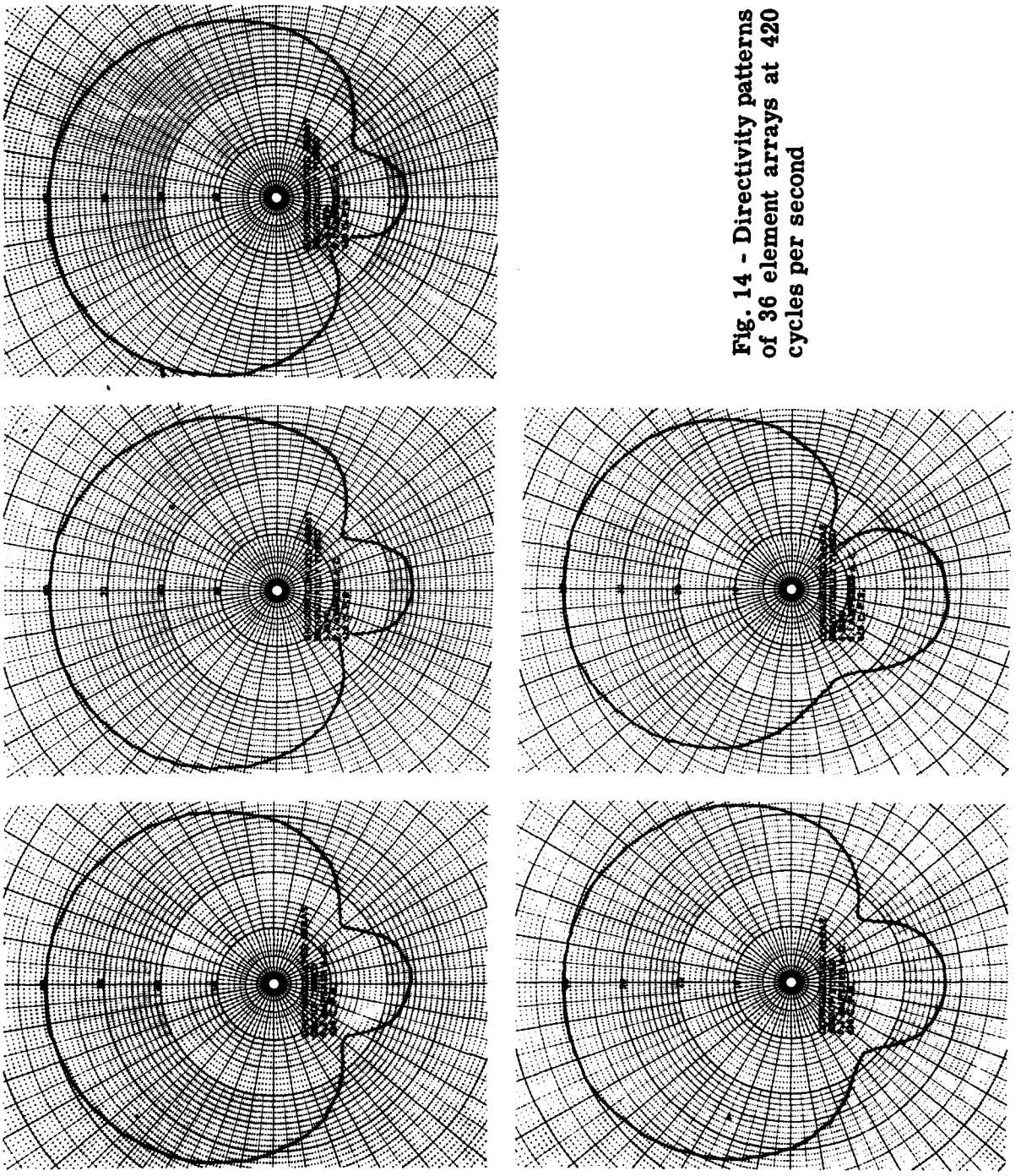

Fig. 14 - Directivity patterns of 36 element arrays at 420 cycles per second

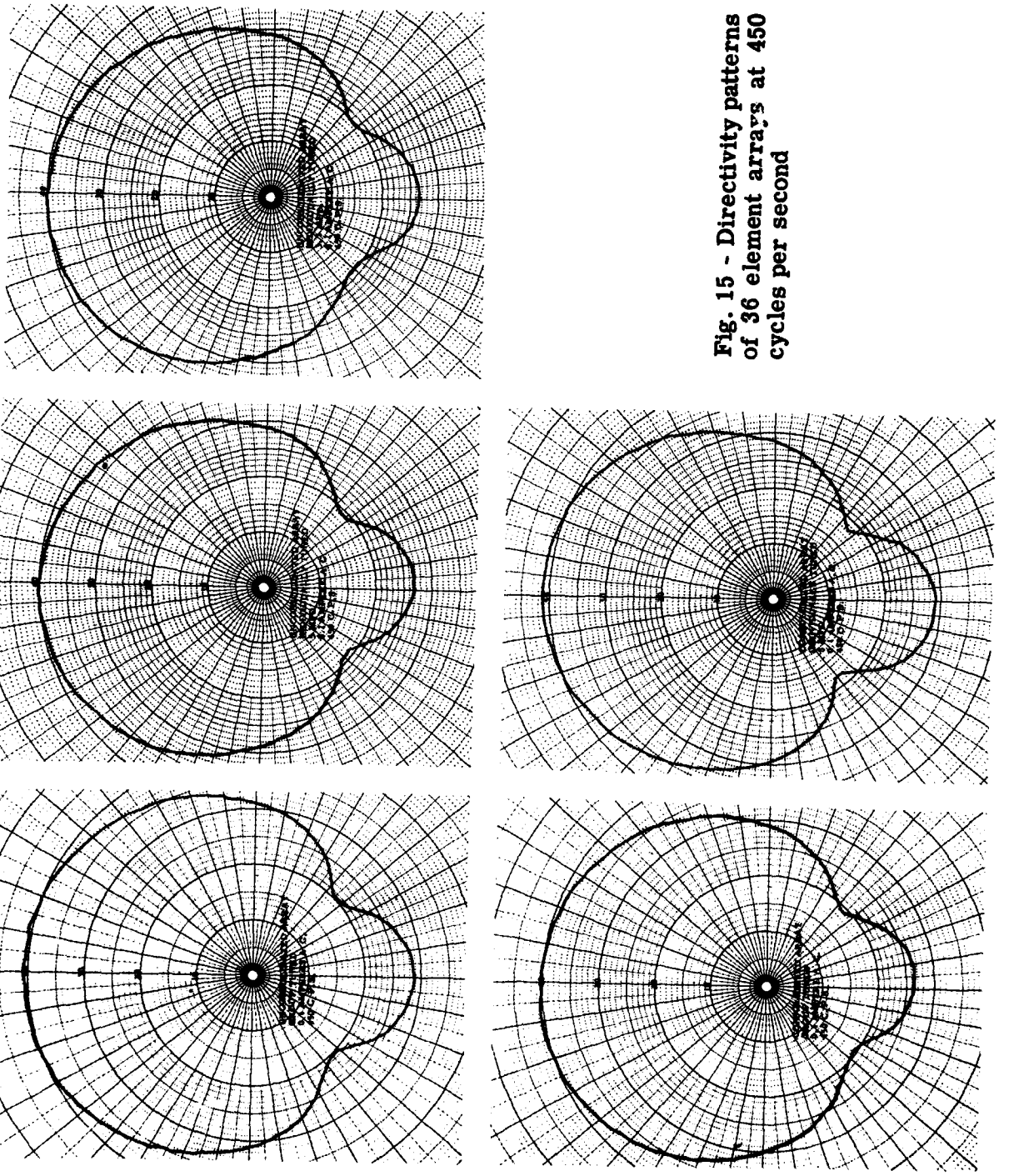

Fig. 15 - Directivity patterns of 36 element arrays at 450 cycles per second

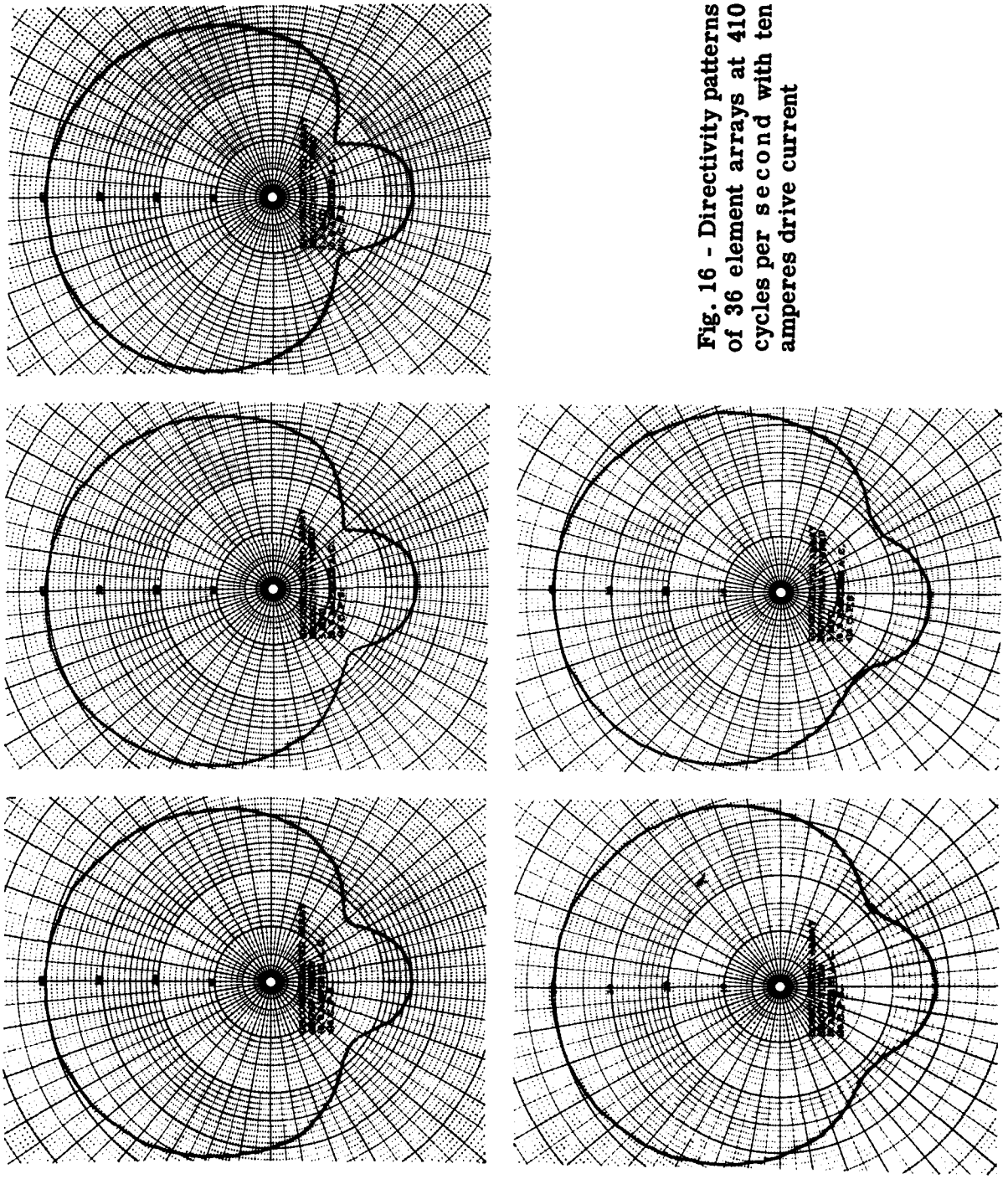

Fig. 16 - Directivity patterns of 36 element arrays at 410 cycles per second with ten amperes drive current

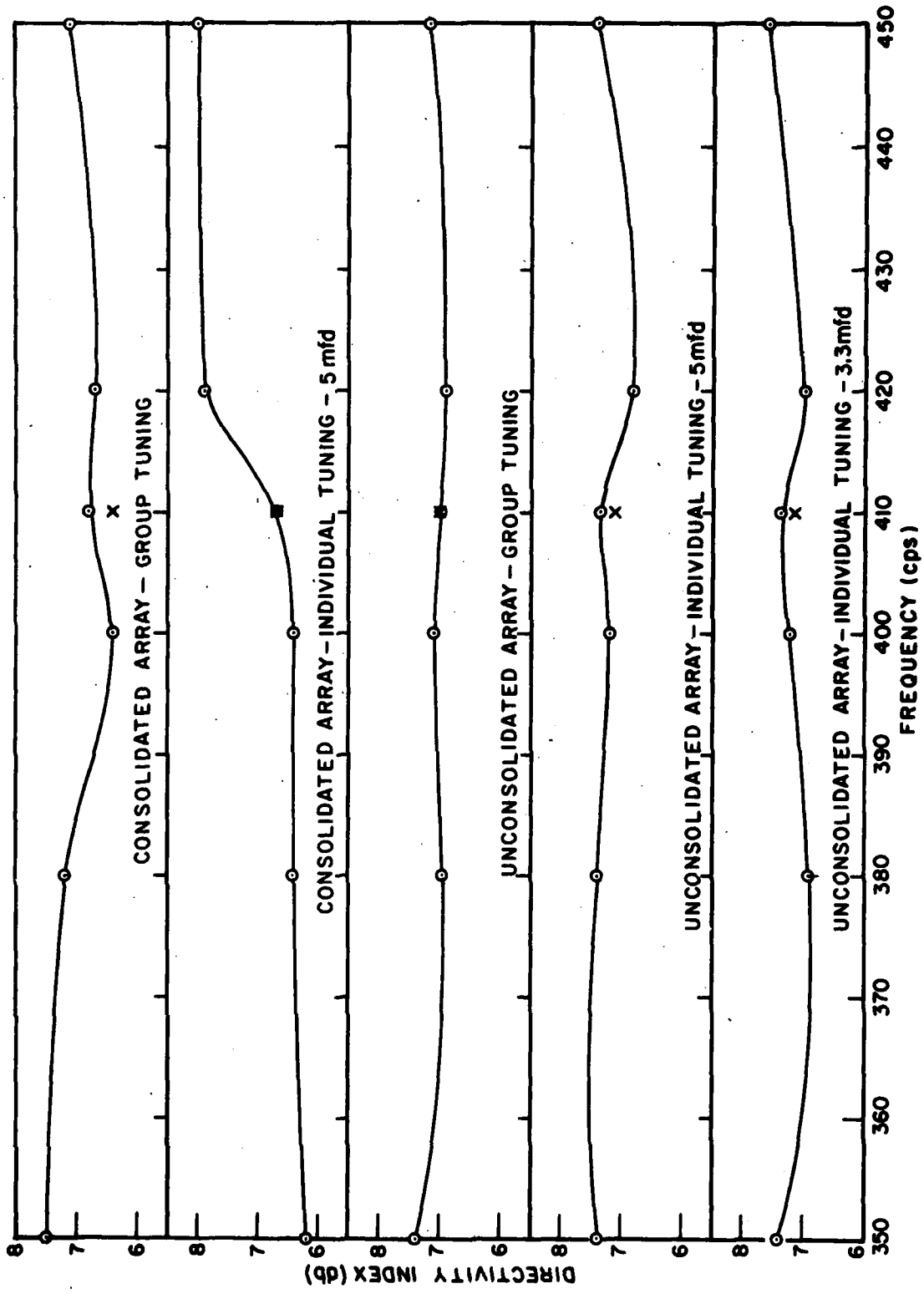

Fig. 17 - Directivity indices for 36 element arrays

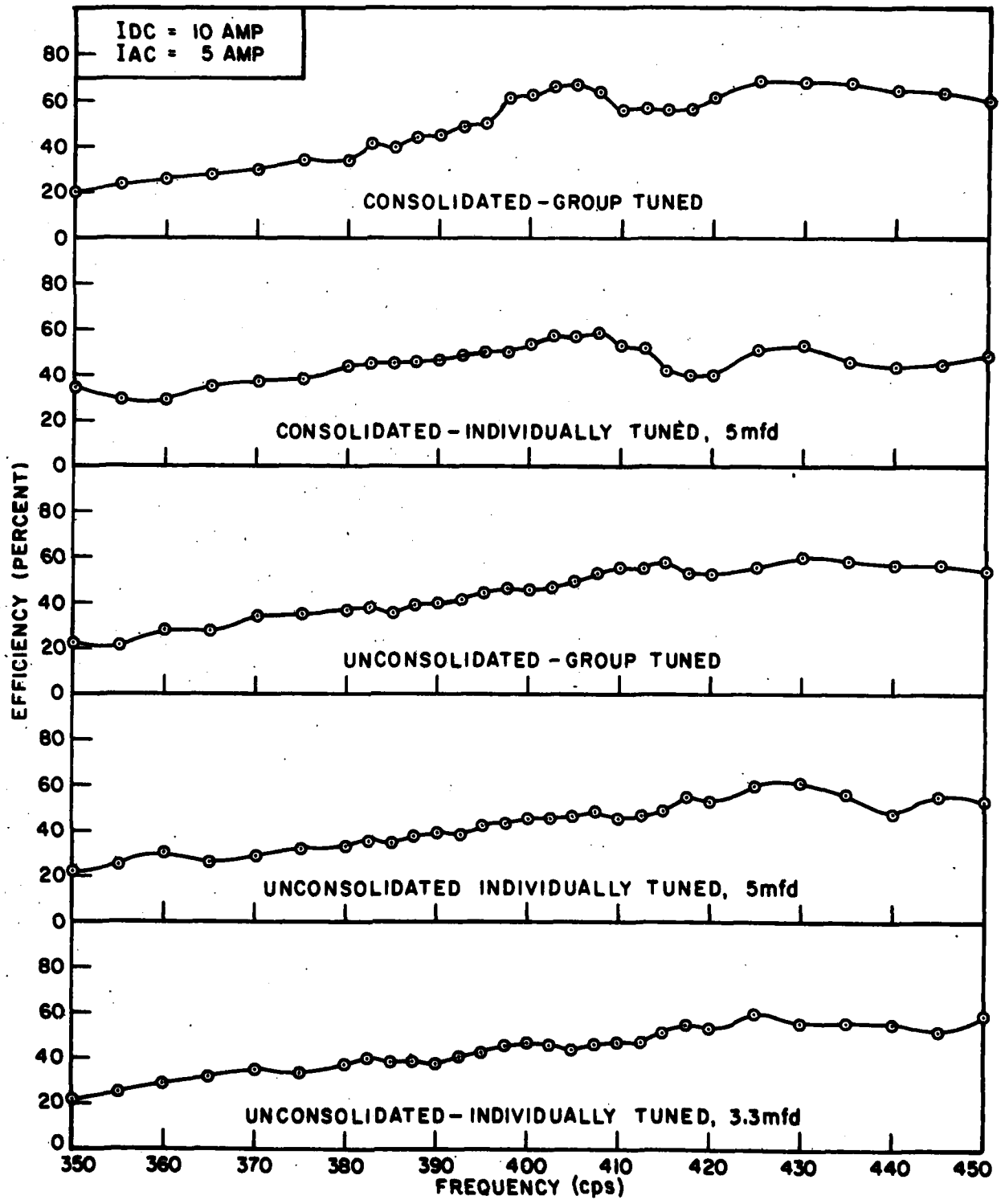

Fig. 18 - Electroacoustic efficiencies of the 36 element arrays

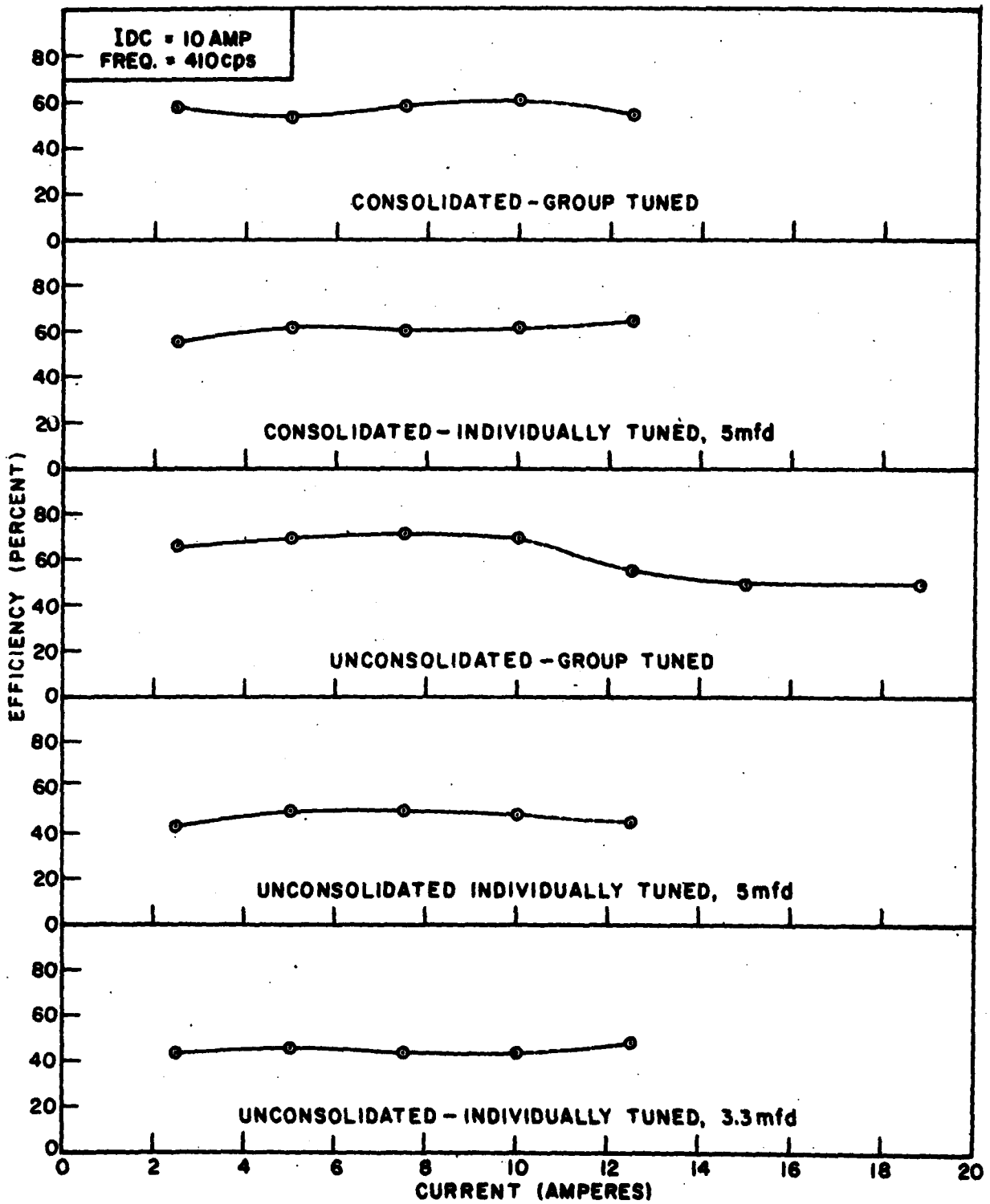

Fig. 19 - Dependence of efficiency on acoustic power

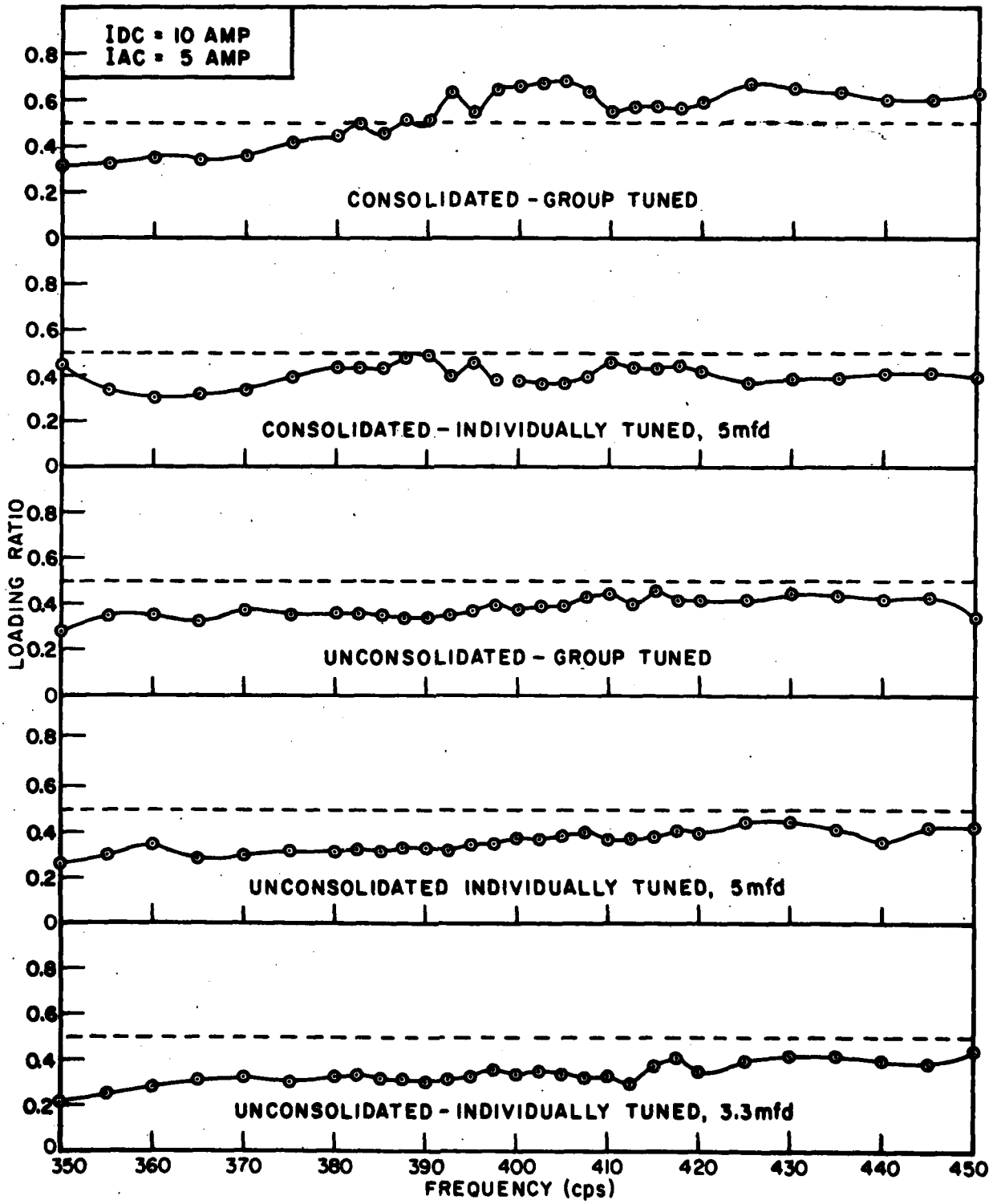

Fig. 20 - Computed loading ratios for the 36 element arrays

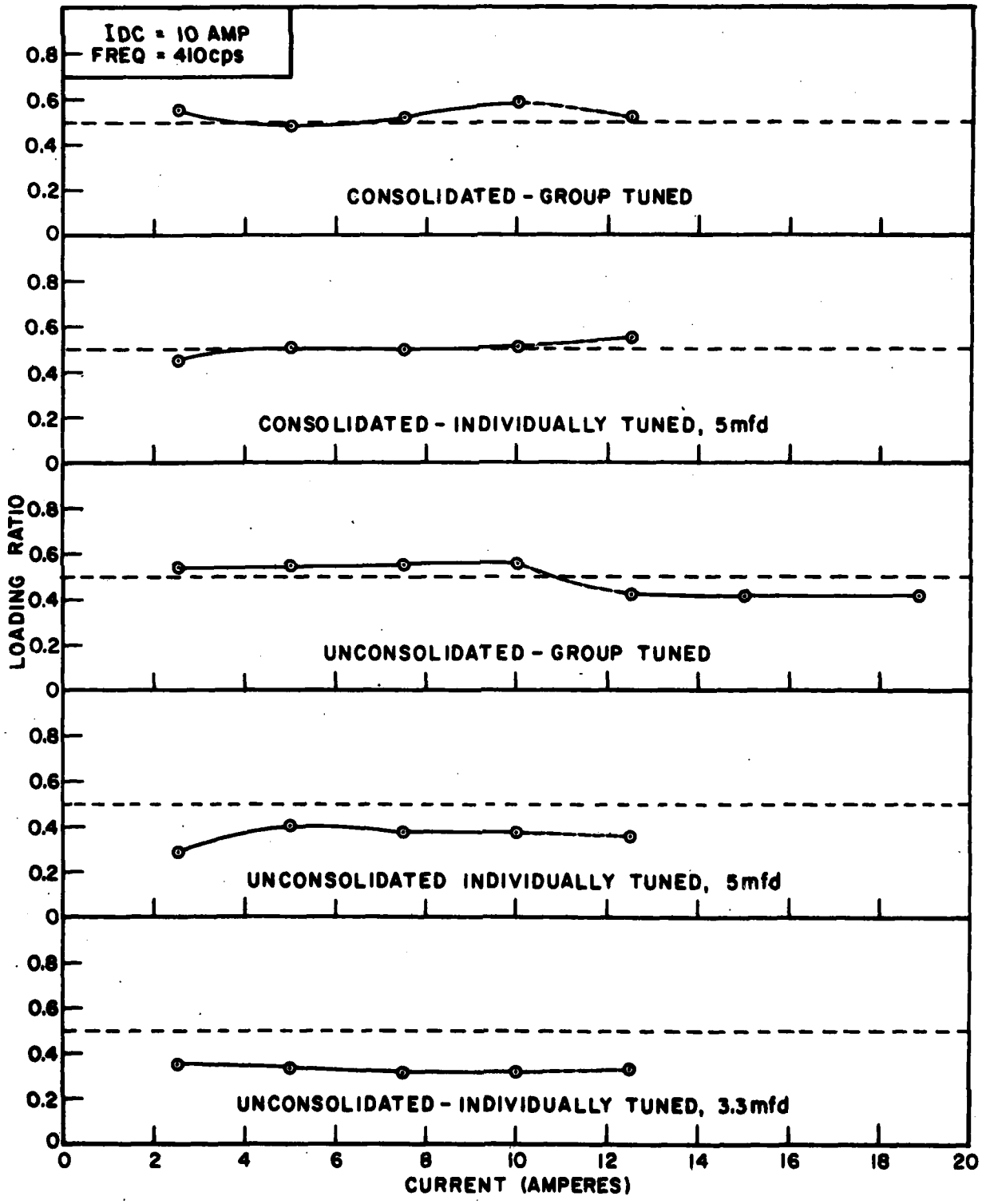

Fig. 21 - Power dependence of loading ratio for the 36 element array

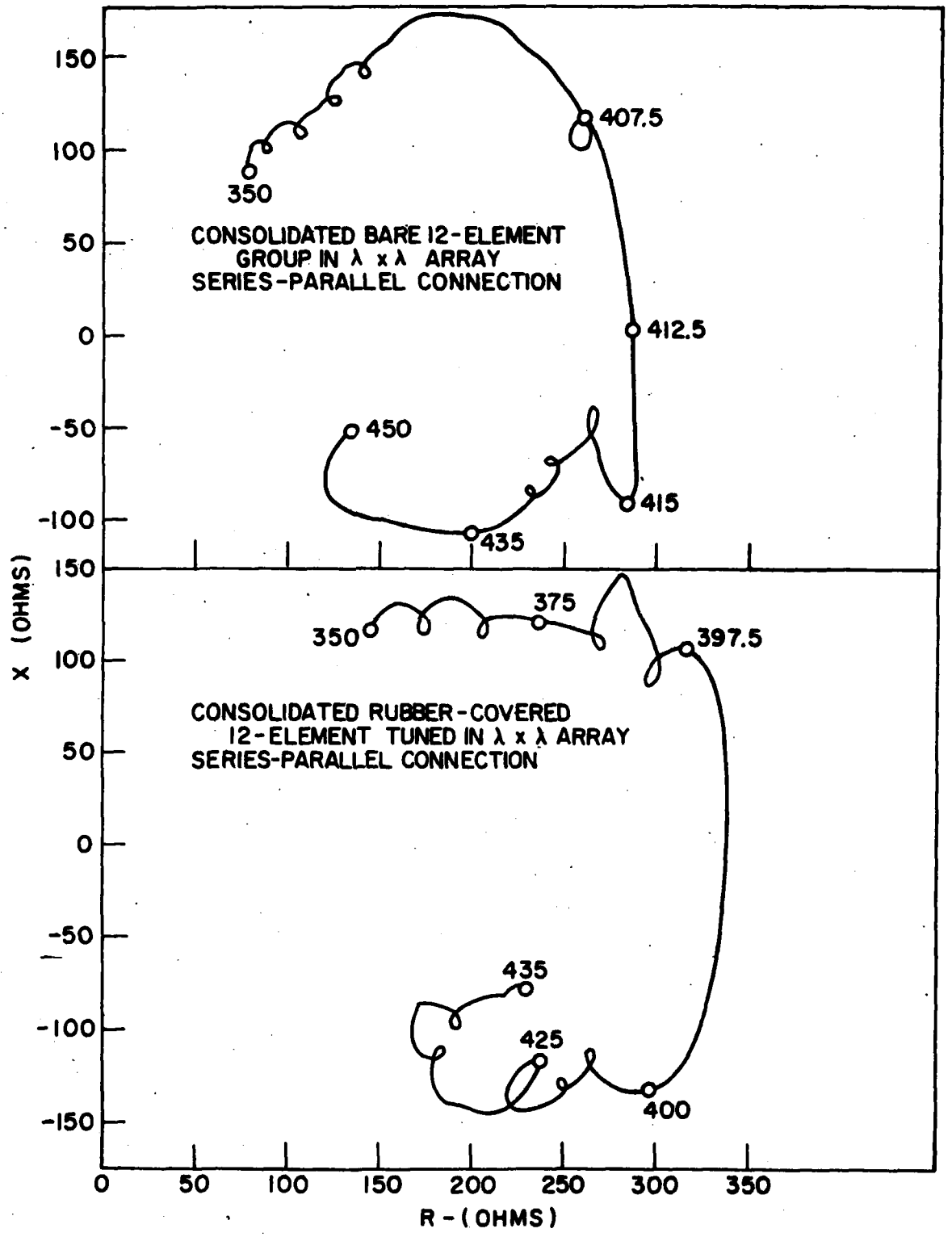

Fig. 22 - Vector impedance loci

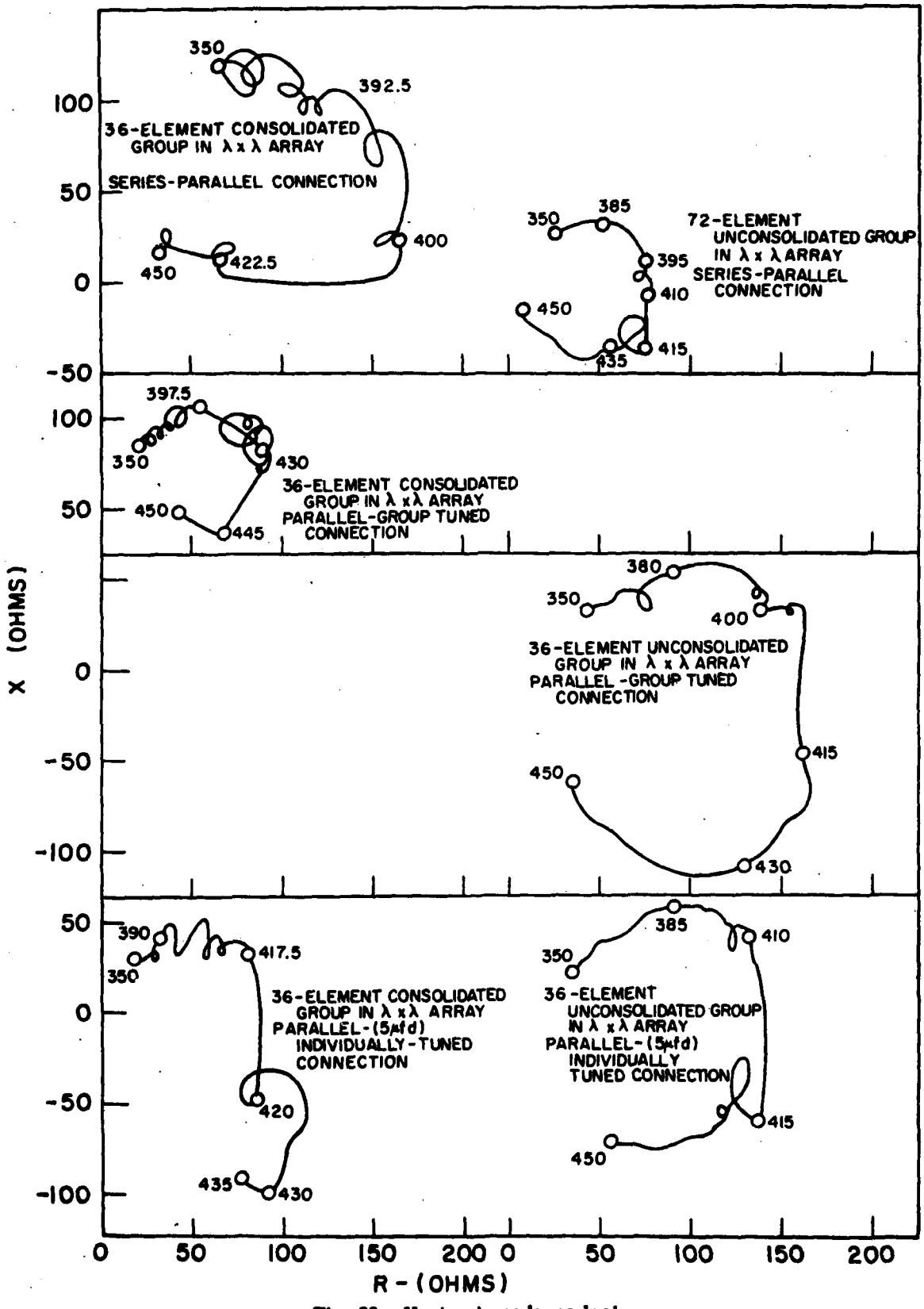

Fig. 23 - Vector impedance loci

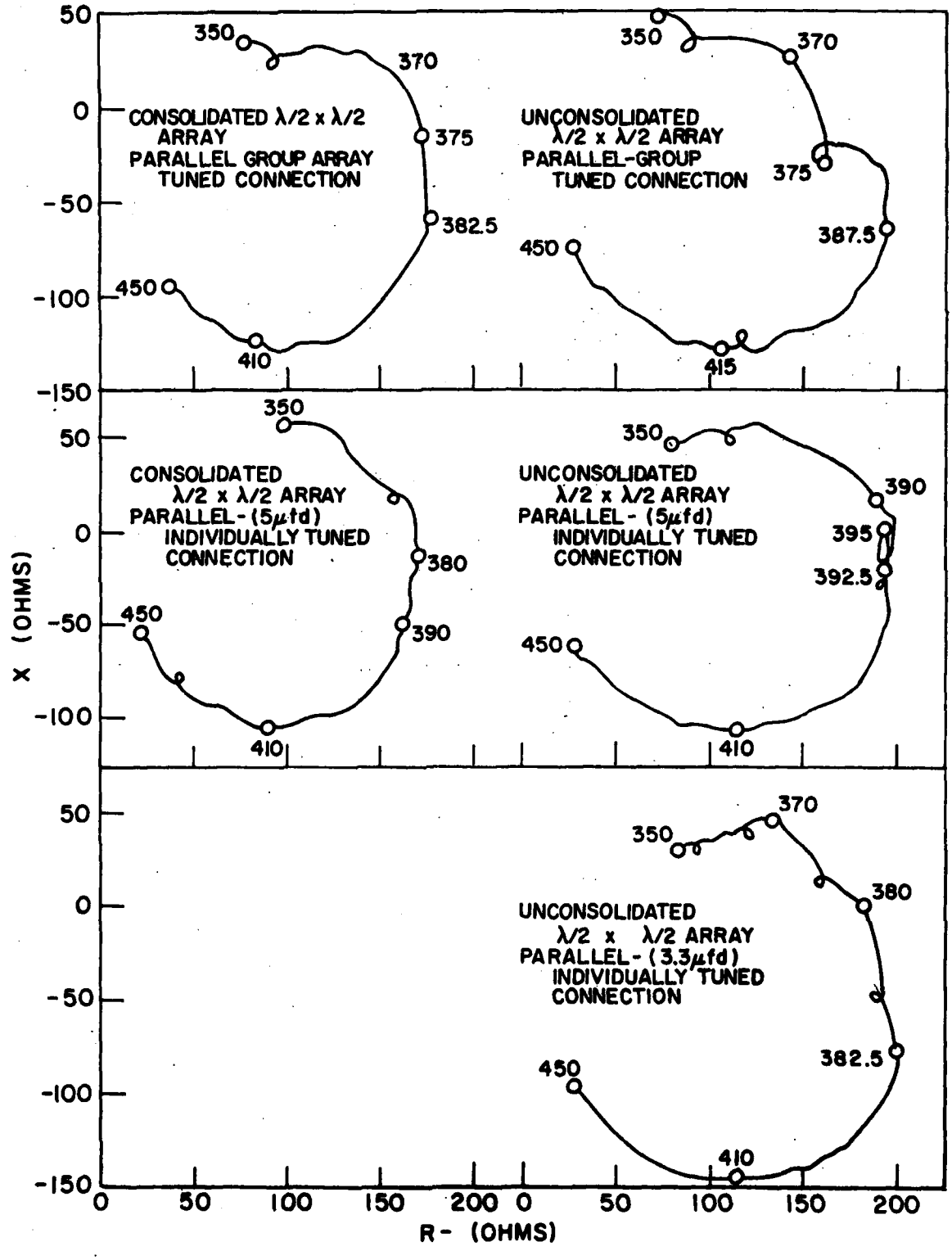

Fig. 24 - Vector impedance loci

CONFIDENTIAL

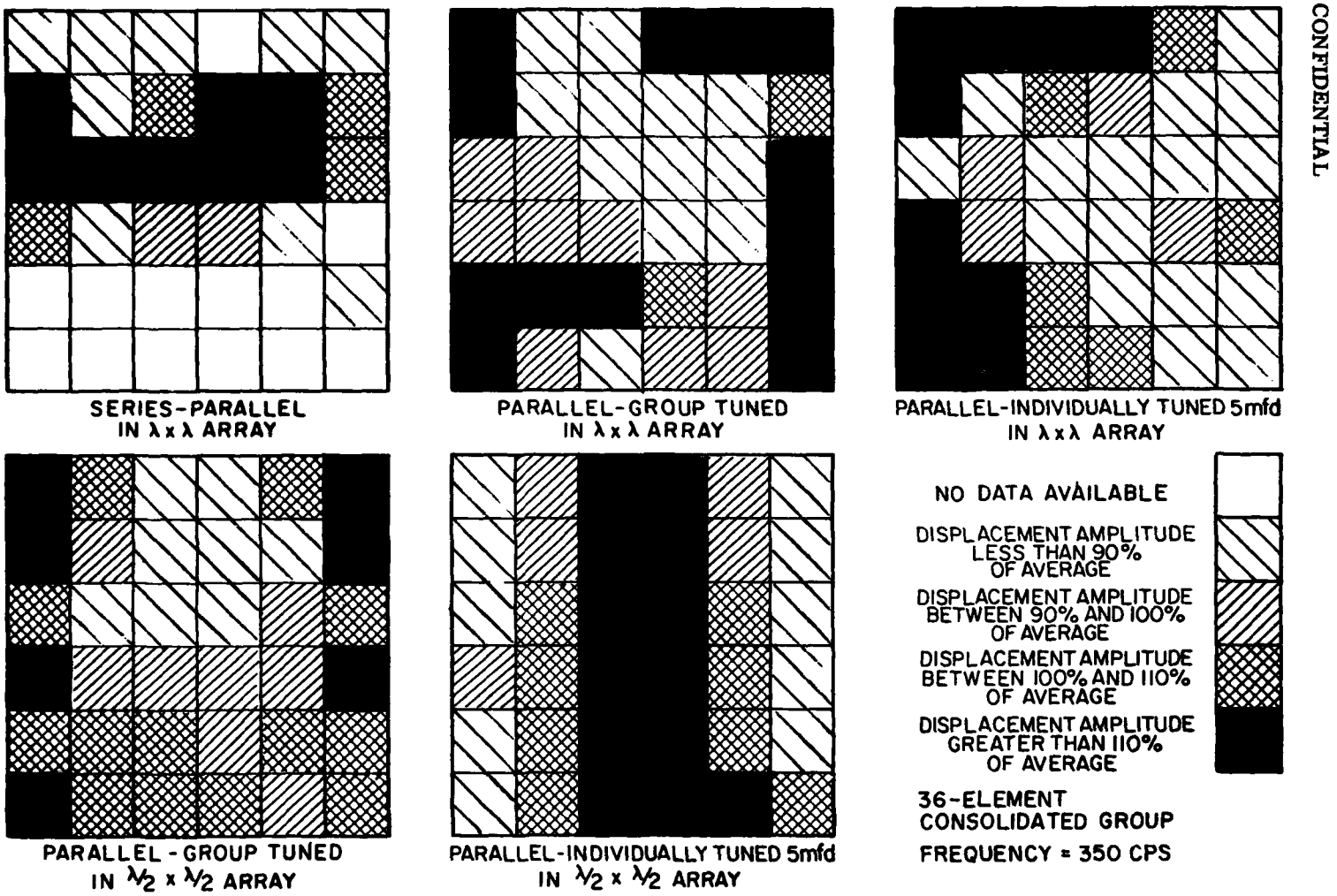

Fig. 25 - Displacement amplitude distribution over array face

CONFIDENTIAL

CONFIDENTIAL

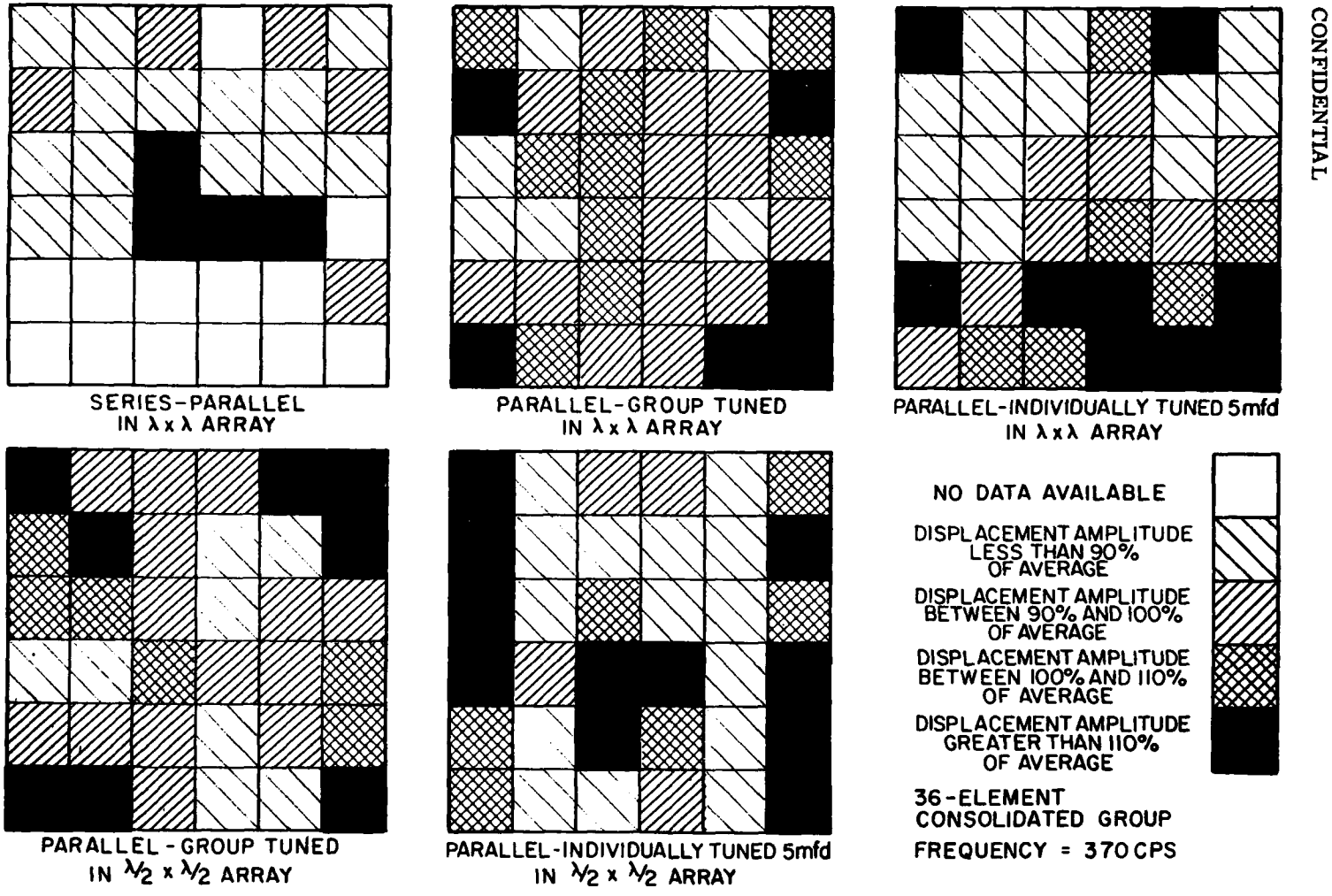

Fig. 26 - Displacement amplitude distribution over array face

CONFIDENTIAL

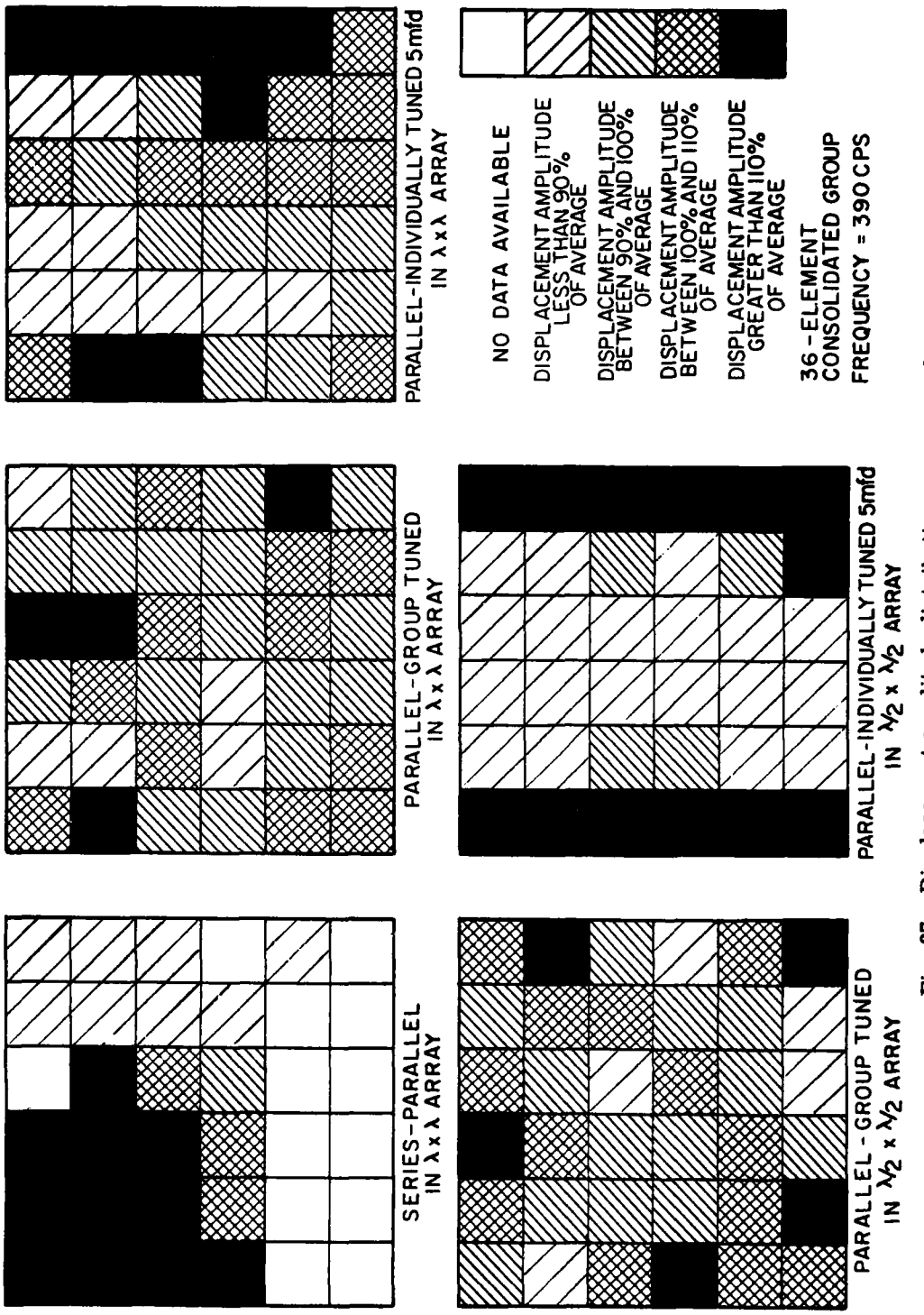

Fig. 27 - Displacement amplitude distribution over array face

CONFIDENTIAL

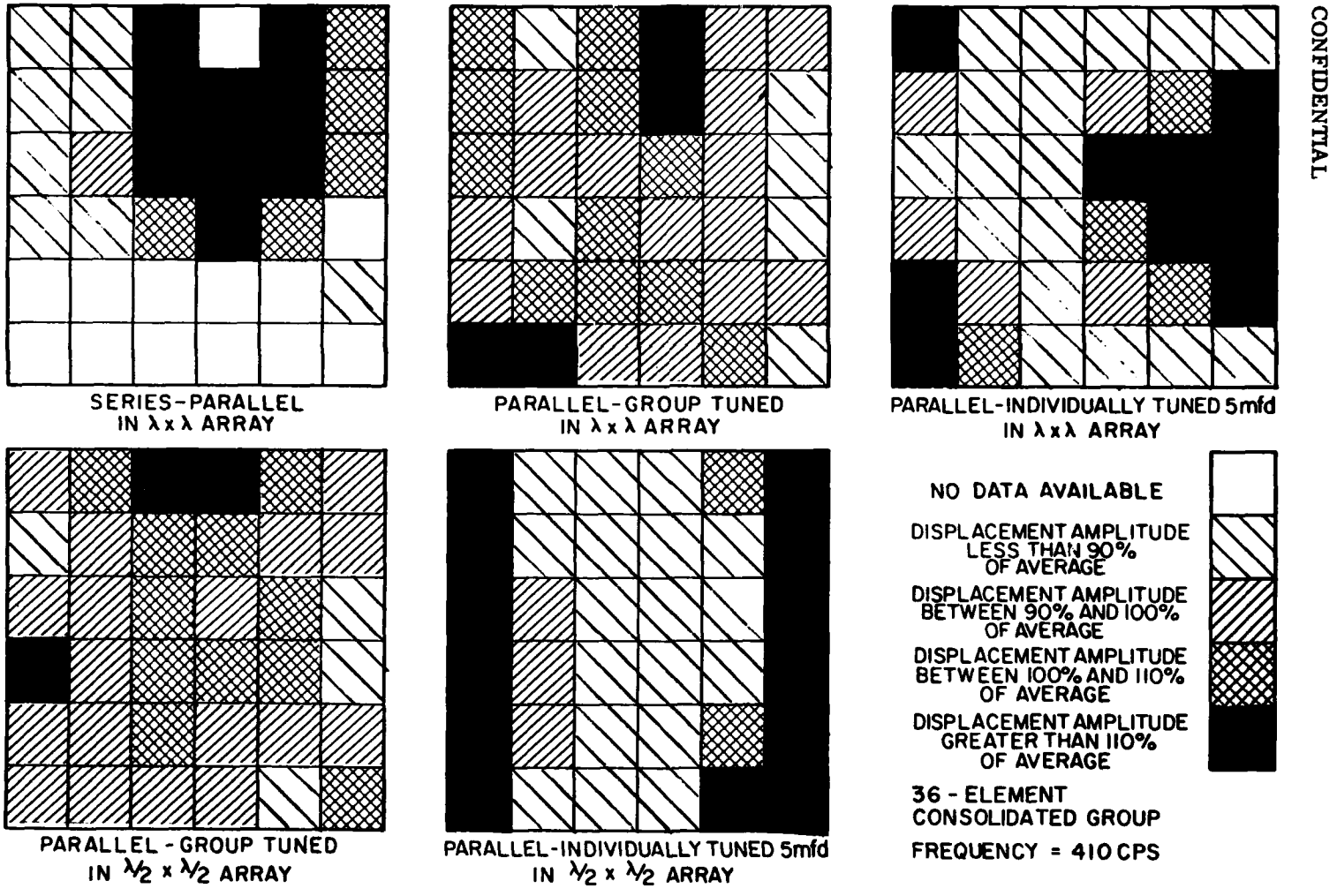

Fig. 28 - Displacement amplitude distribution over array face

CONFIDENTIAL

CONFIDENTIAL

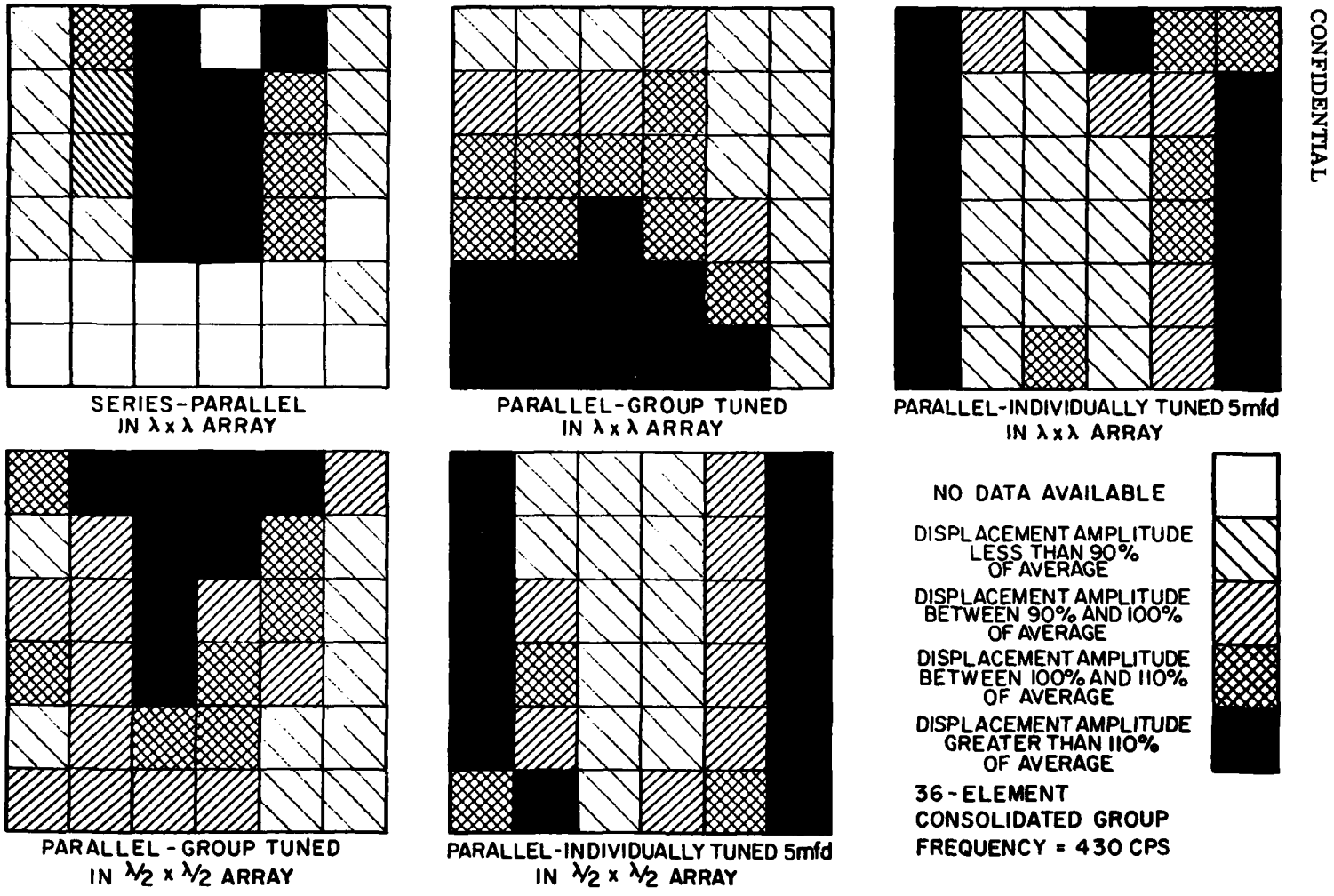

Fig. 29 - Displacement amplitude distribution over array face

CONFIDENTIAL

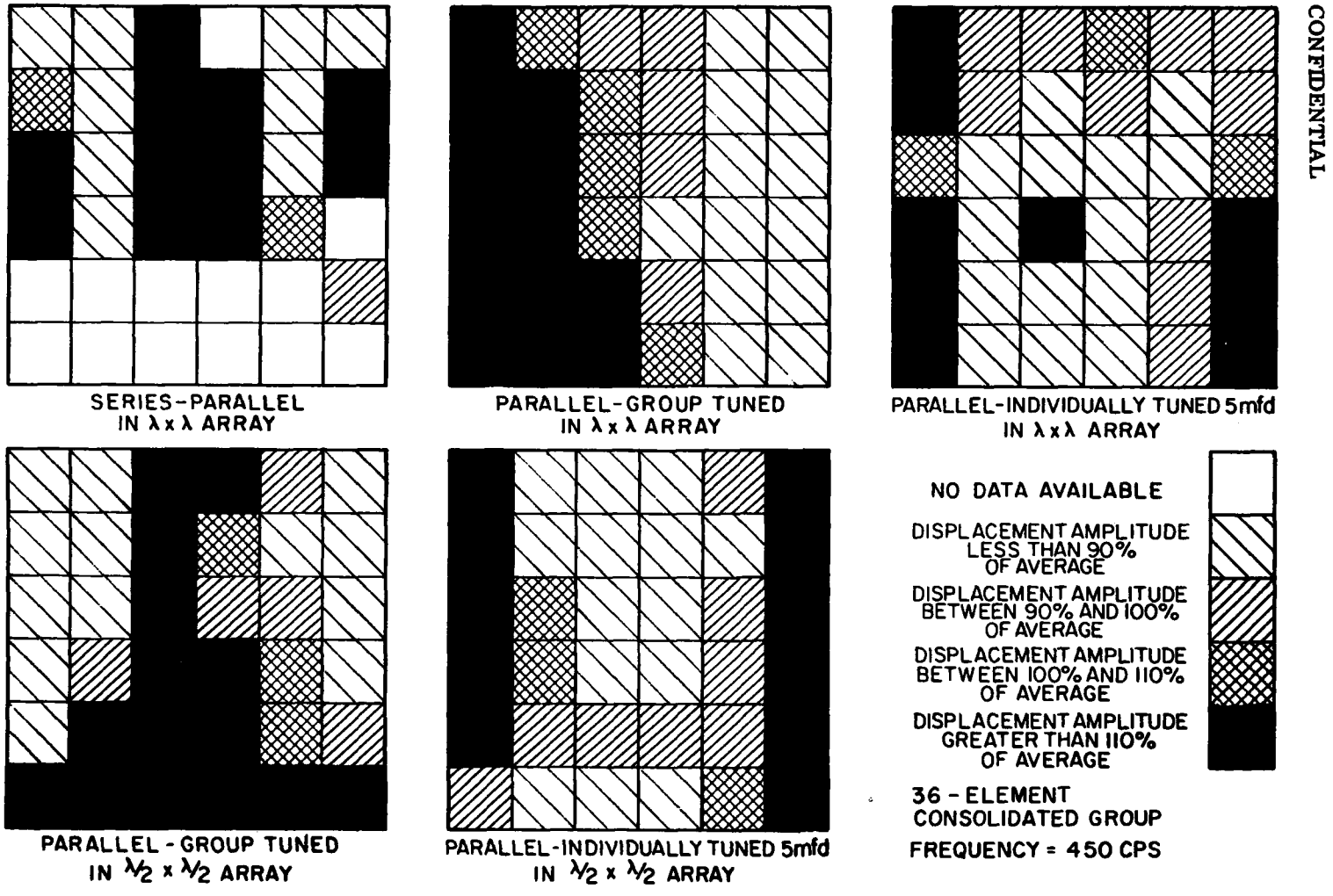

Fig. 30 - Displacement amplitude distribution over array face

CONFIDENTIAL

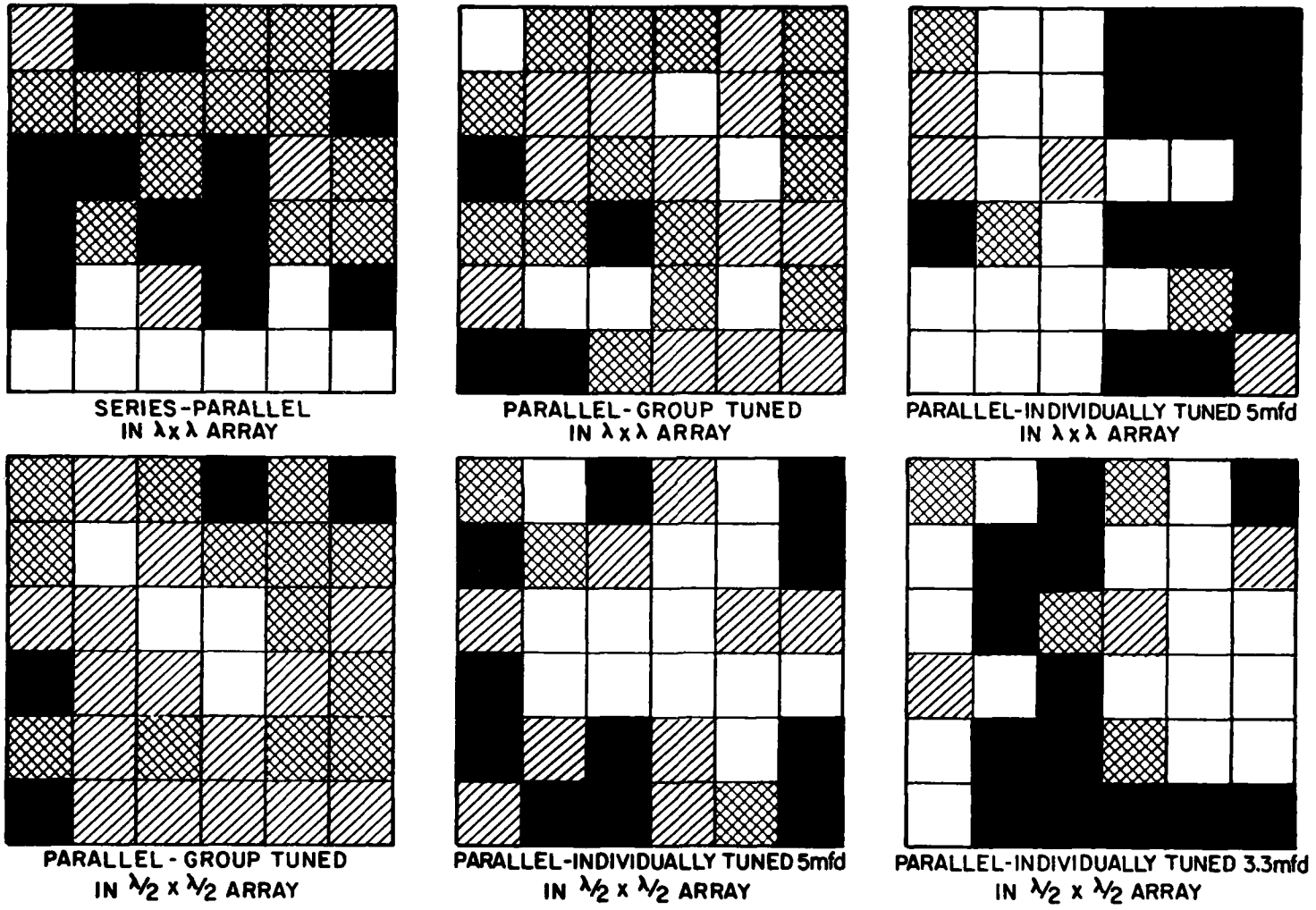

Fig. 31 - Displacement amplitude distribution over array face

CONFIDENTIAL

CONFIDENTIAL

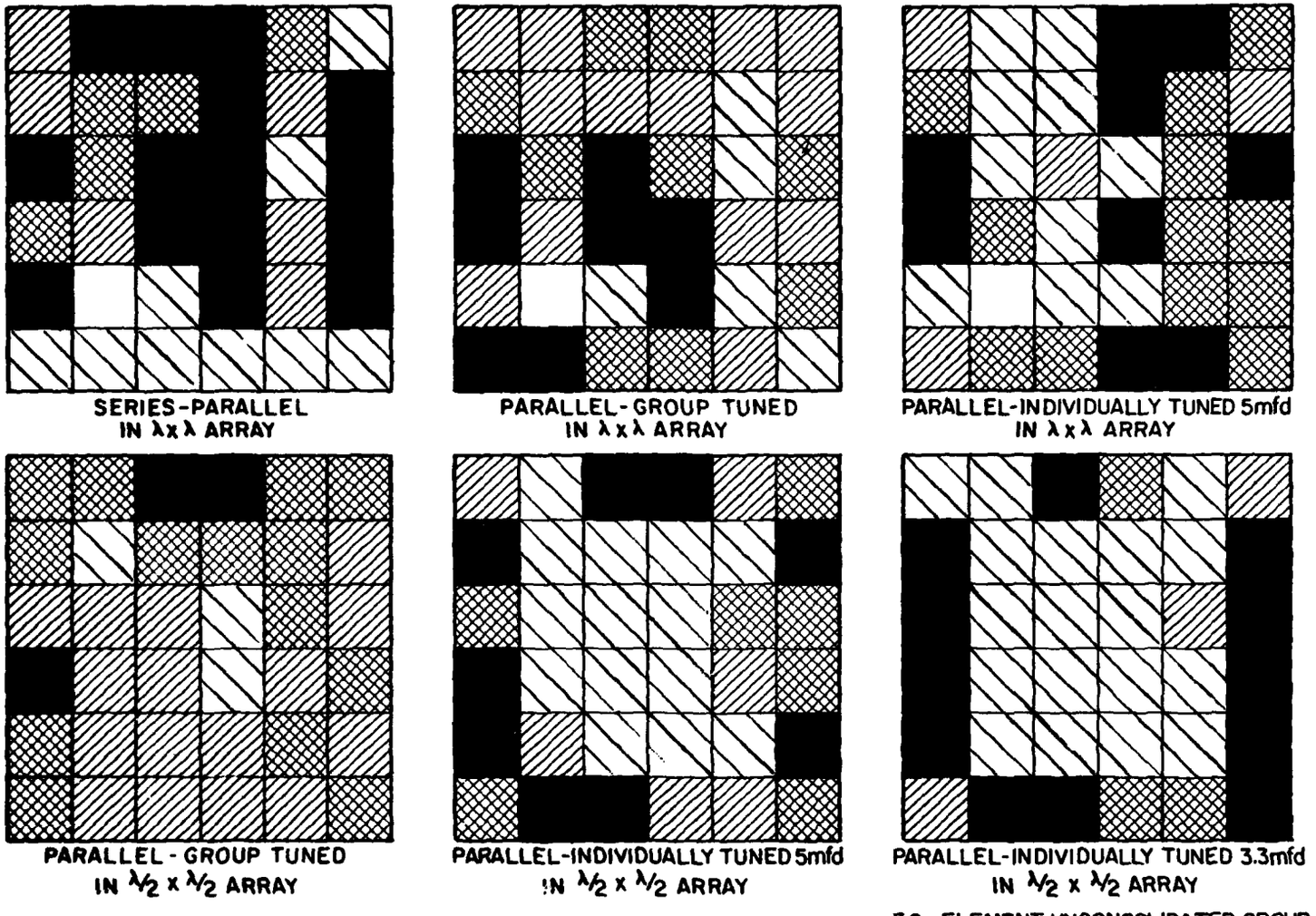

Fig. 32 - Displacement amplitude distribution over array face

CONFIDENTIAL

CONFIDENTIAL

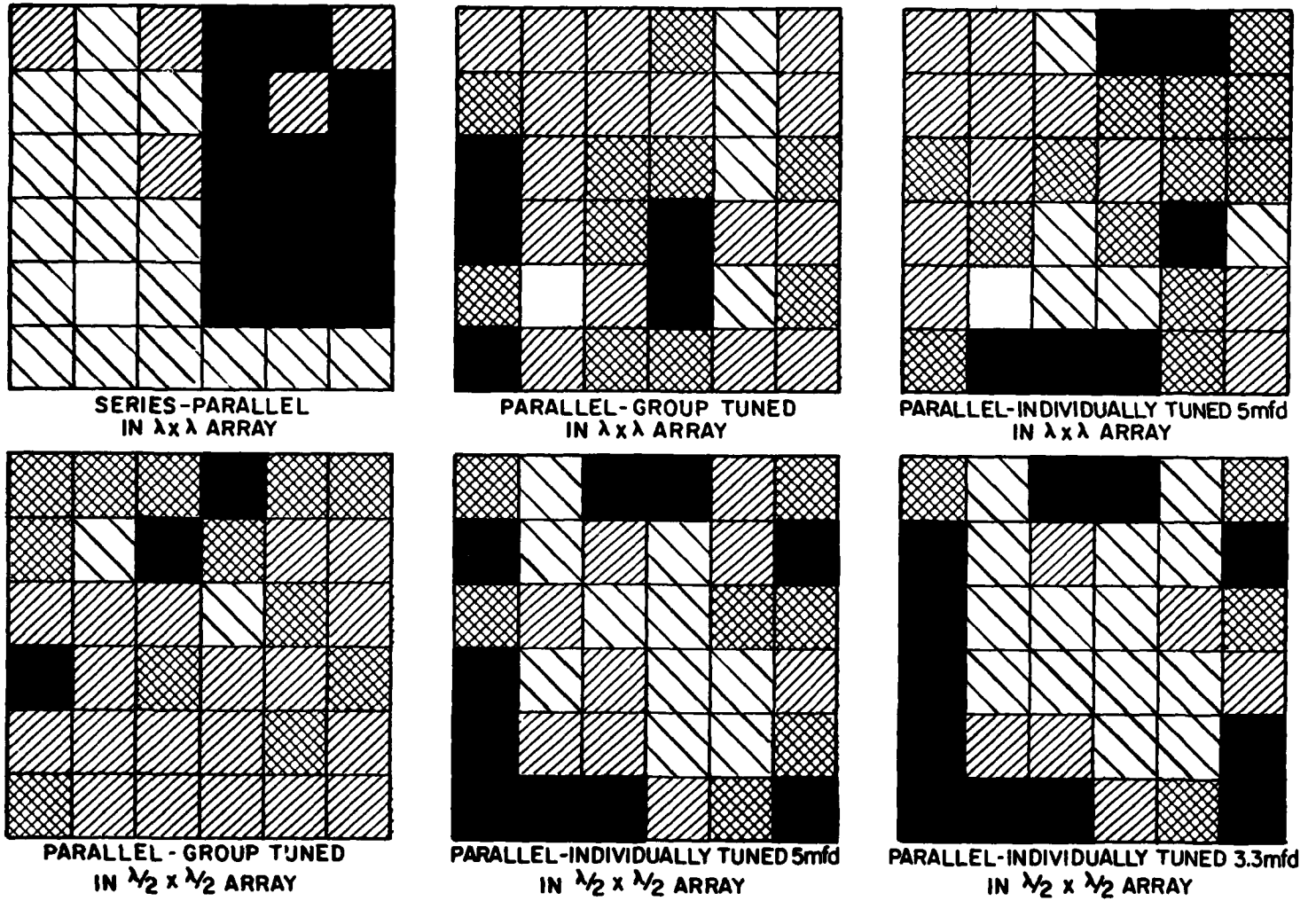

Fig. 33 - Displacement amplitude distribution over array face

CONFIDENTIAL

CONFIDENTIAL

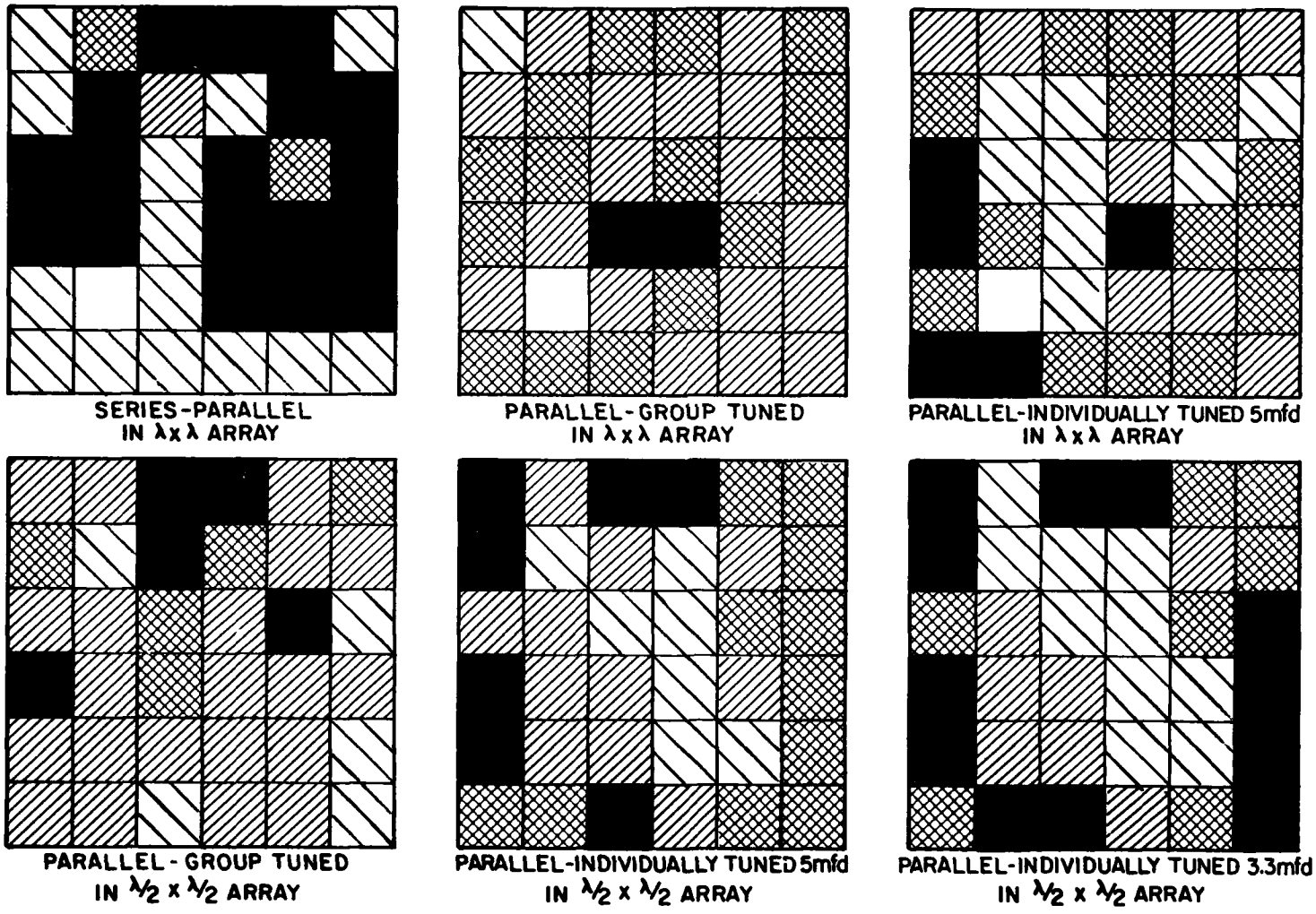

Fig. 34 - Displacement amplitude distribution over array face

CONFIDENTIAL

CONFIDENTIAL

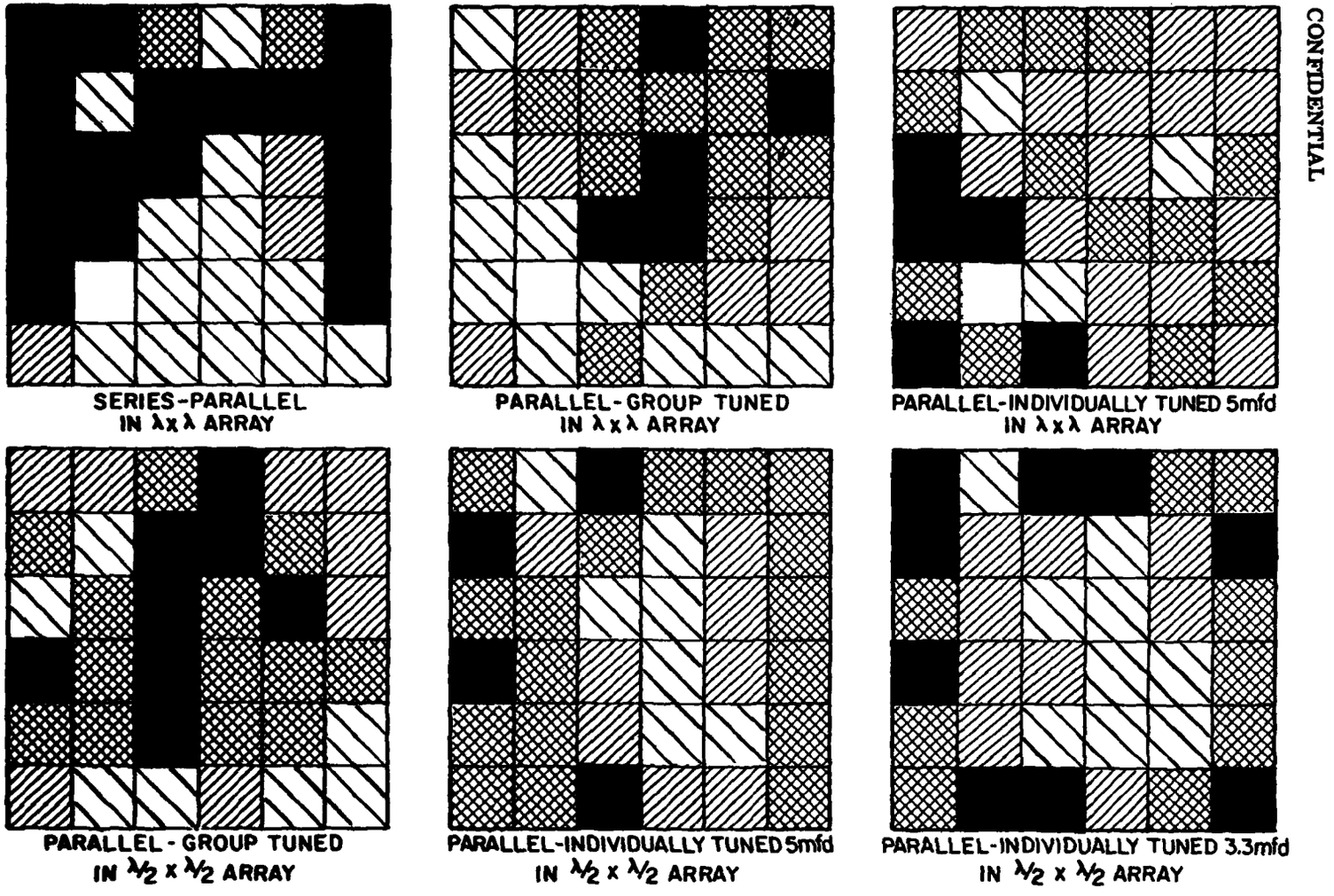

Fig. 35 - Displacement amplitude distribution over array face

CONFIDENTIAL

CONFIDENTIAL

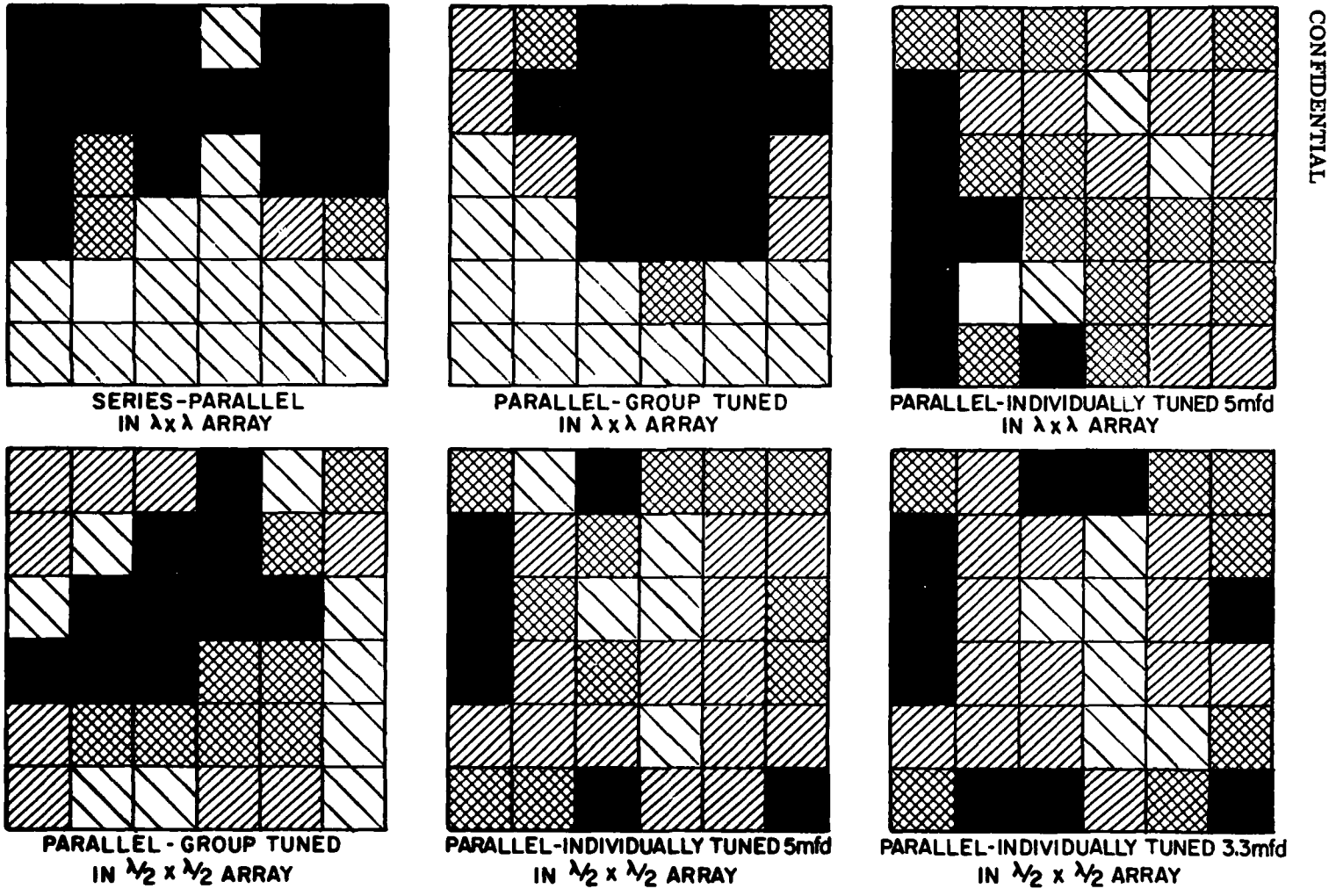

Fig. 36 - Displacement amplitude distribution over array face

CONFIDENTIAL

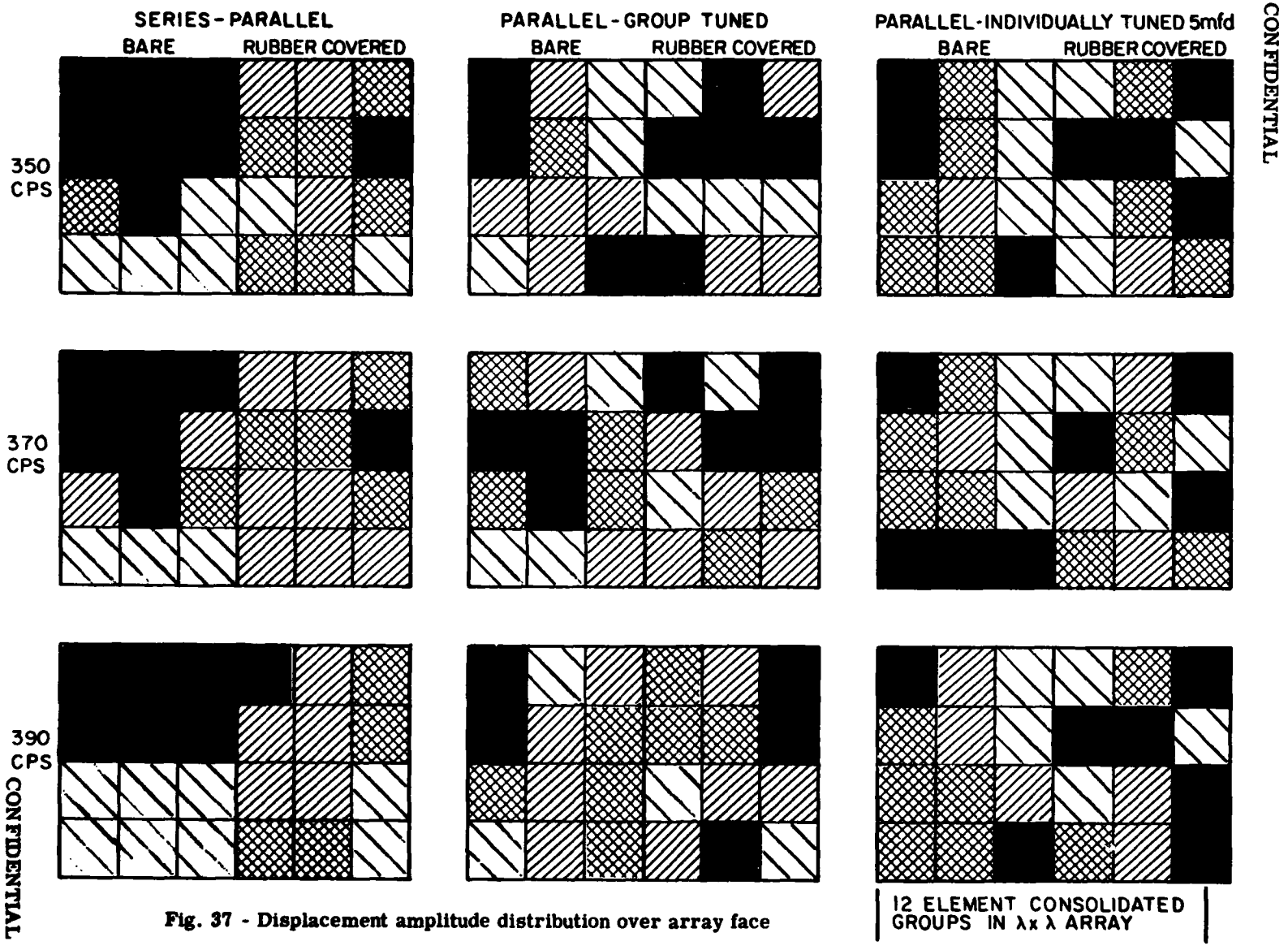

Fig. 37 - Displacement amplitude distribution over array face

CONFIDENTIAL

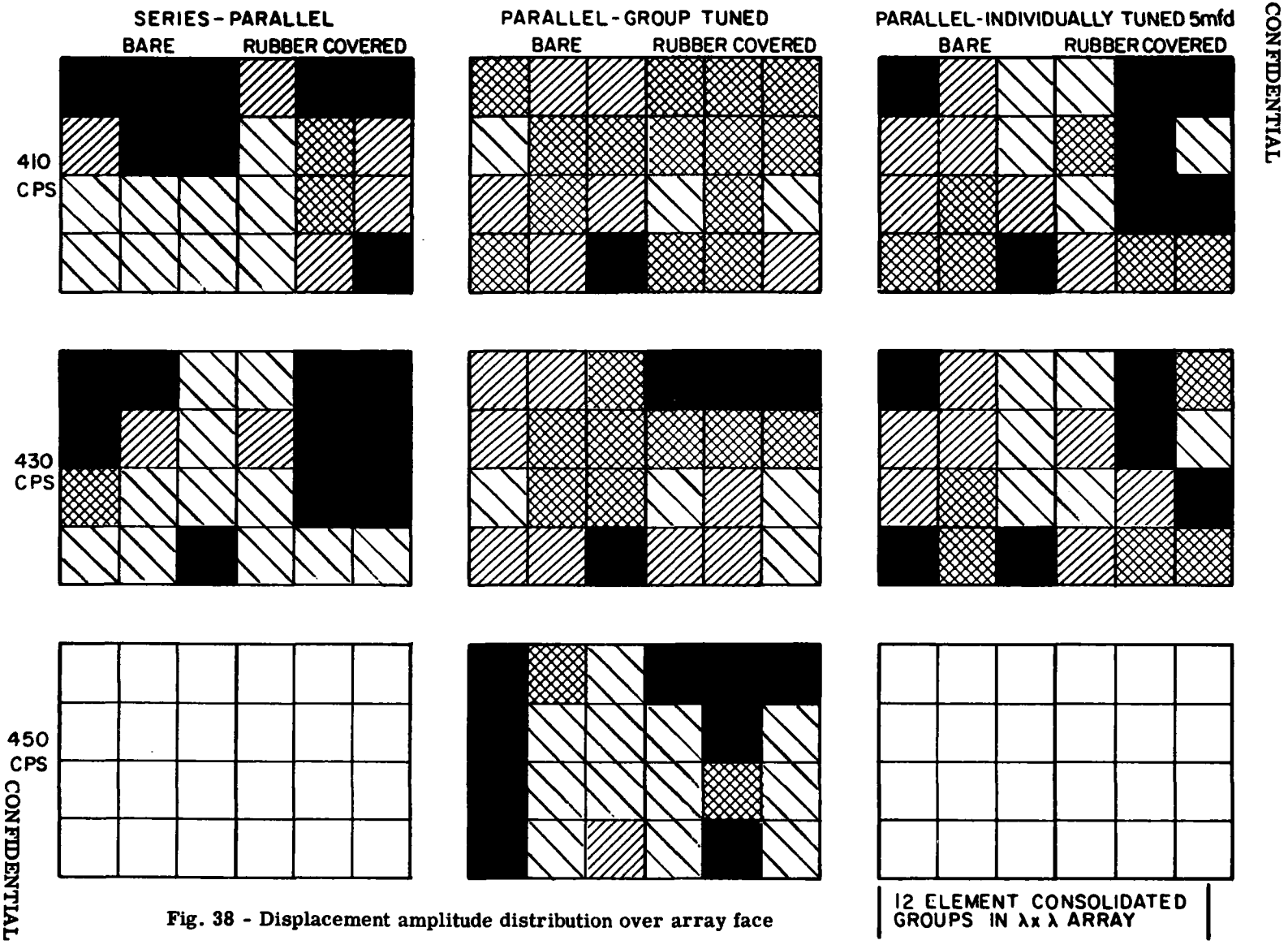

Fig. 38 - Displacement amplitude distribution over array face

CONFIDENTIAL

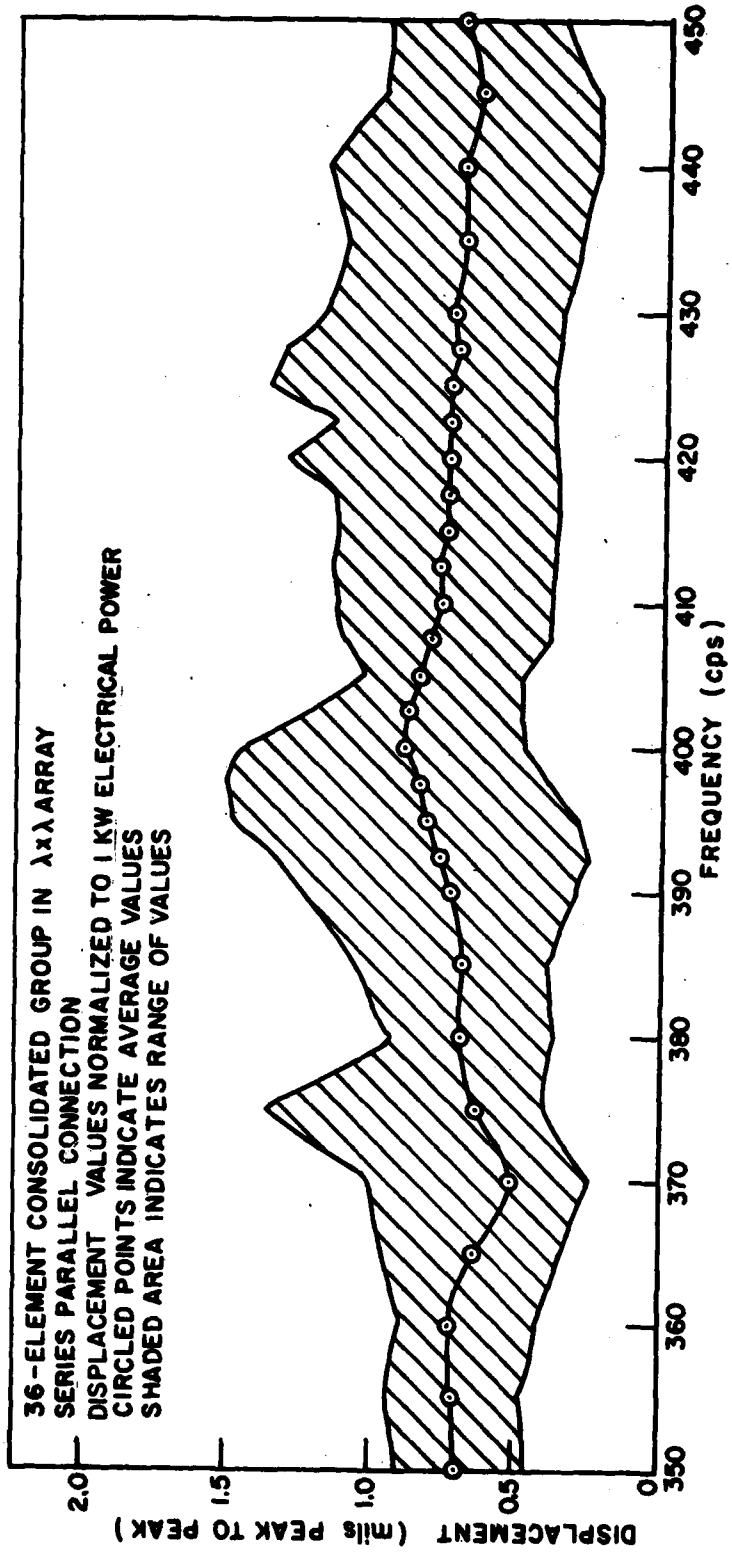

Fig. 39 - Average displacement of outer masses

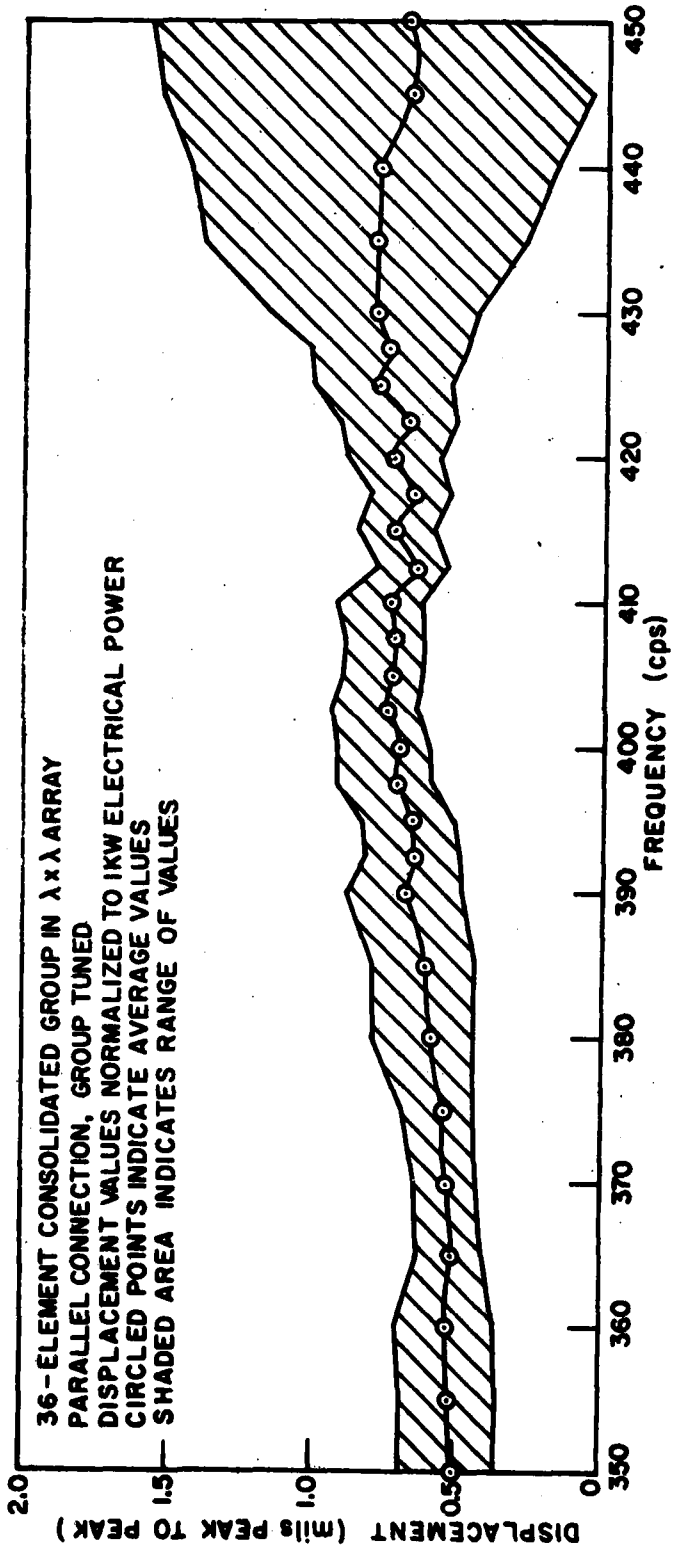

Fig. 40 - Average displacement of outer masses

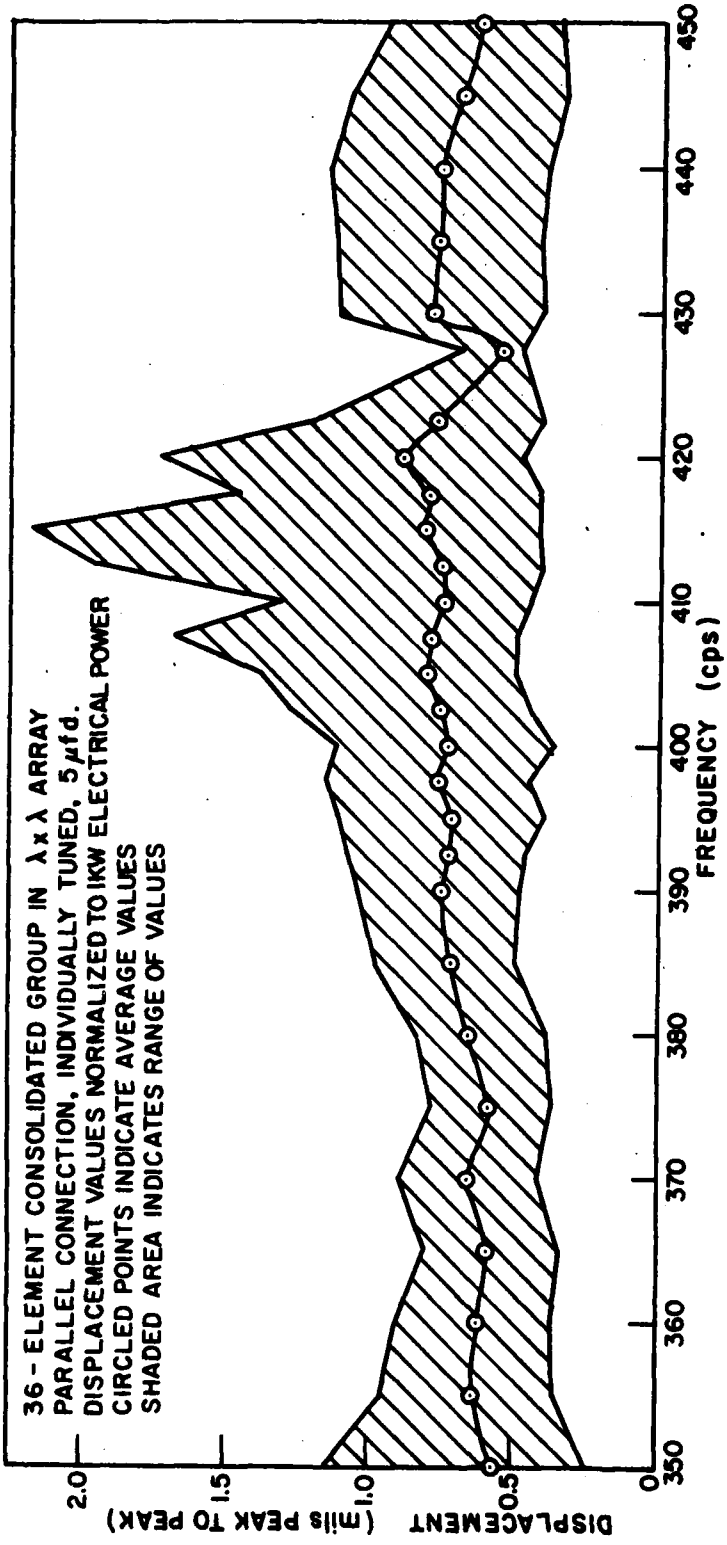

Fig. 41 - Average displacement of outer masses

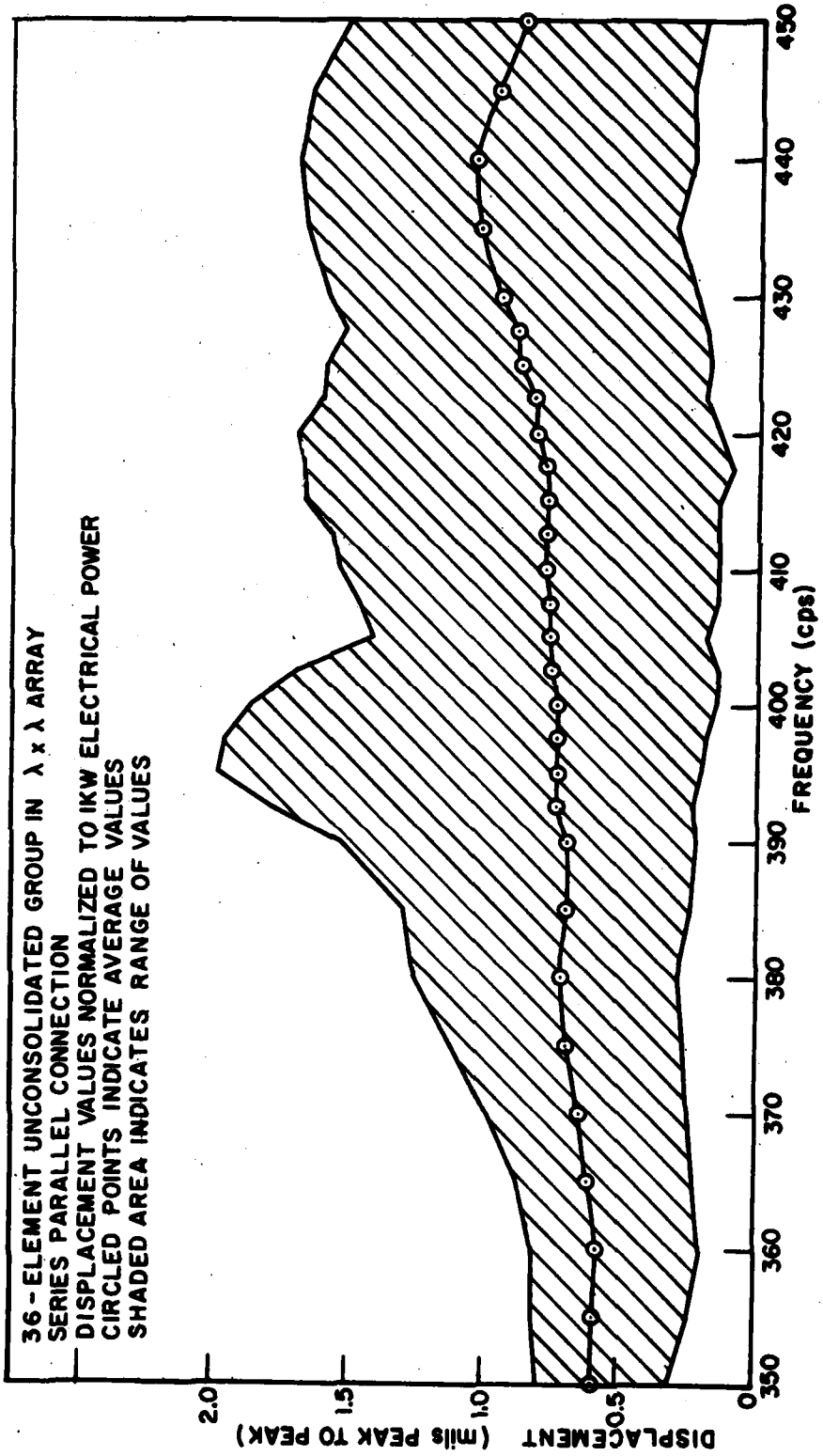

Fig. 42 - Average displacement of outer masses

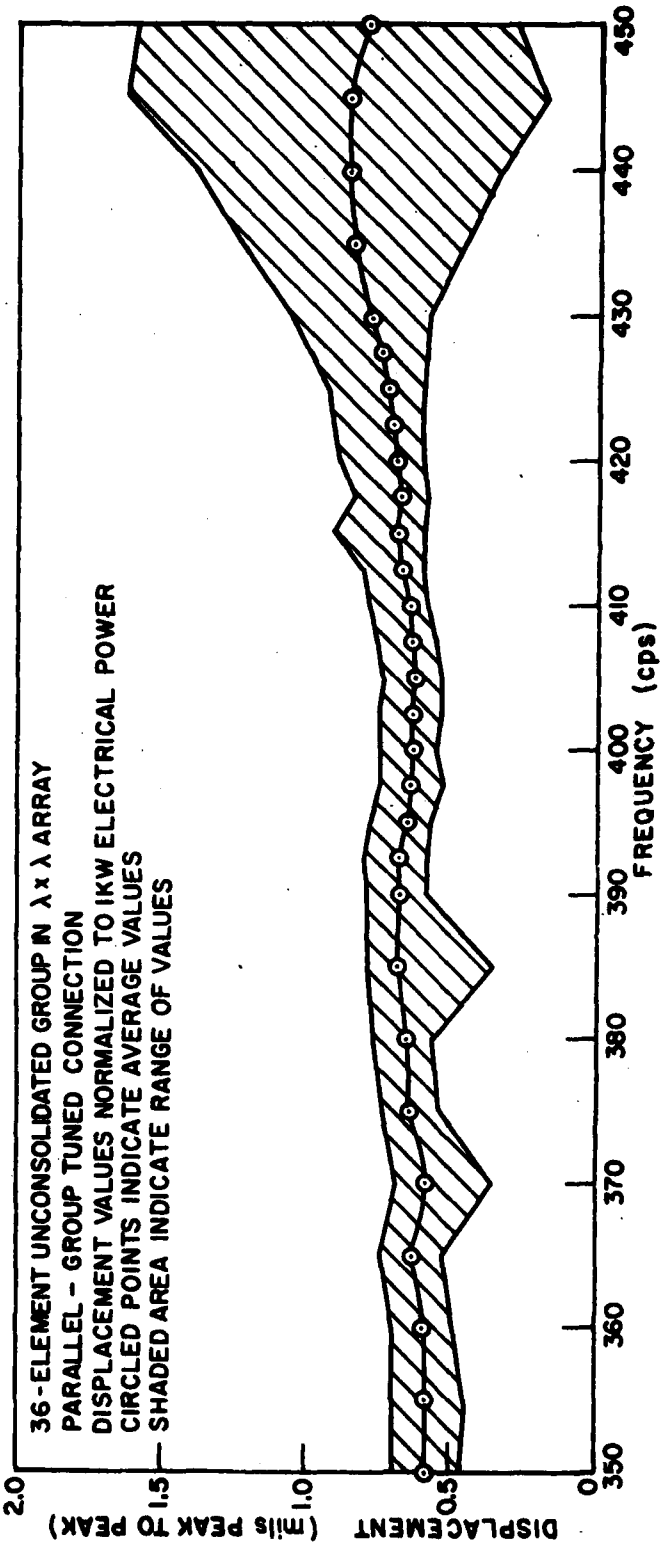

Fig. 43 - Average displacement of outer masses

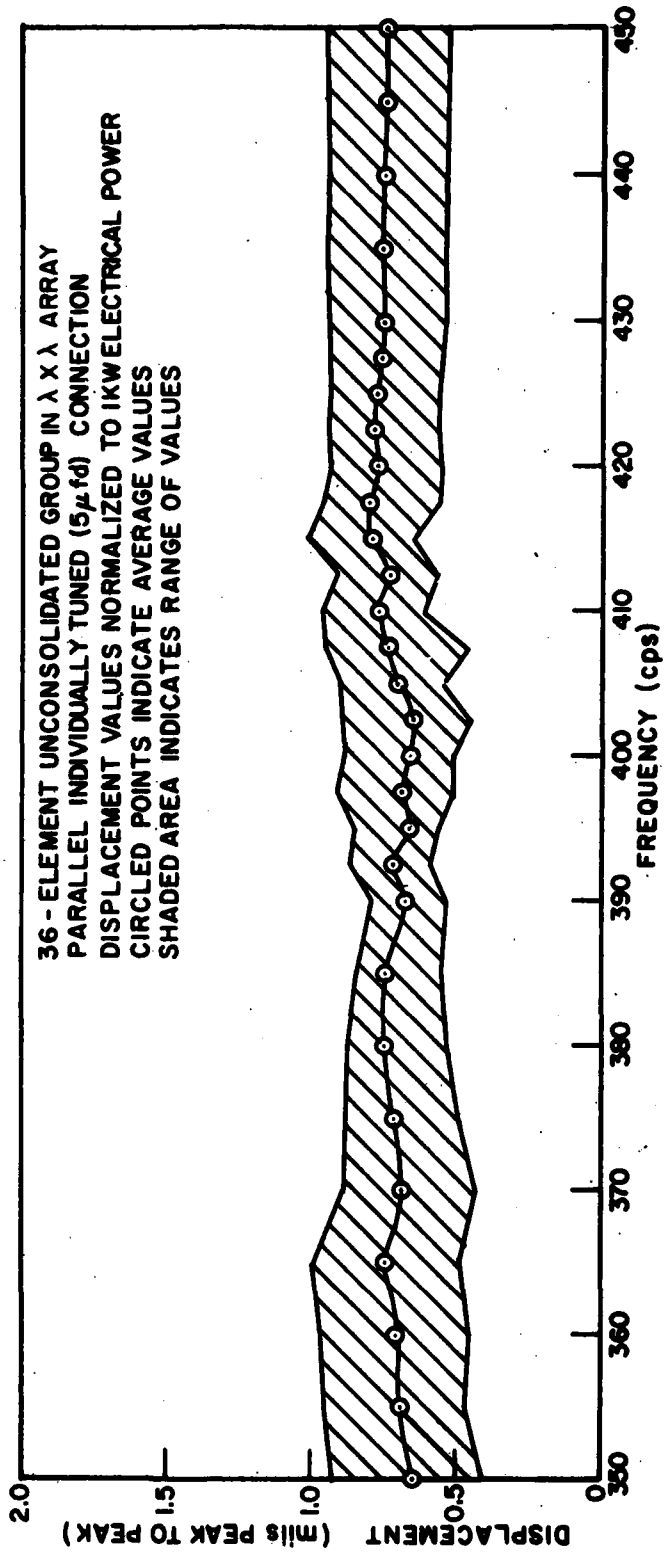

Fig. 44 - Average displacement of outer masses

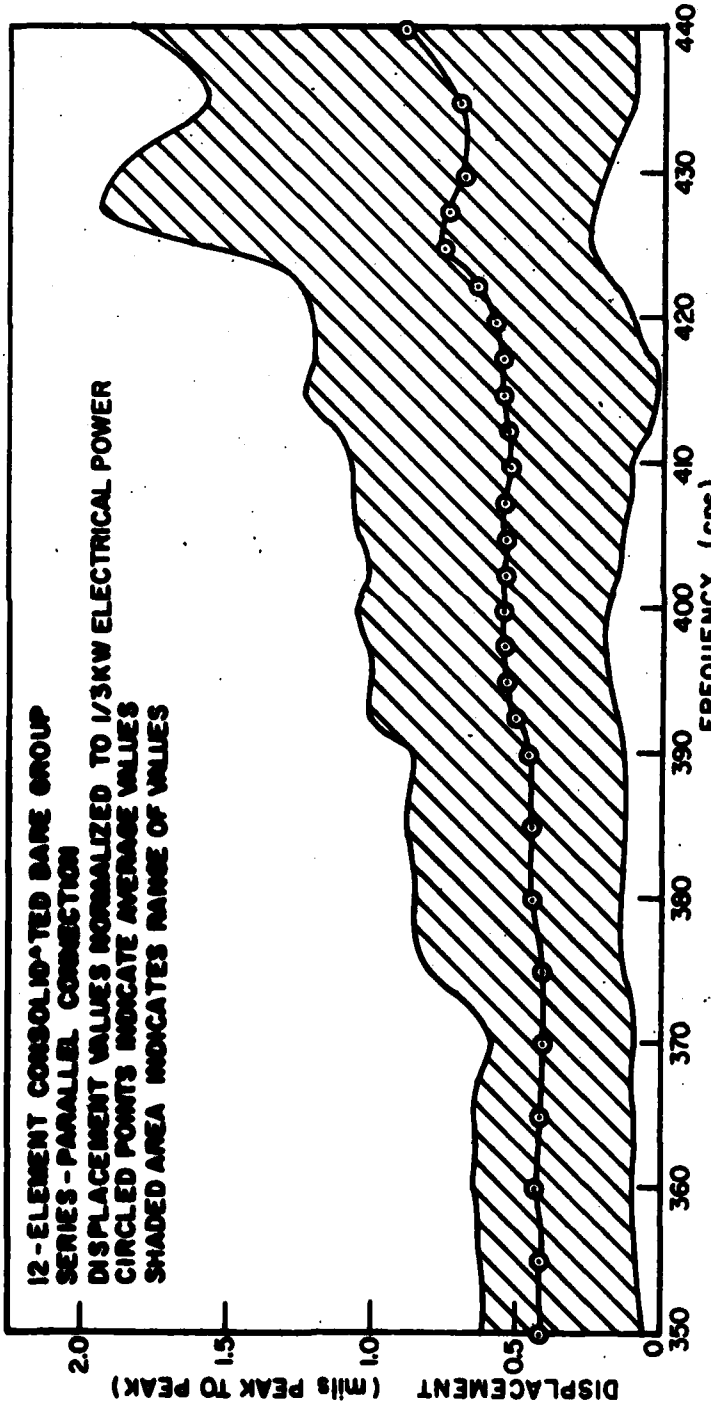

Fig. 45 - Average displacement of outer masses

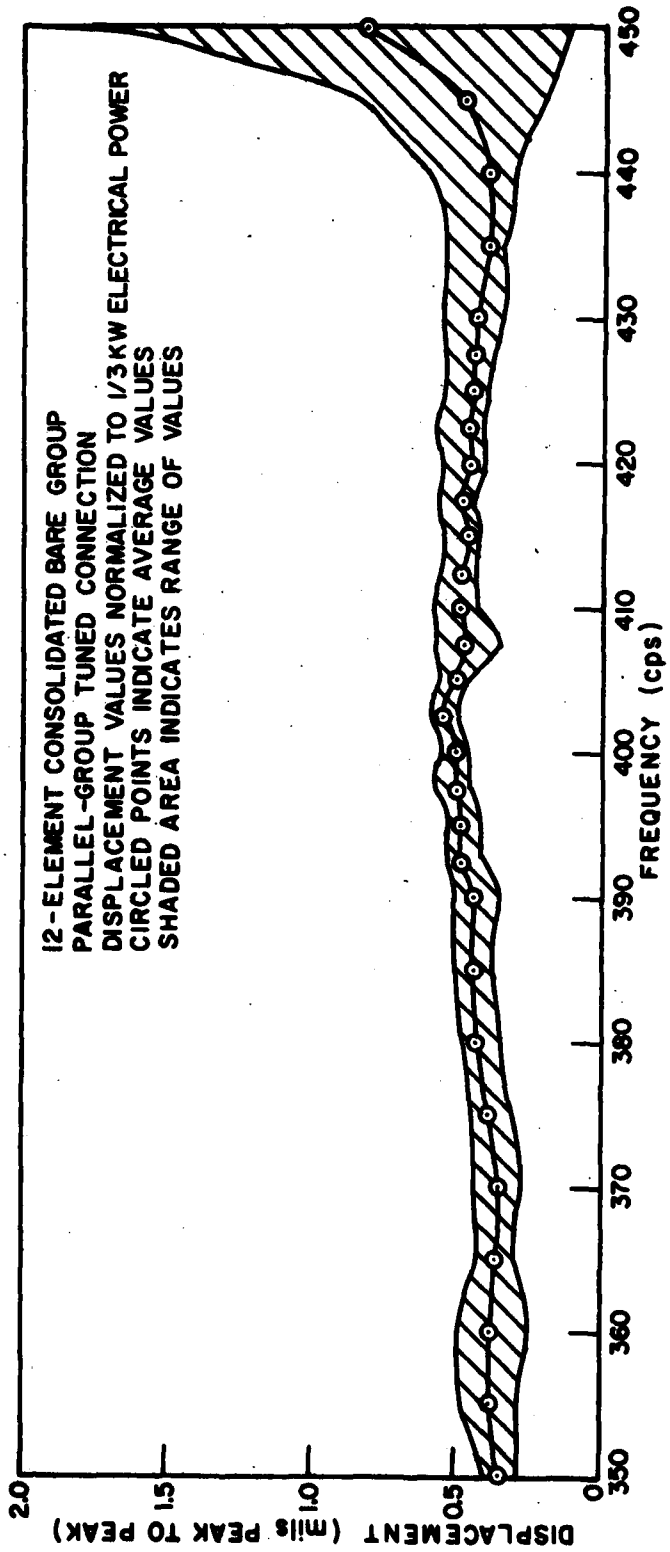

Fig. 46 - Average displacement of outer masses

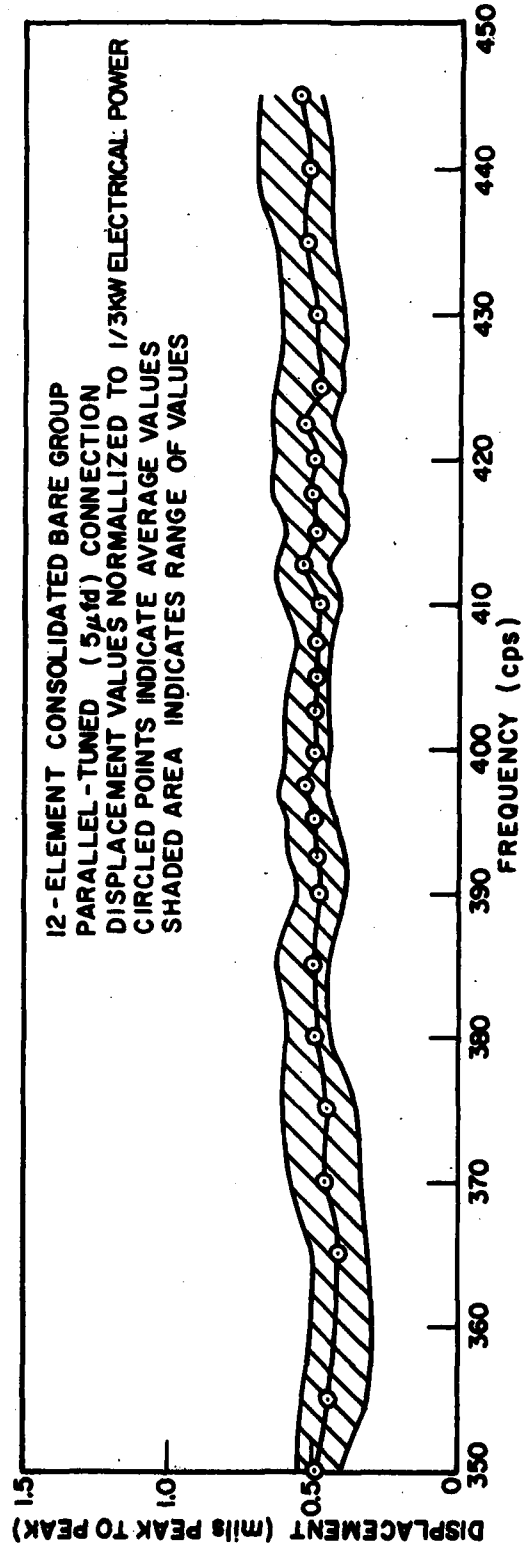

Fig. 47 - Average displacement of outer masses

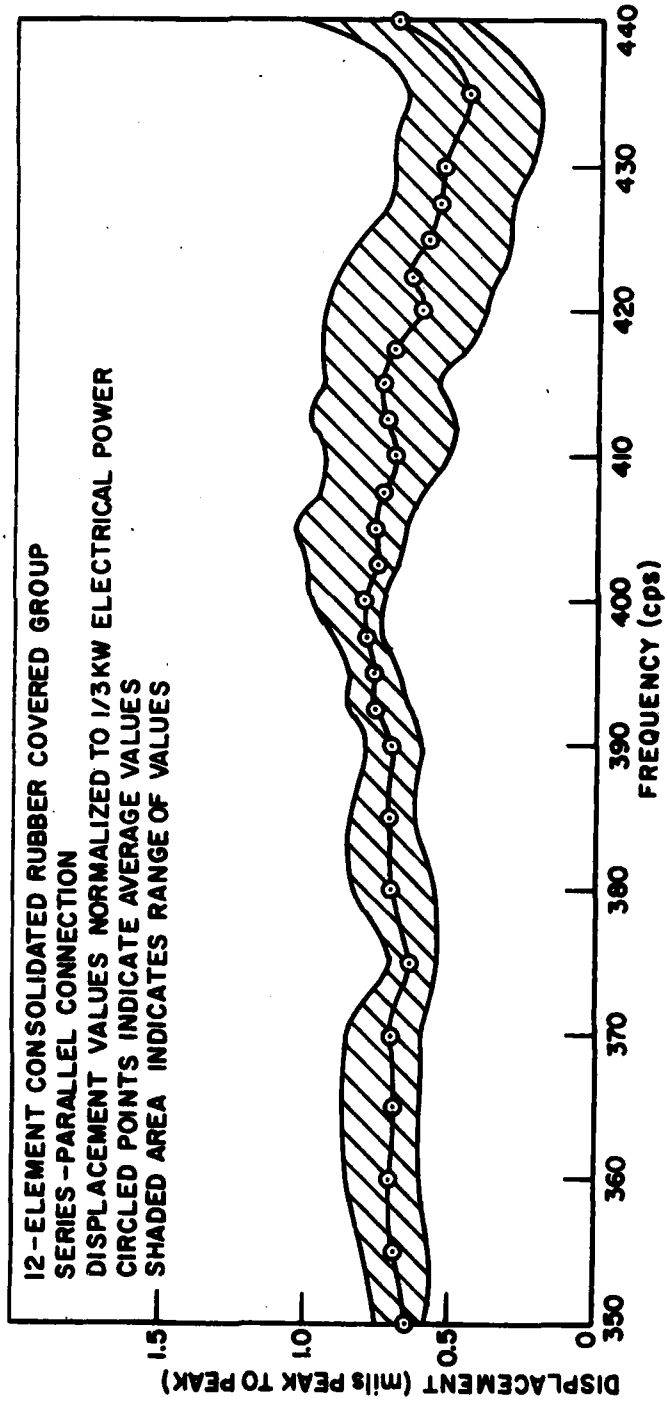

Fig. 48 - Average displacement of outer masses

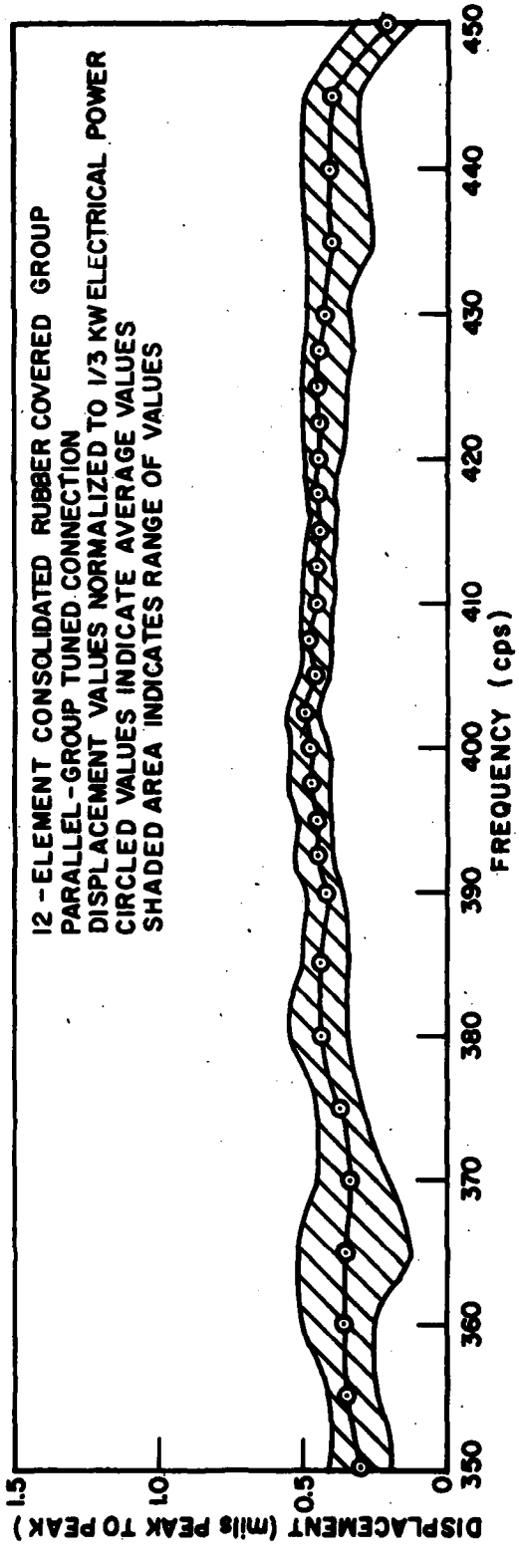

Fig. 49 - Average displacement of outer masses

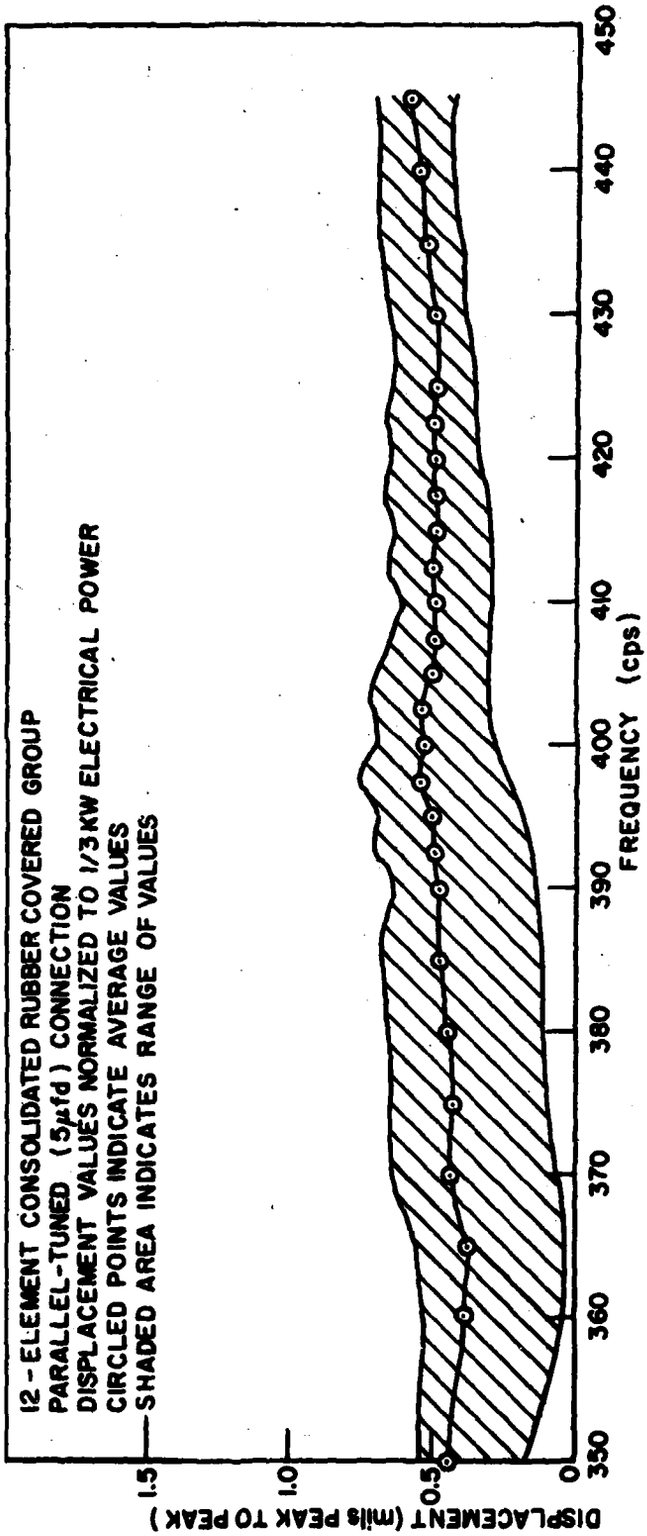

Fig. 50 - Average displacement of outer masses

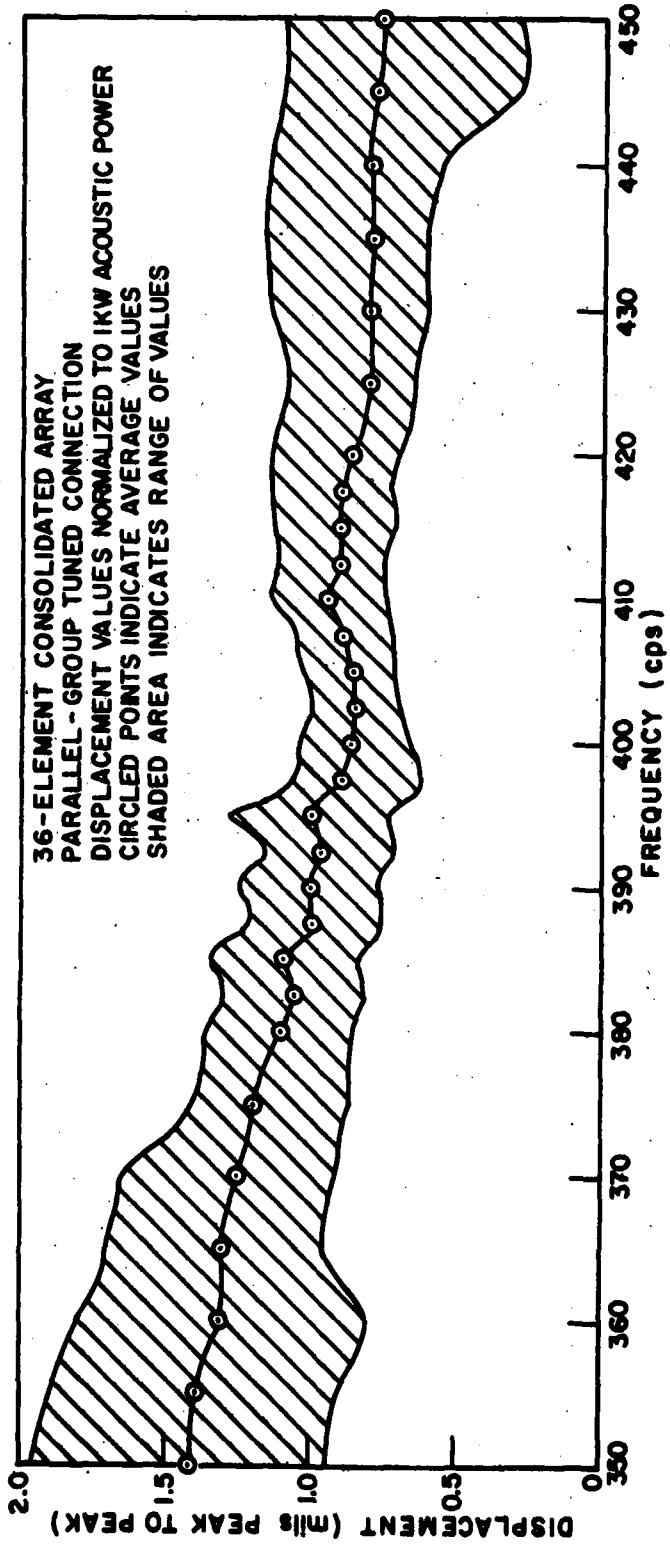

Fig. 51 - Average displacement of outer masses

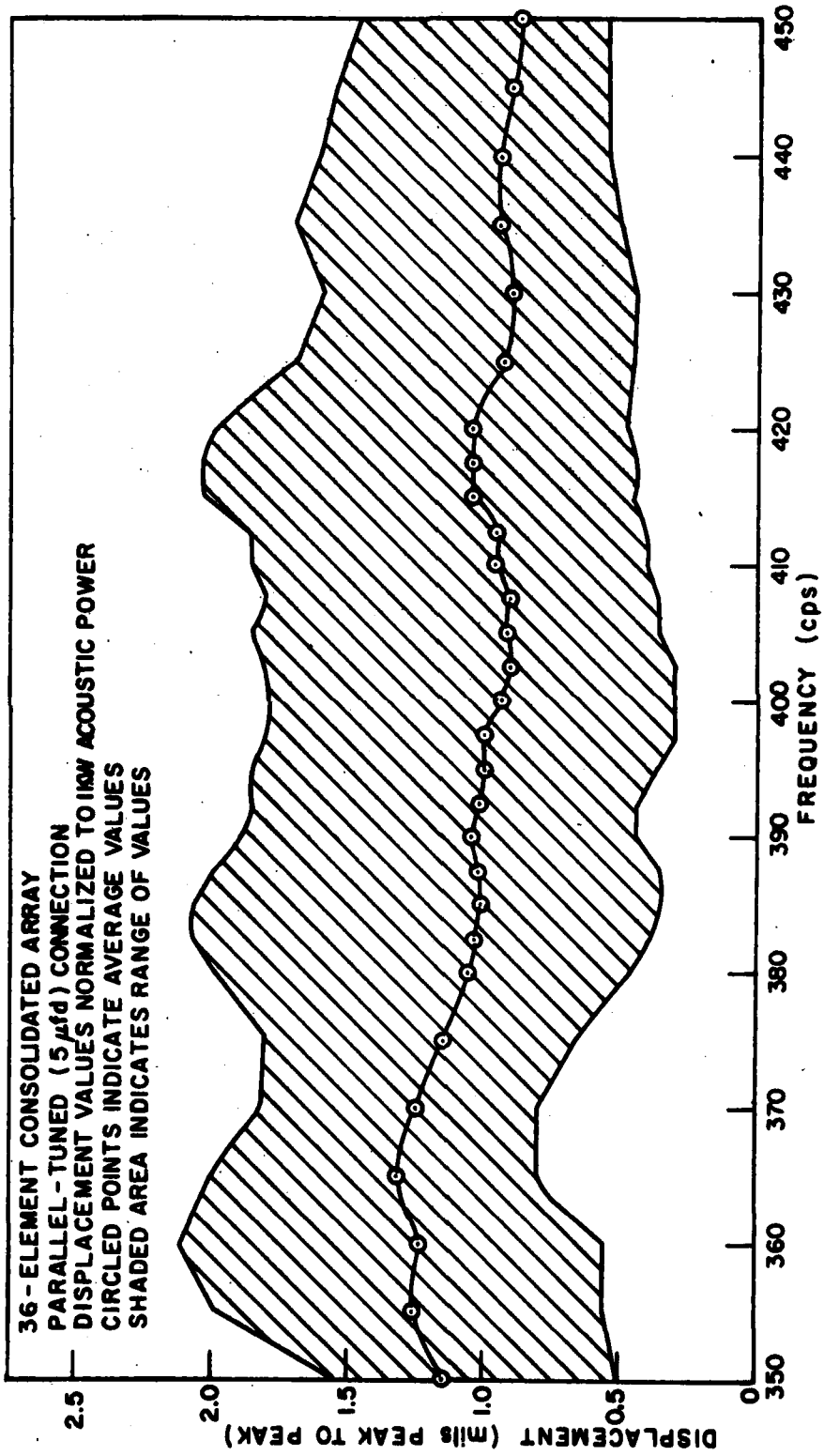

Fig. 52 - Average displacement of outer masses

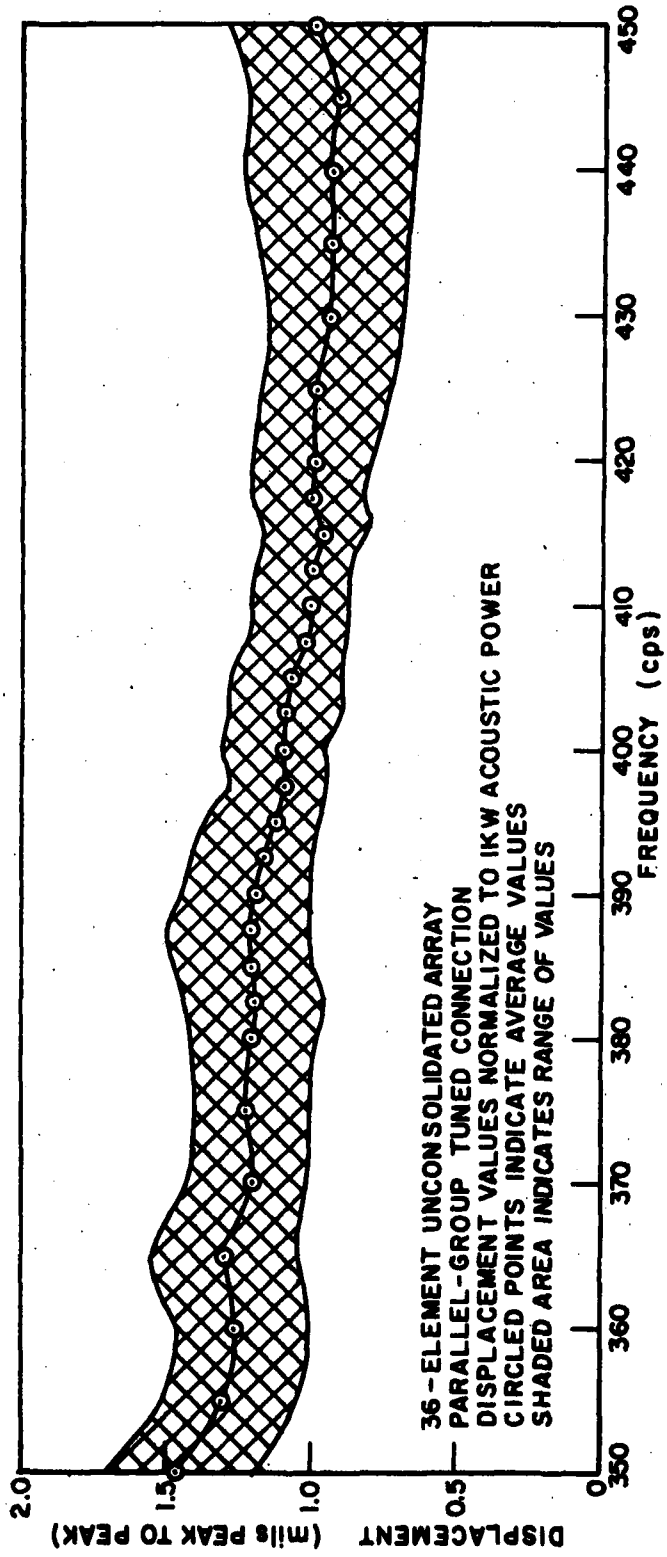

Fig. 53 - Average displacement of outer masses

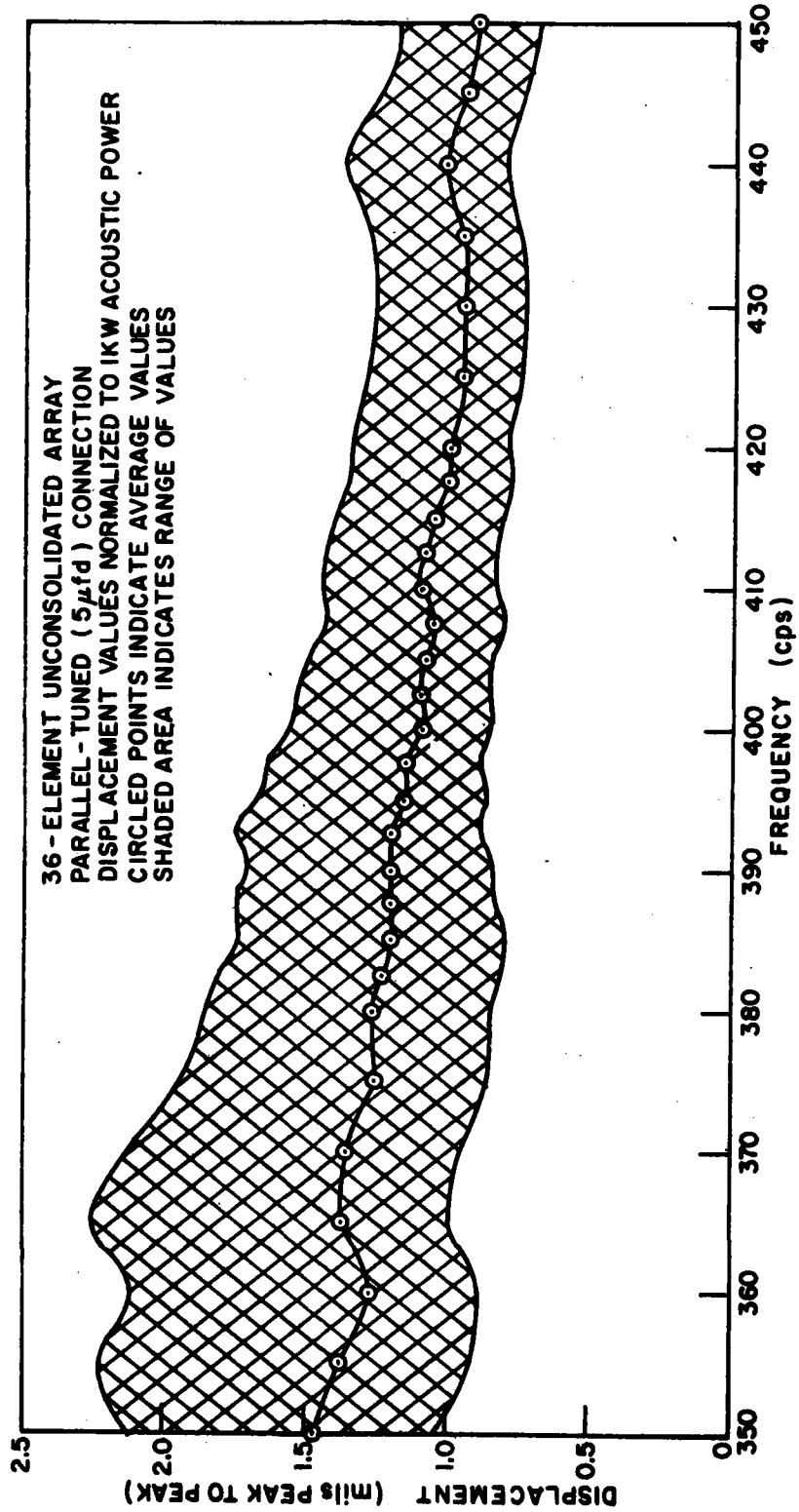

Fig. 54 - Average displacement of outer masses

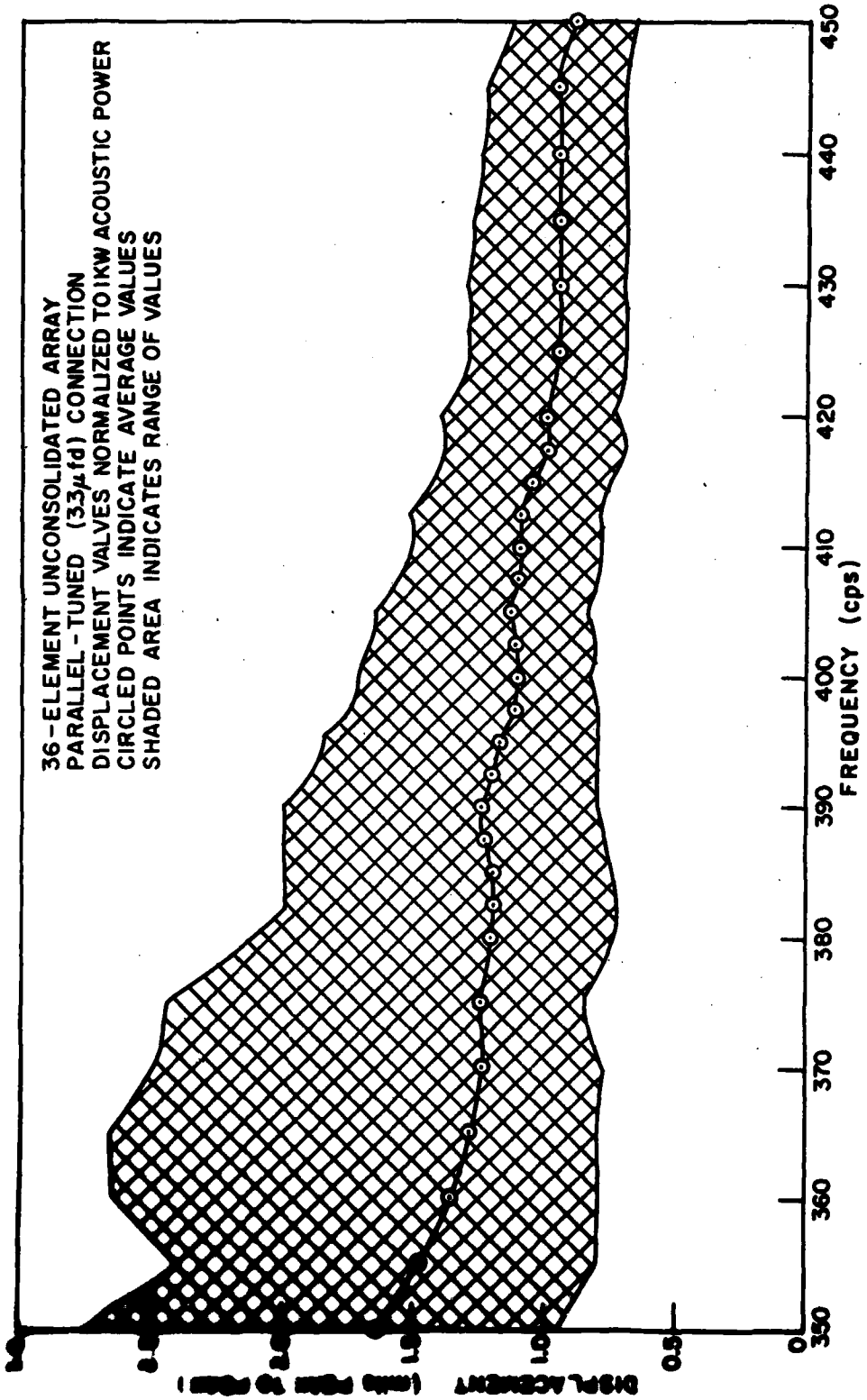

Fig. 55 - Average displacement of outer masses

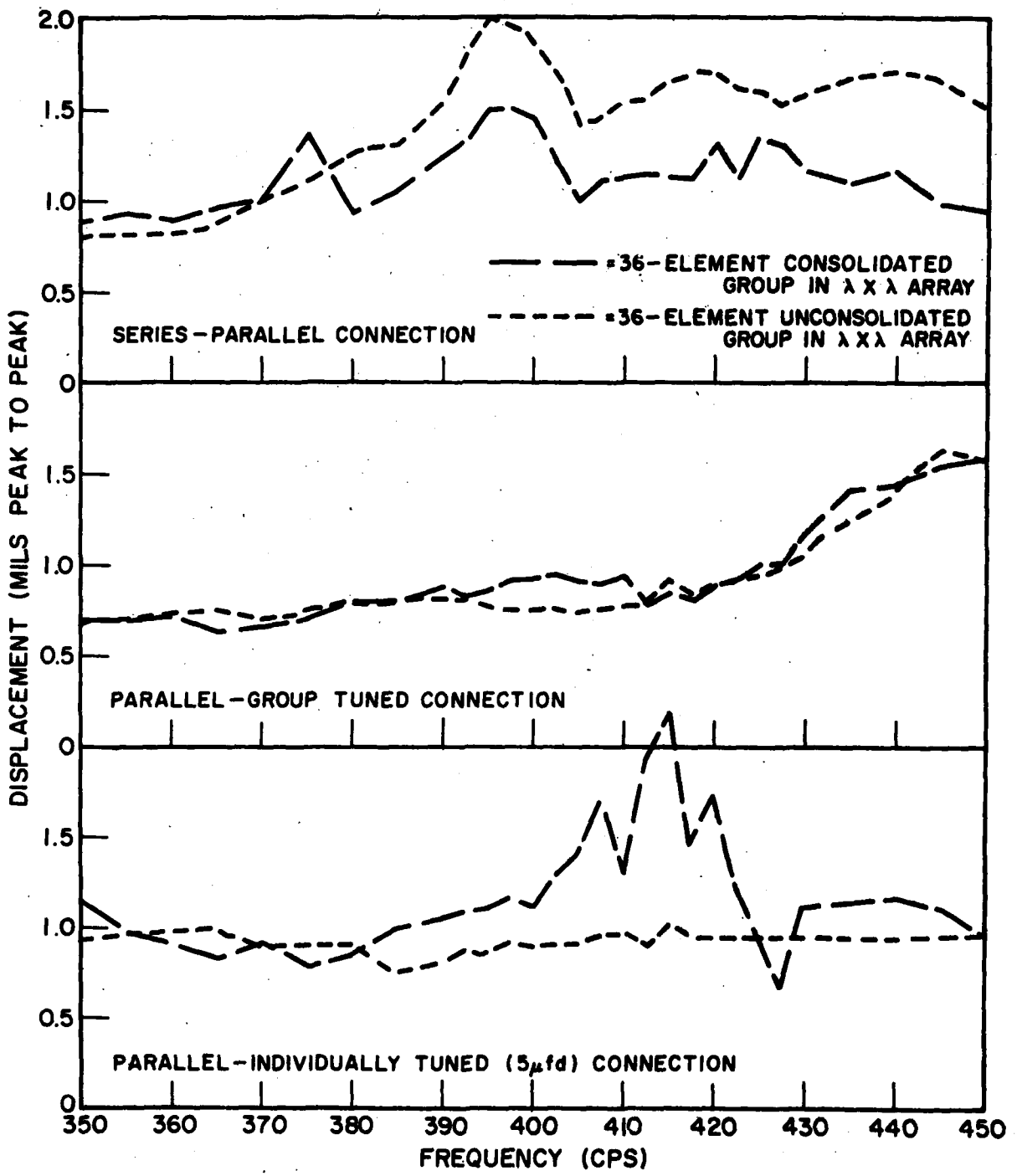

Fig. 56 - Maximum outer mass displacement amplitude

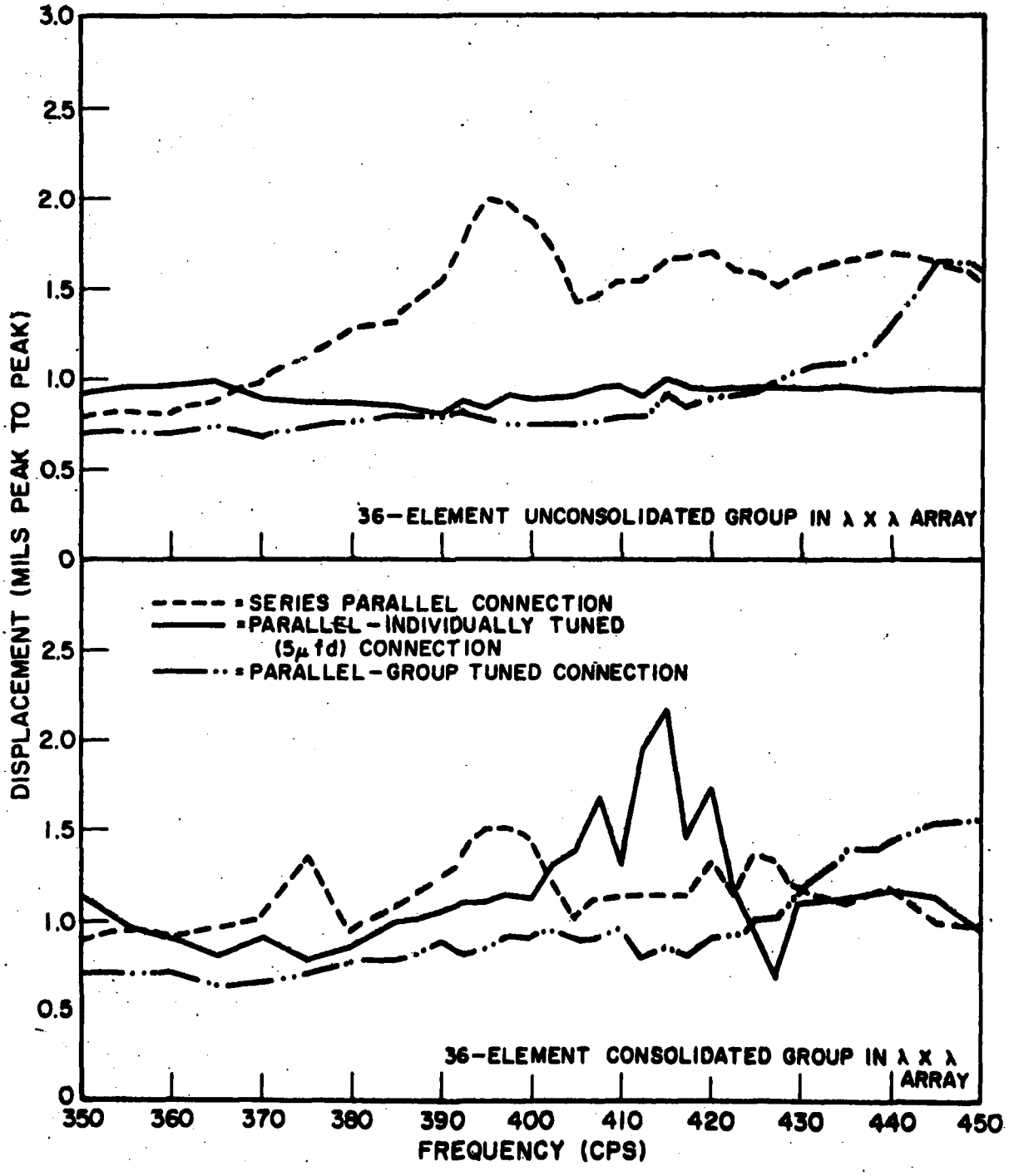

Fig. 57 - Maximum outer mass displacement amplitude

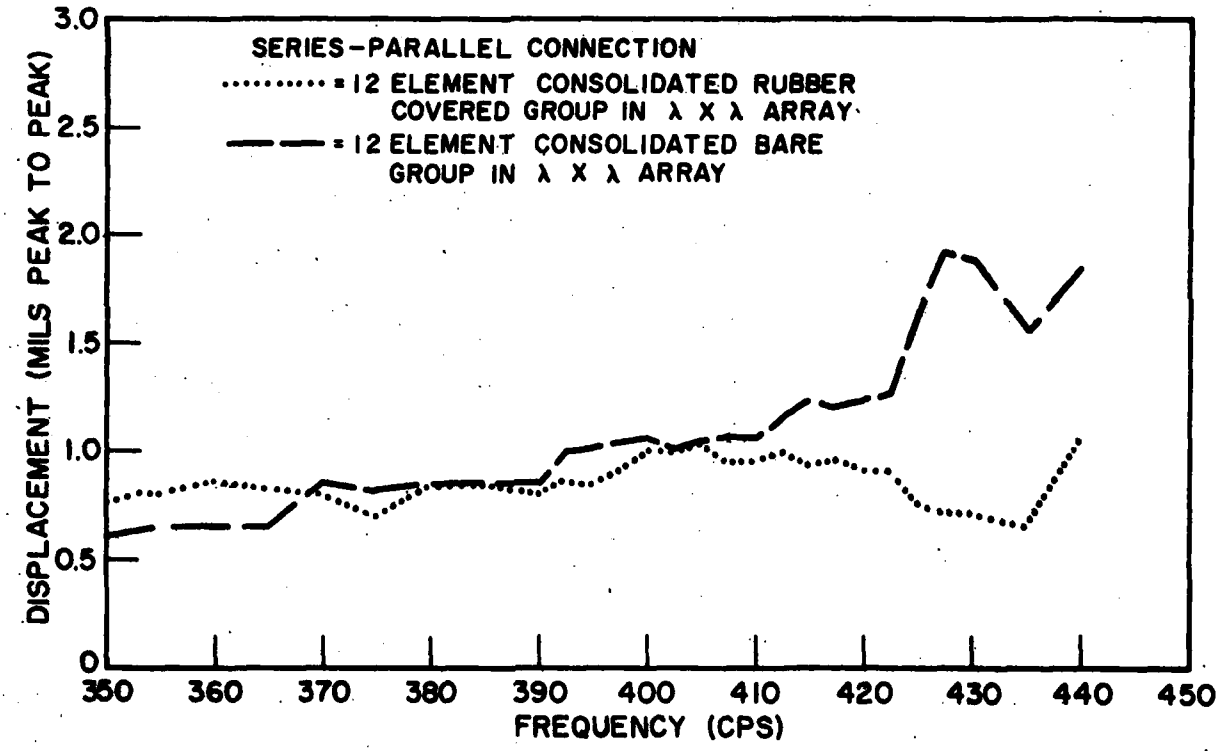

Fig. 58 - Maximum outer mass displacement amplitude

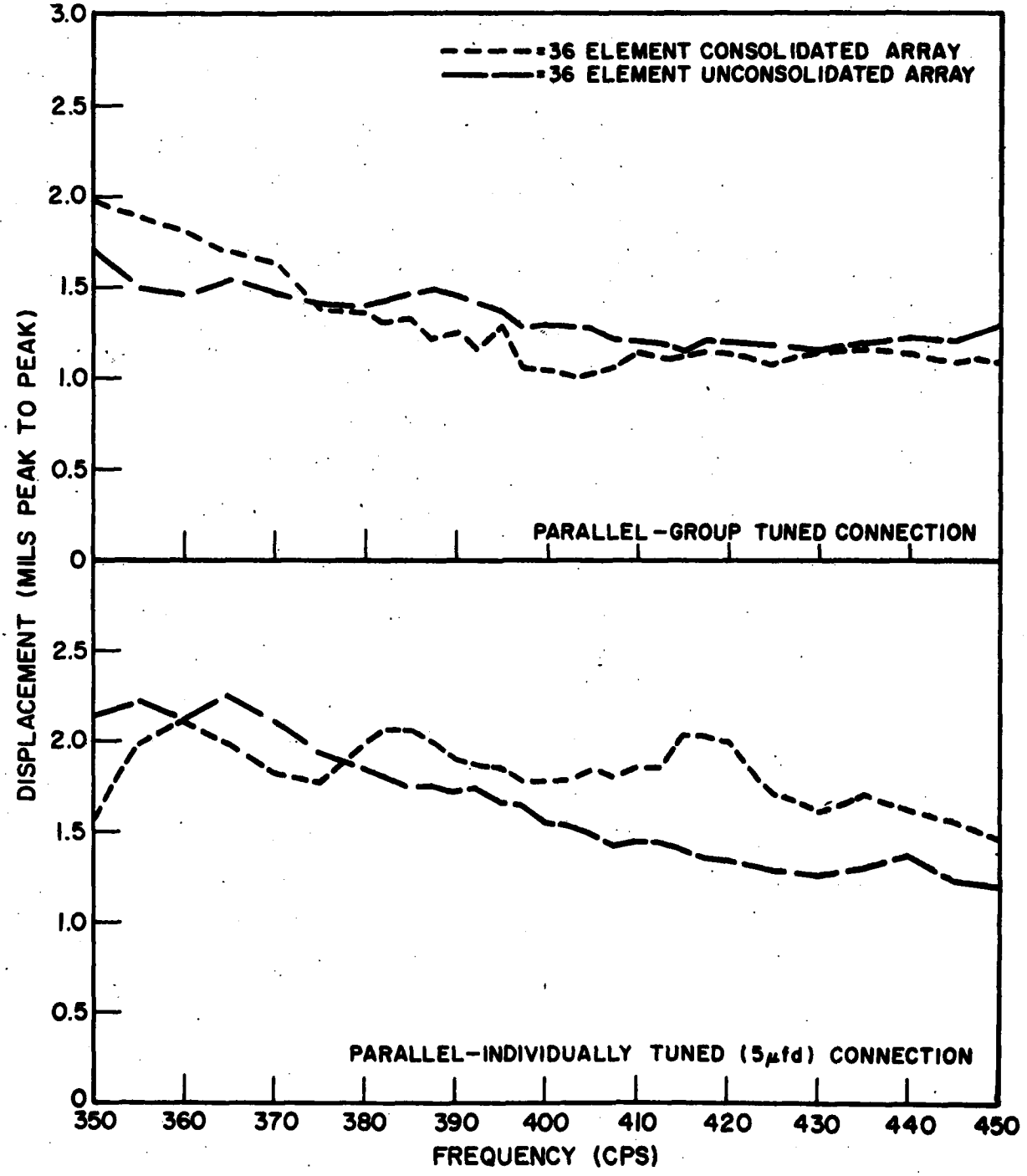

Fig. 59 - Maximum outer mass displacement amplitude

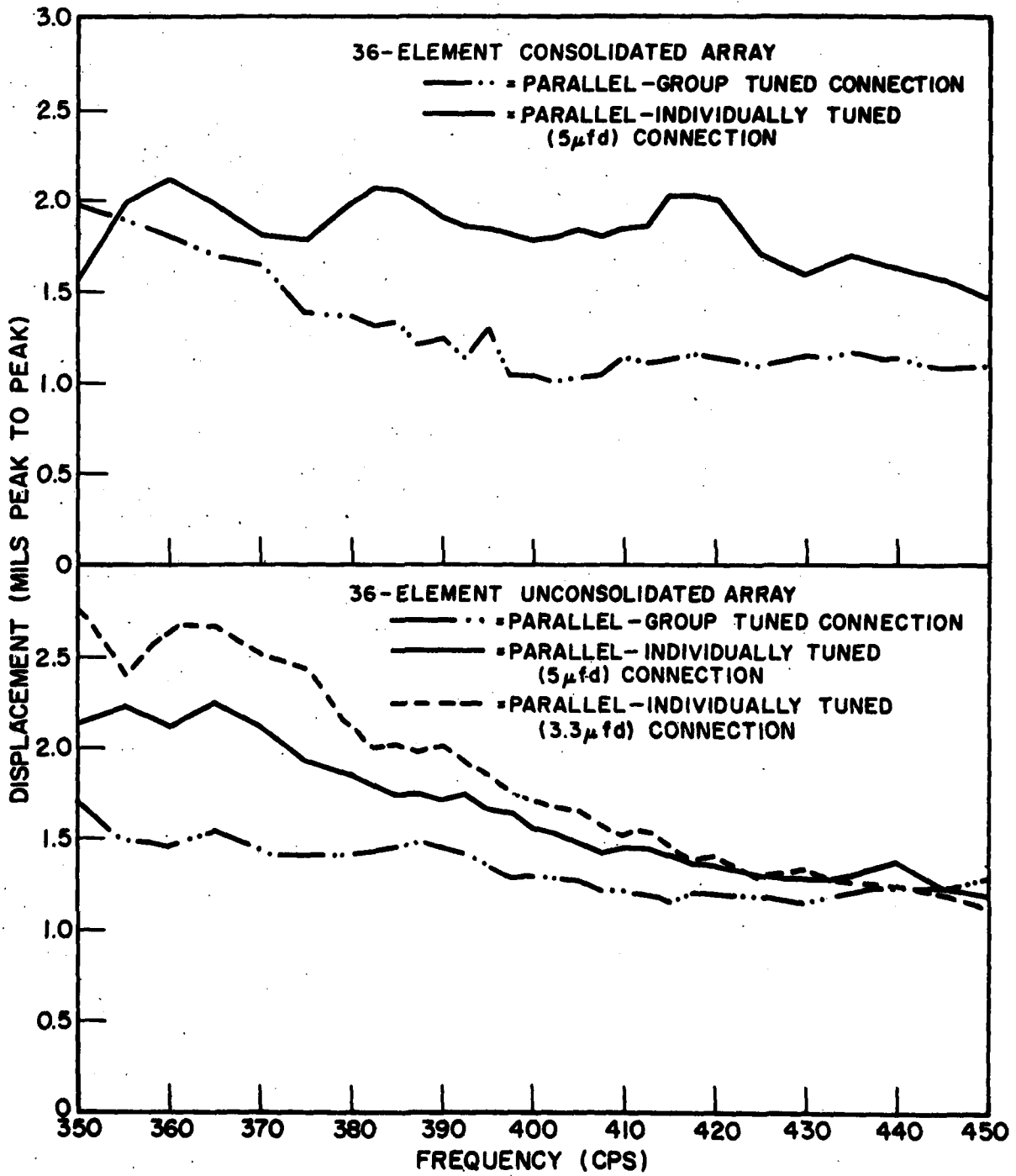

Fig. 60 - Maximum outer mass displacement amplitude

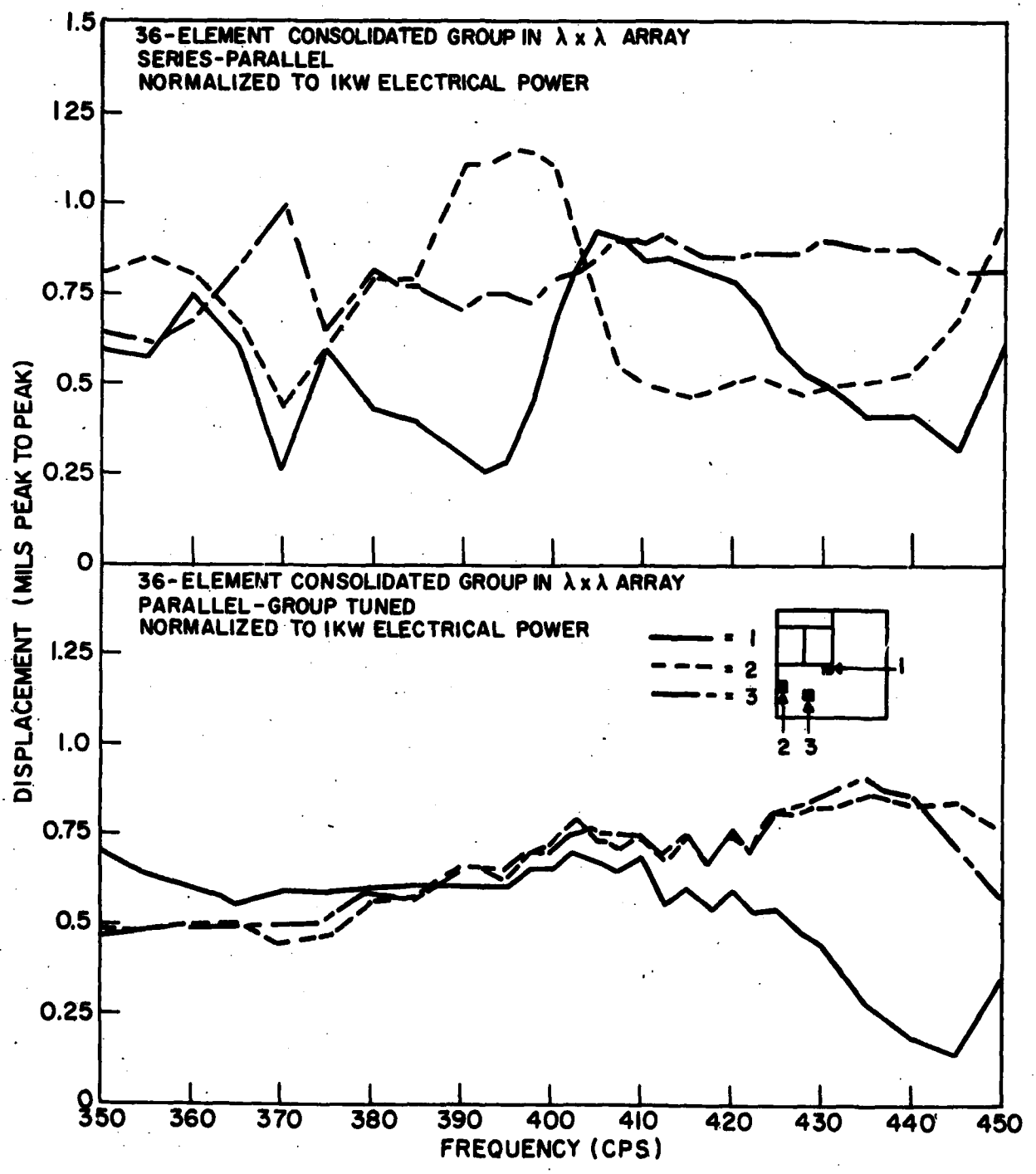

Fig. 61 - Frequency dependence of outer mass displacement for individual transducer elements

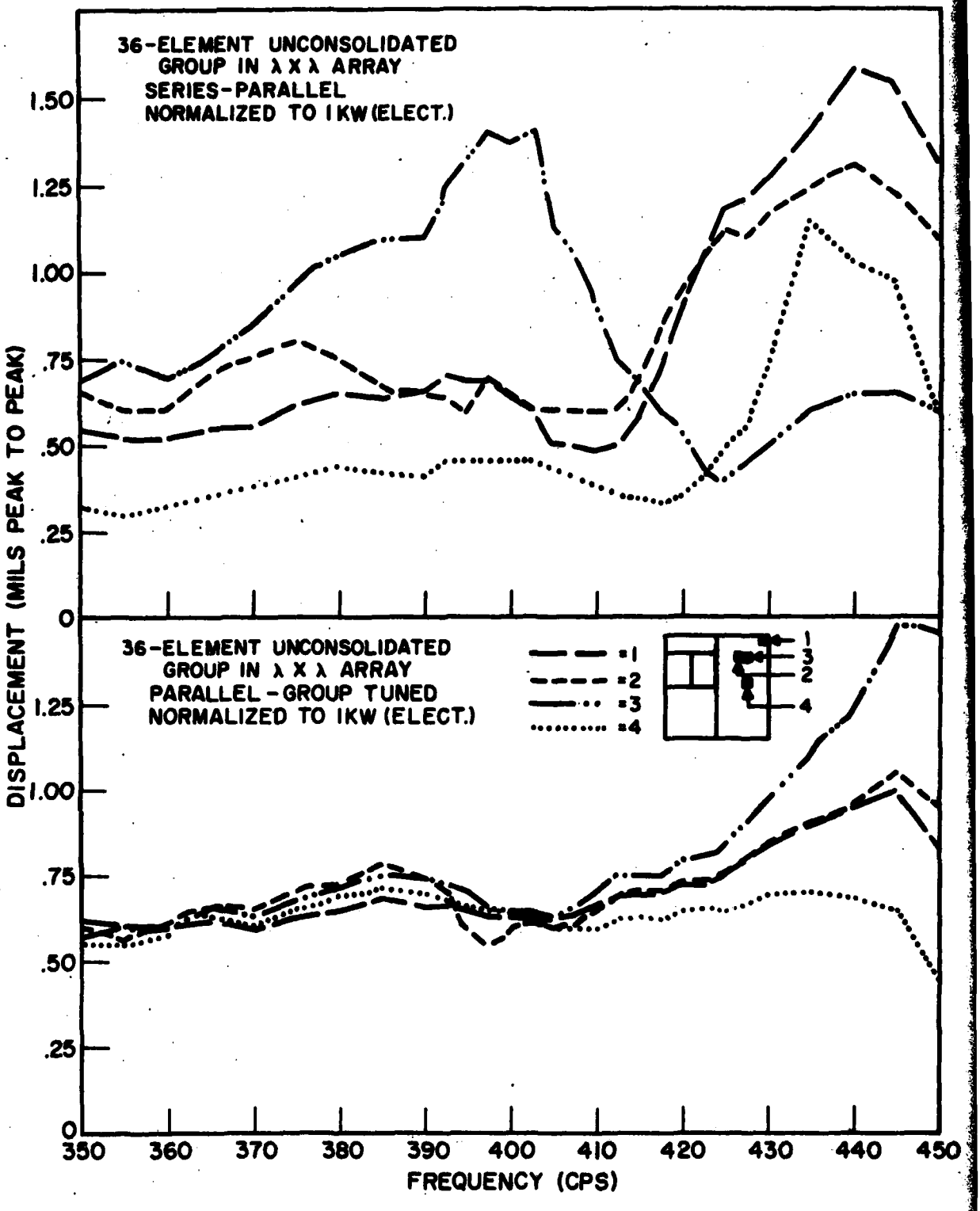

Fig. 62 - Frequency dependence of outer mass displacement for individual transducer elements

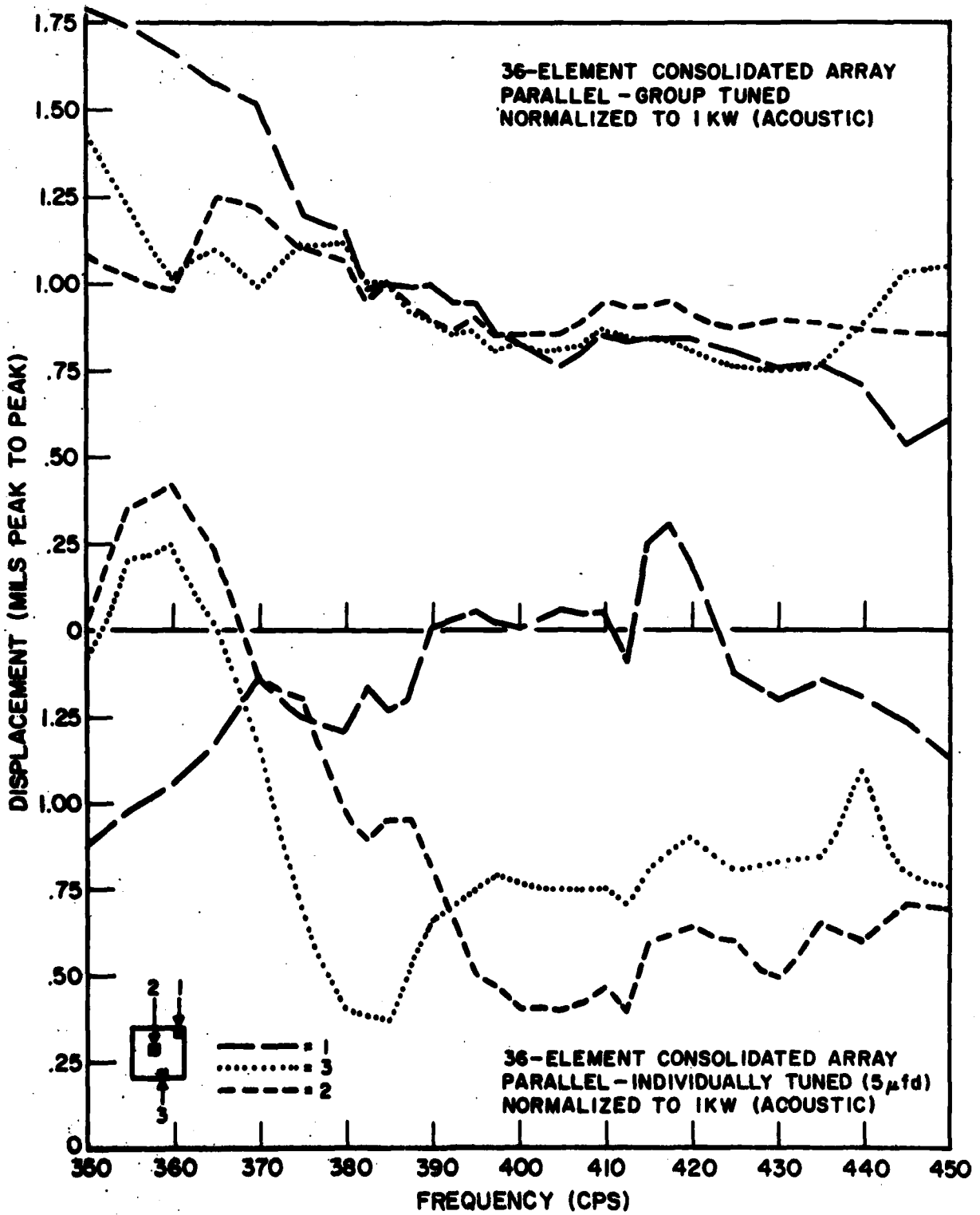

Fig. 63 - Frequency dependence of outer mass displacement for individual transducer elements

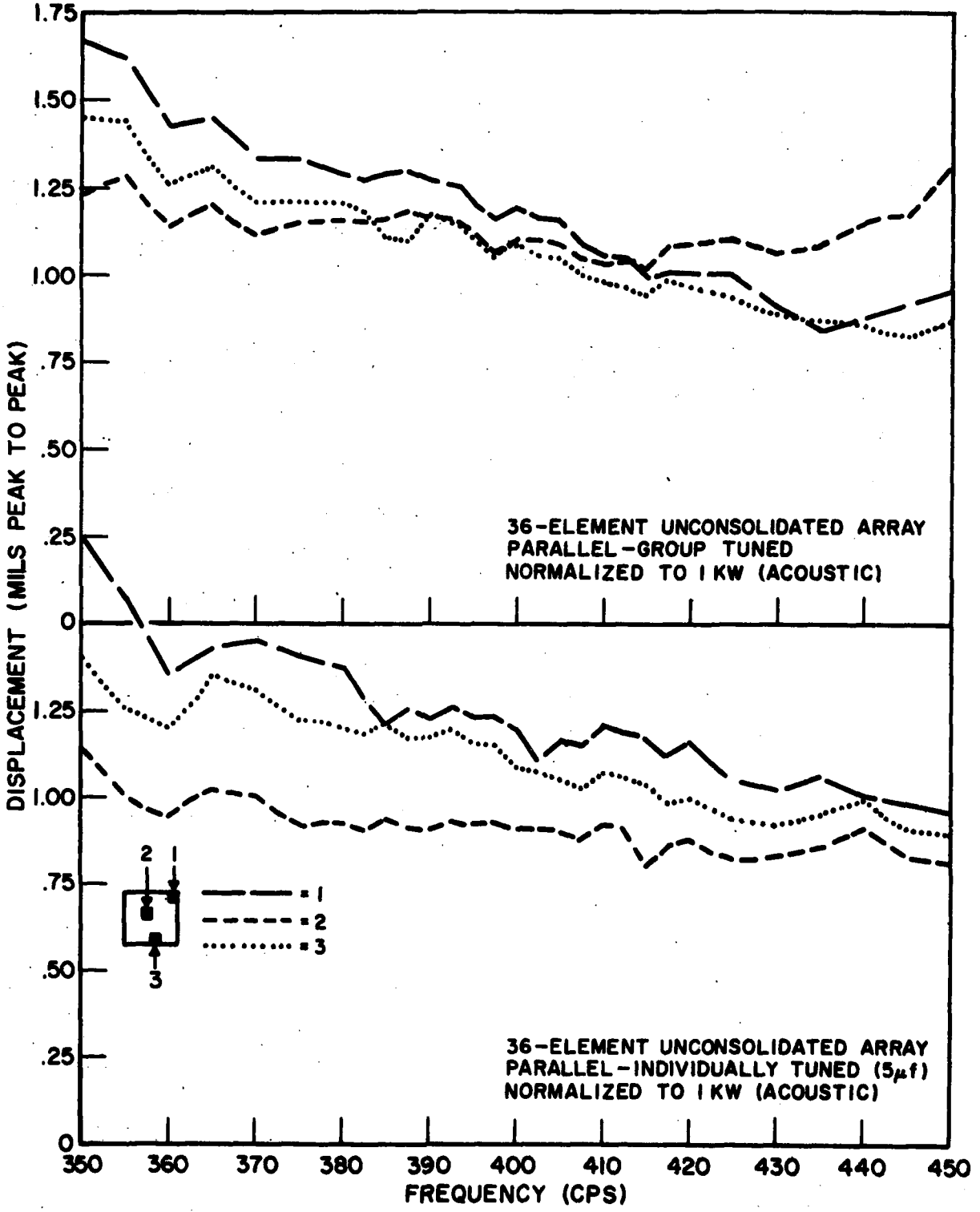

Fig. 64 - Frequency dependence of outer mass displacement for individual transducer elements

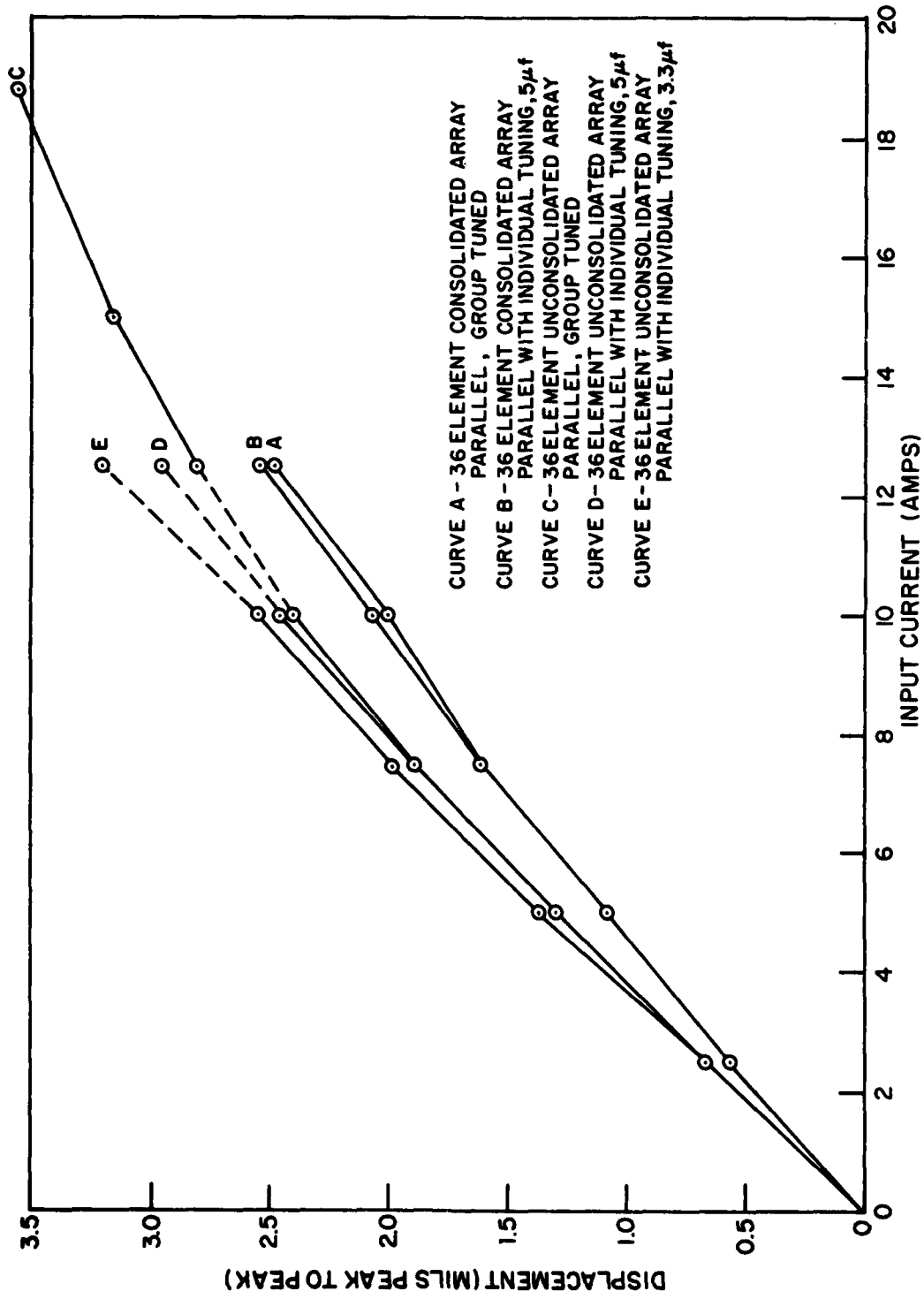

Fig. 65 - Linearity of average outer mass displacement

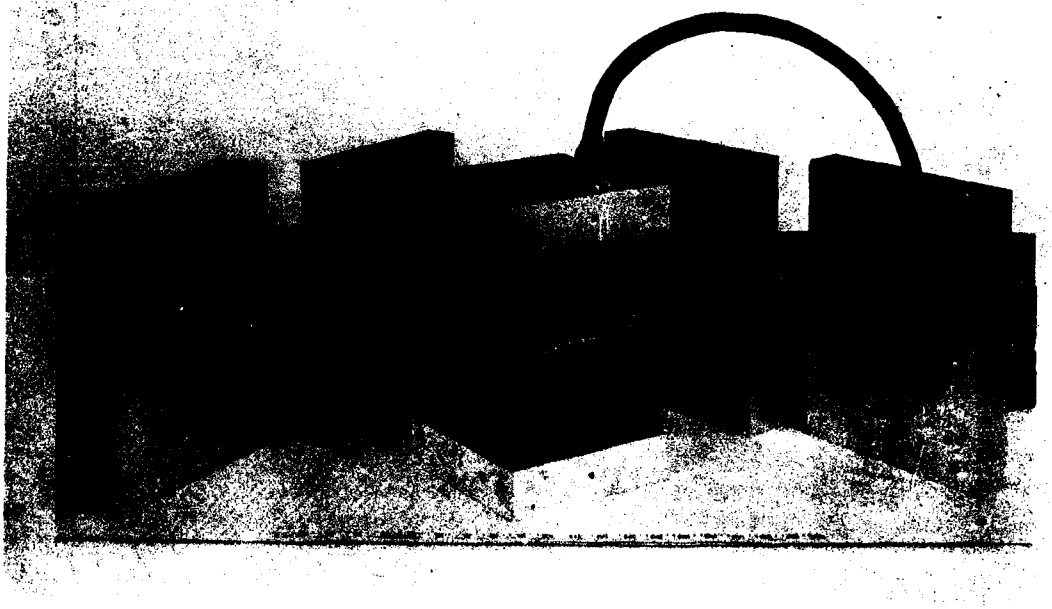

Fig. 66 - View of Massa model TR-11B transducer element with side plates removed showing spring location

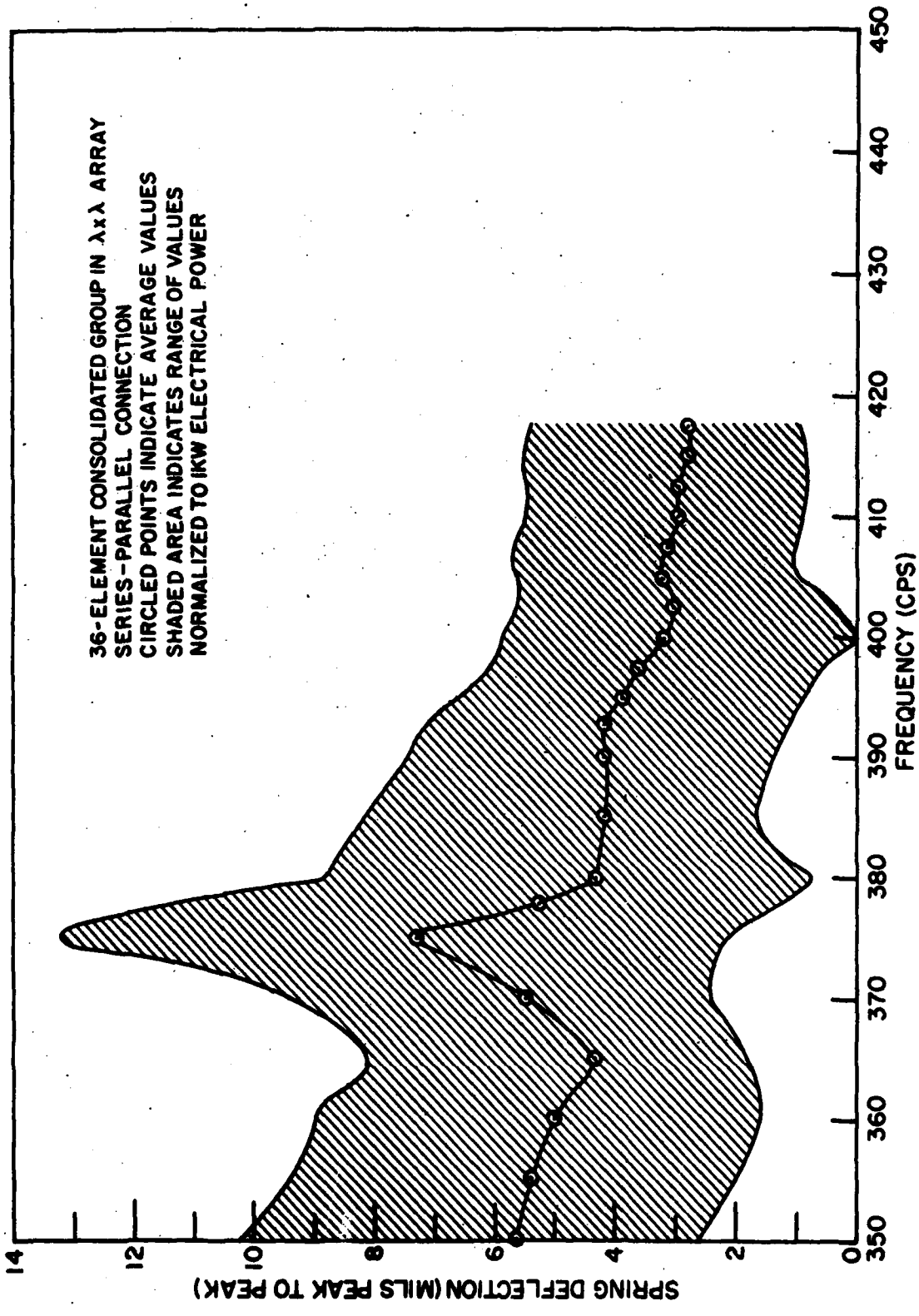

Fig. 67 - Average spring deflections

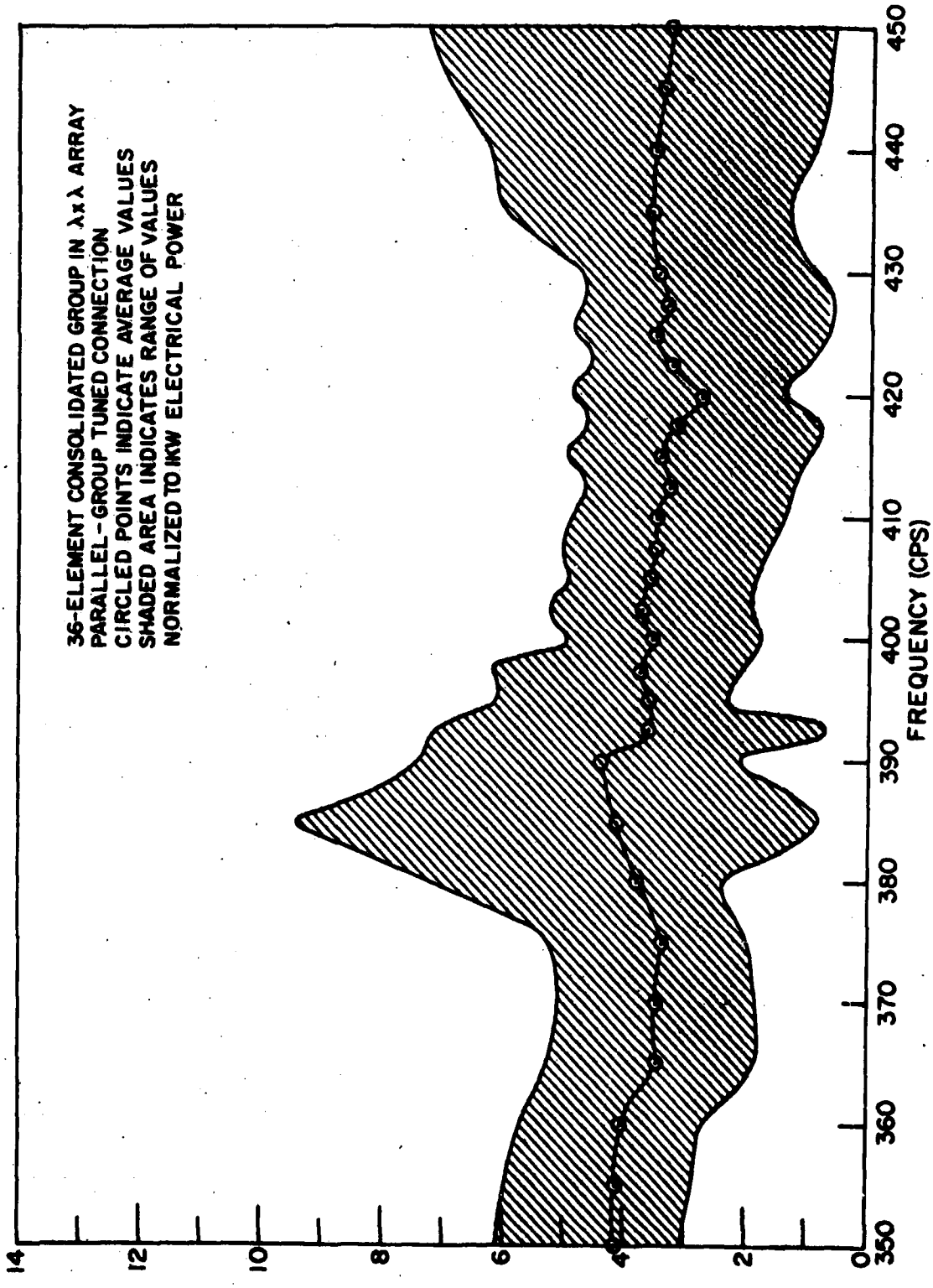

Fig. 68 - Average spring deflections

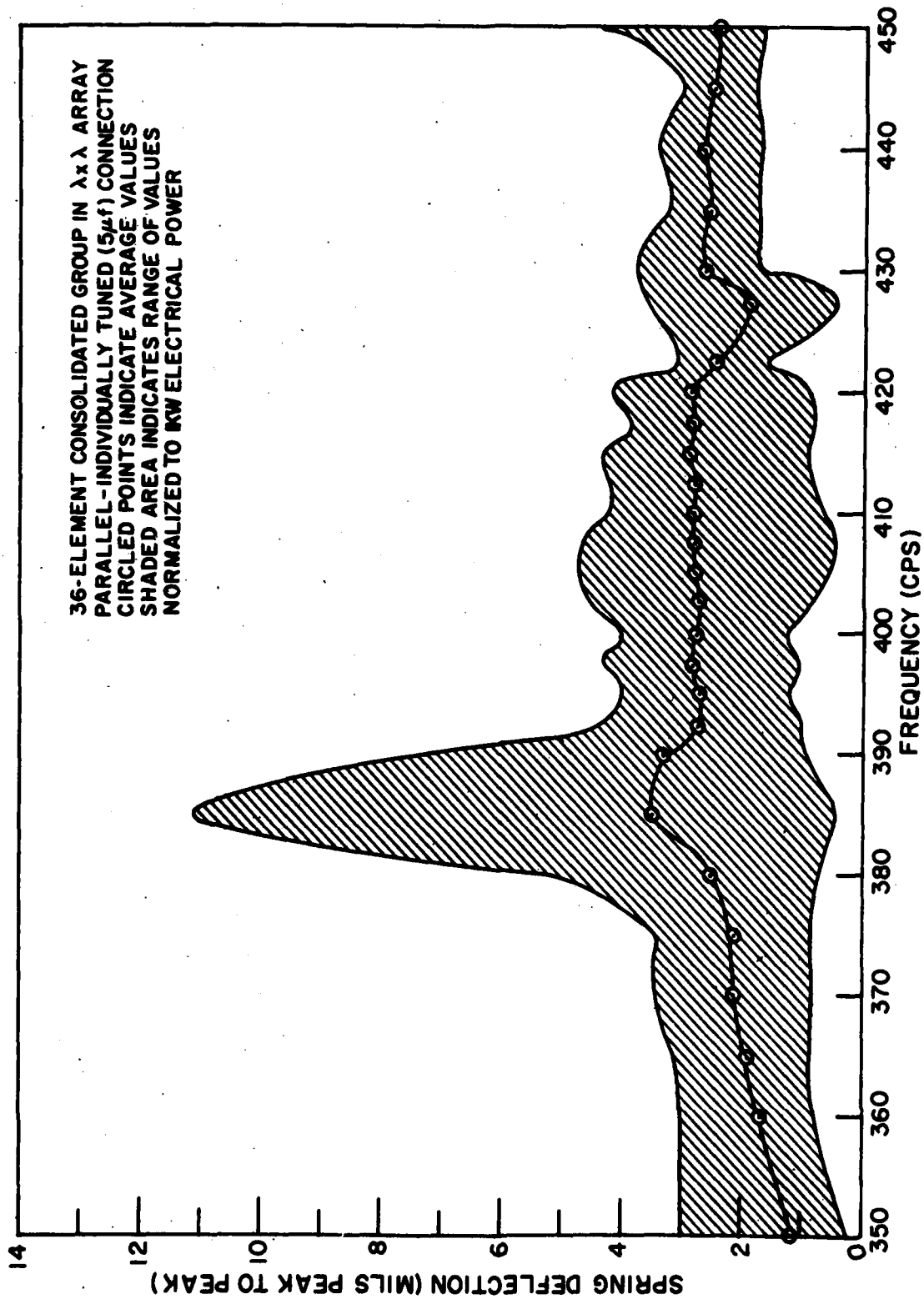

Fig. 69 - Average spring deflections

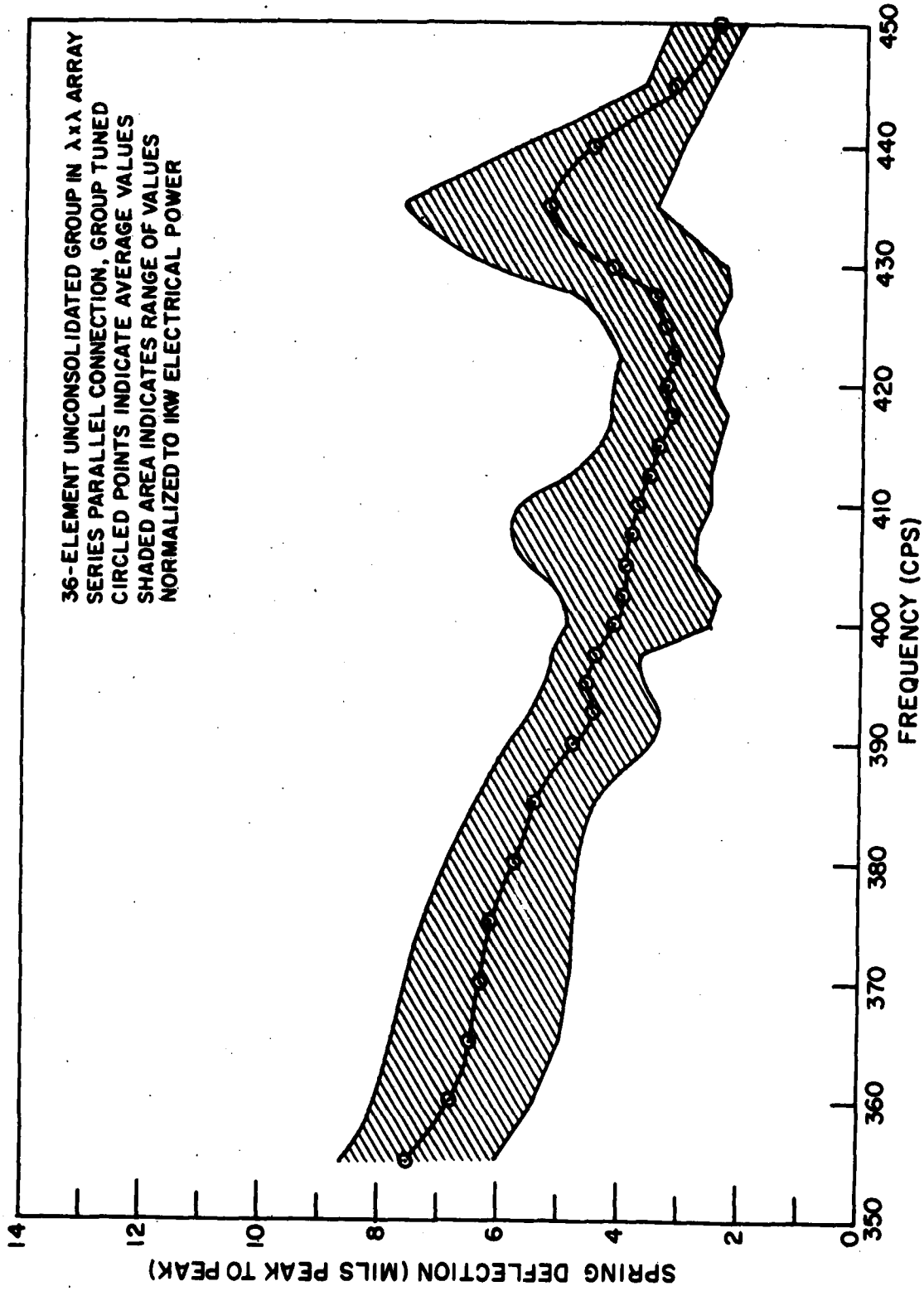

Fig. 70 - Average spring deflections

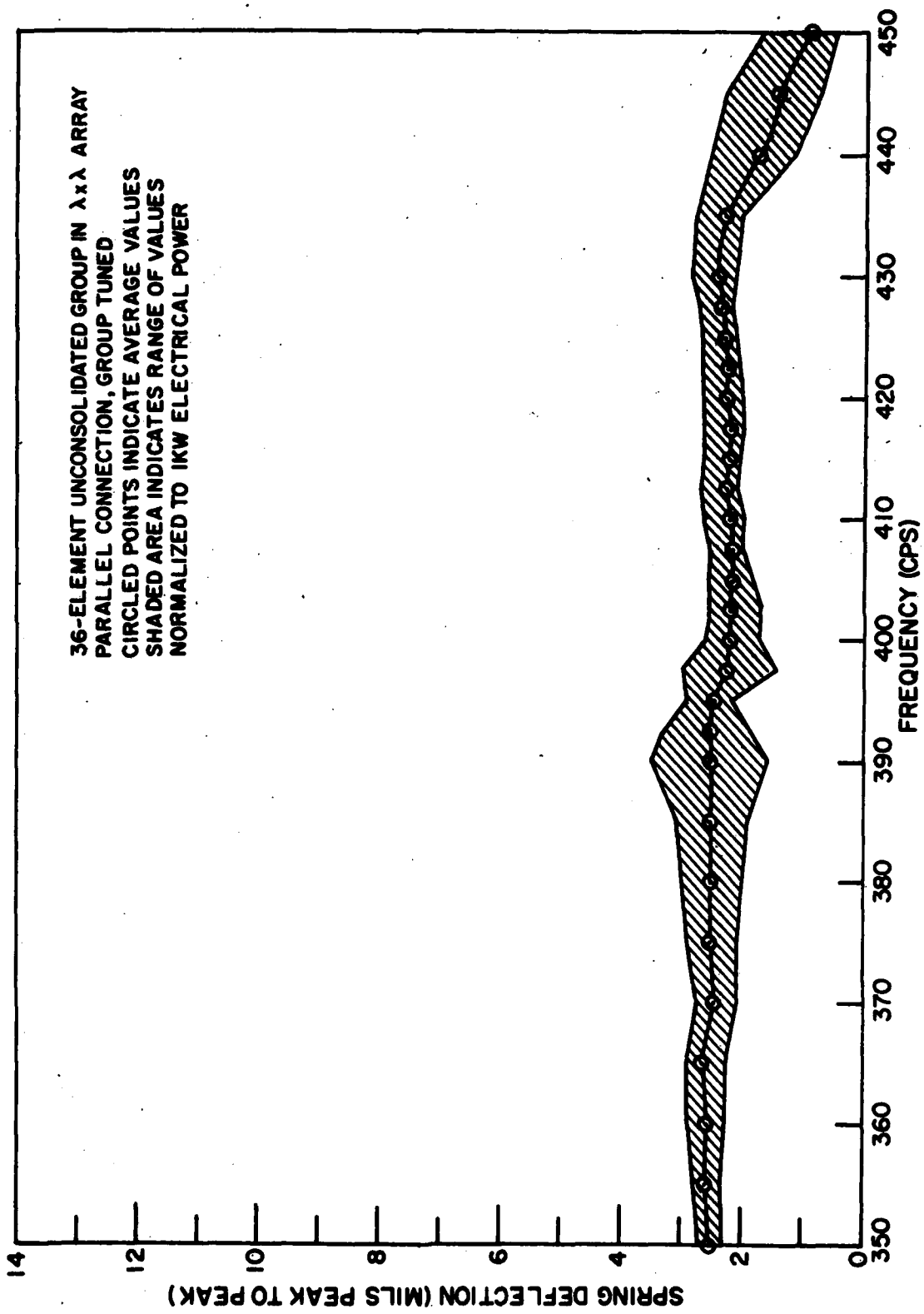

Fig. 71 - Average spring deflections

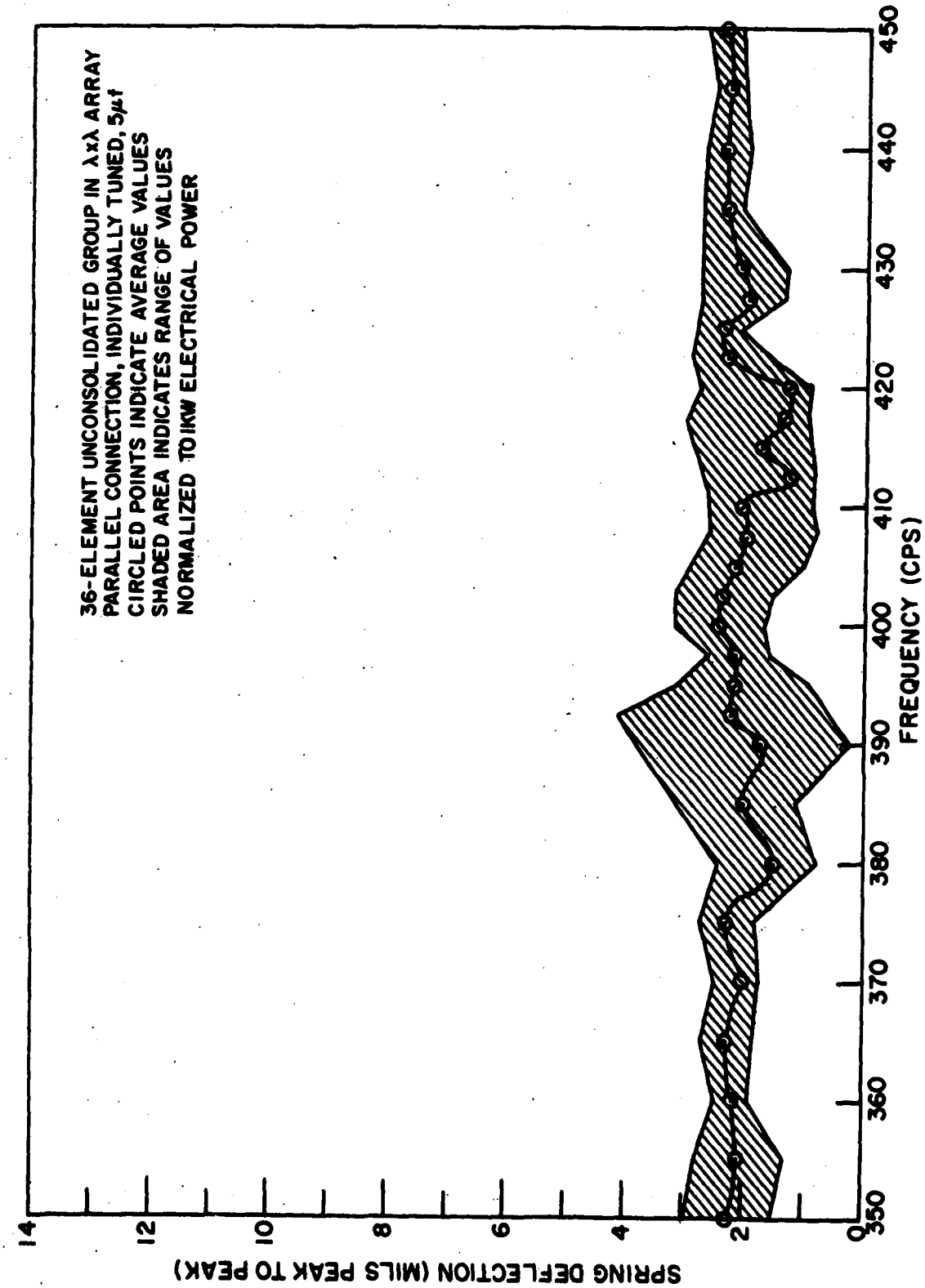

Fig. 72 - Average spring deflections

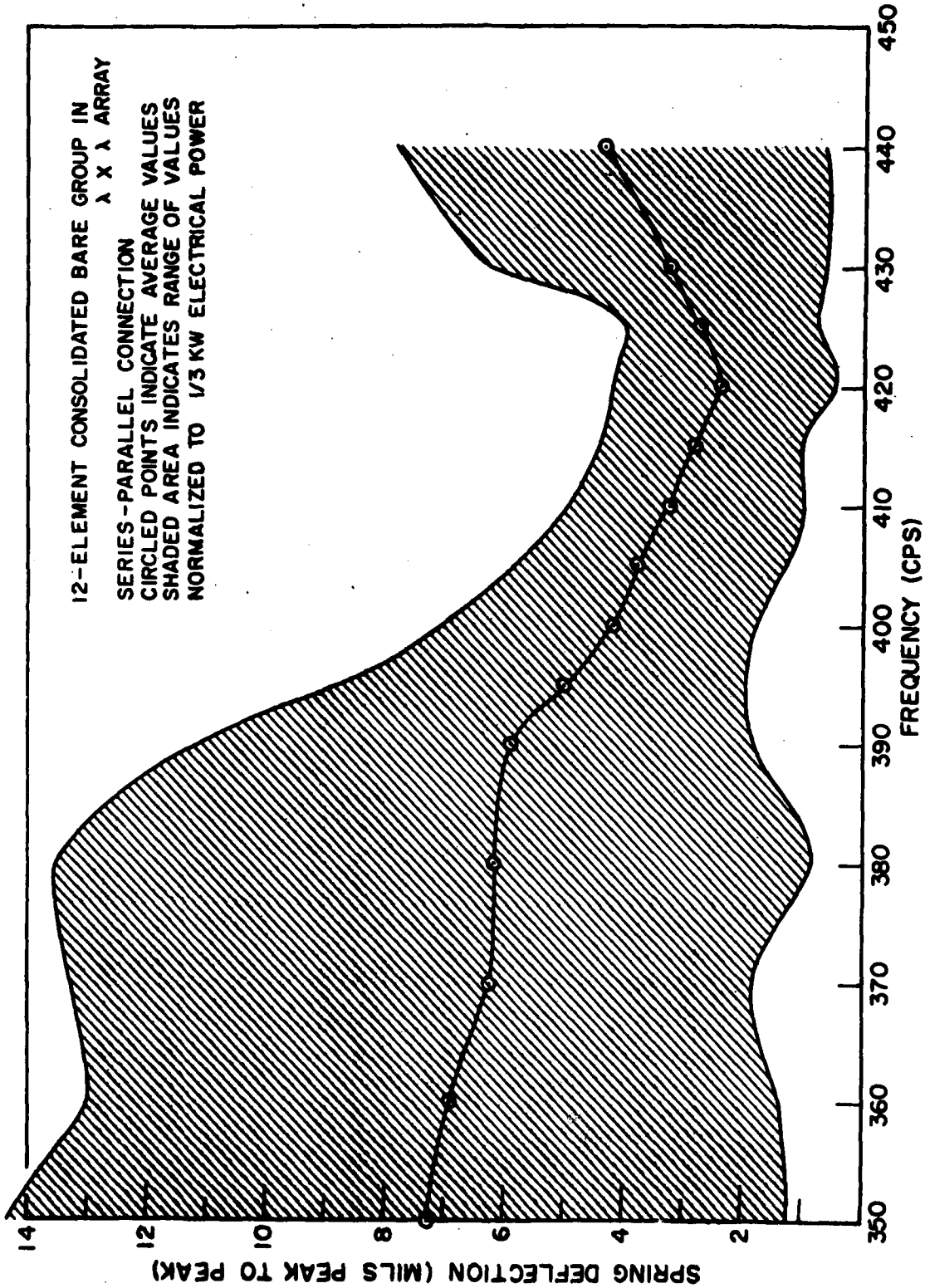

Fig. 73 - Average spring deflections

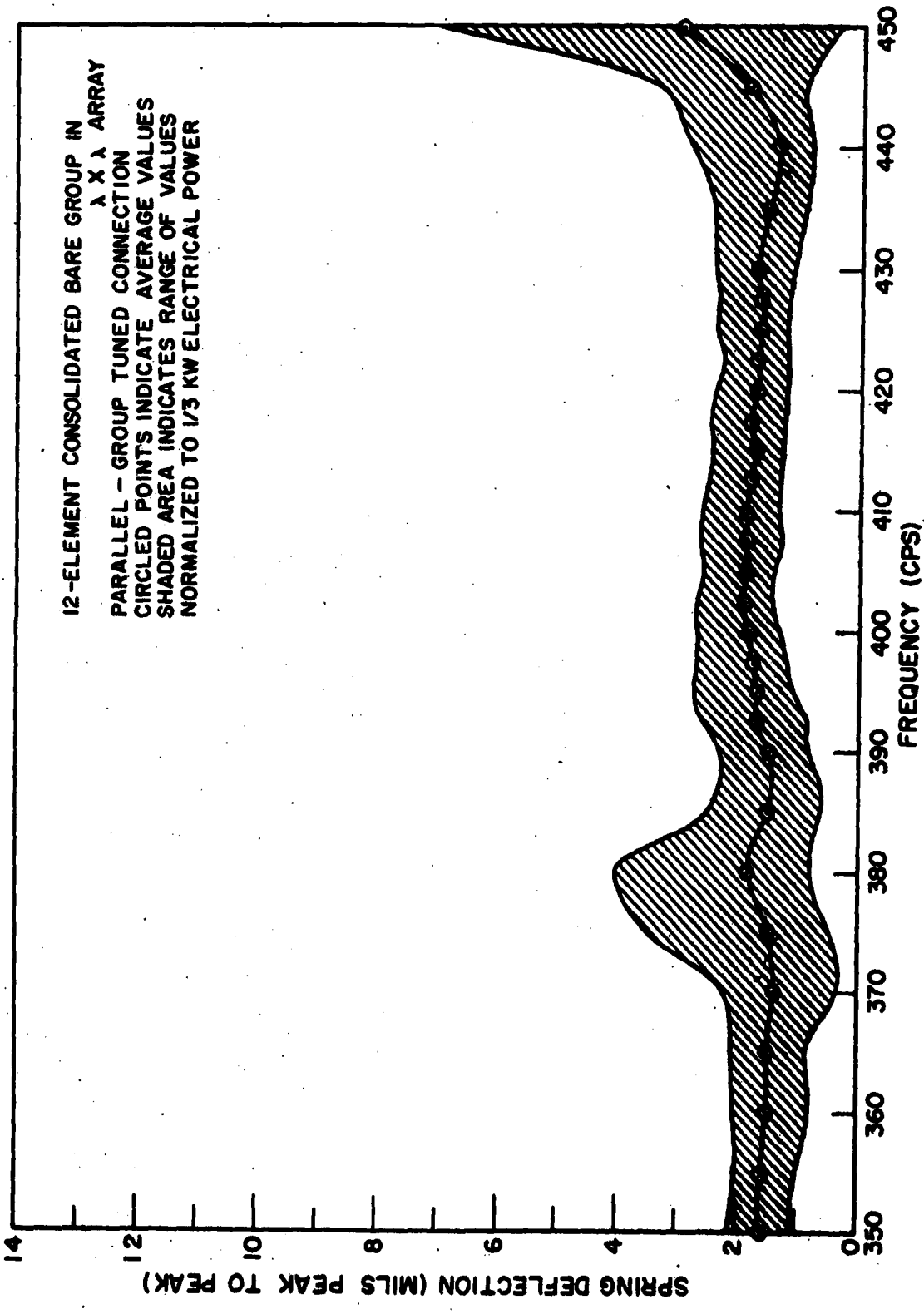

Fig. 74 - Average spring deflections

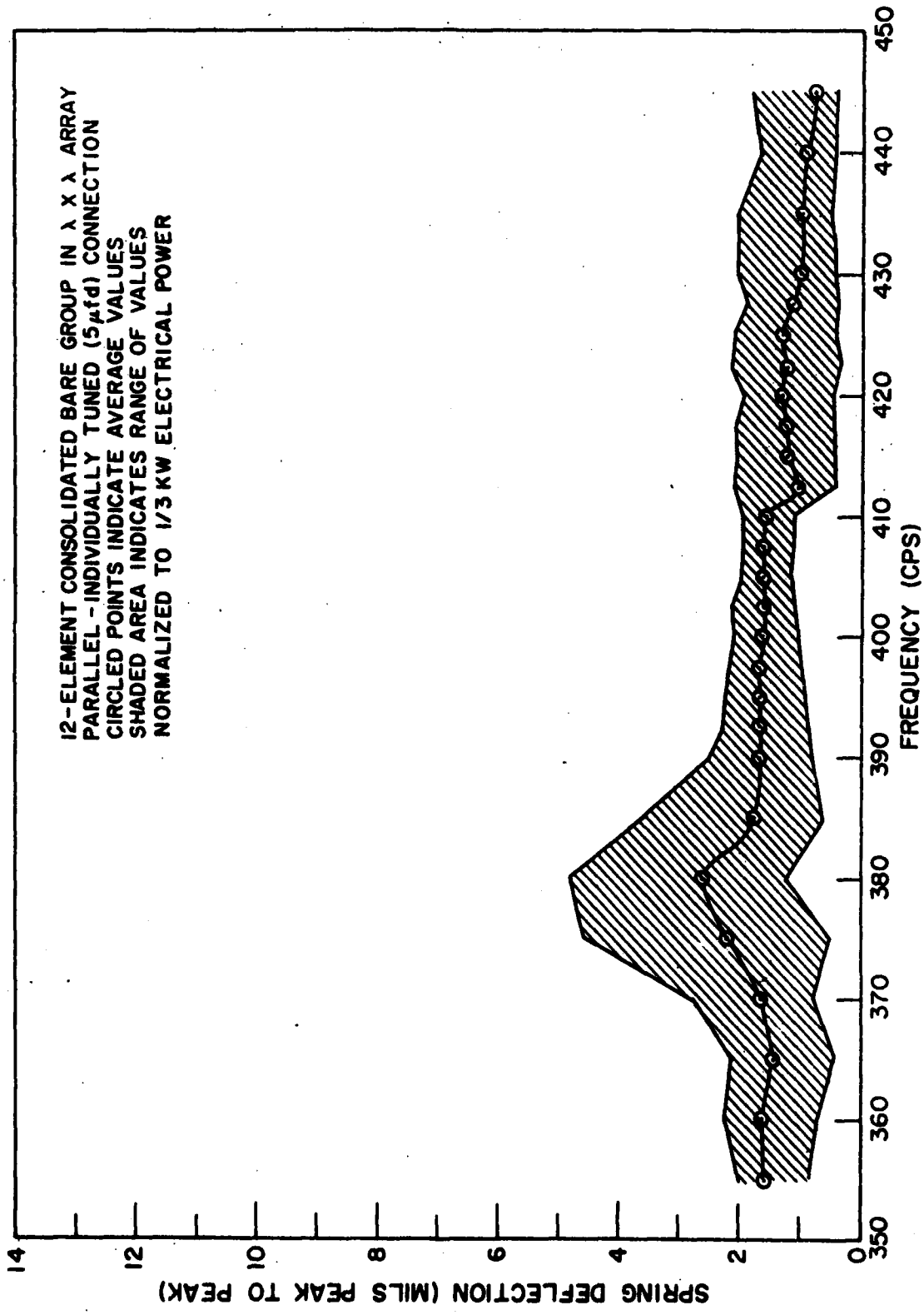

Fig. 75 - Average spring deflections

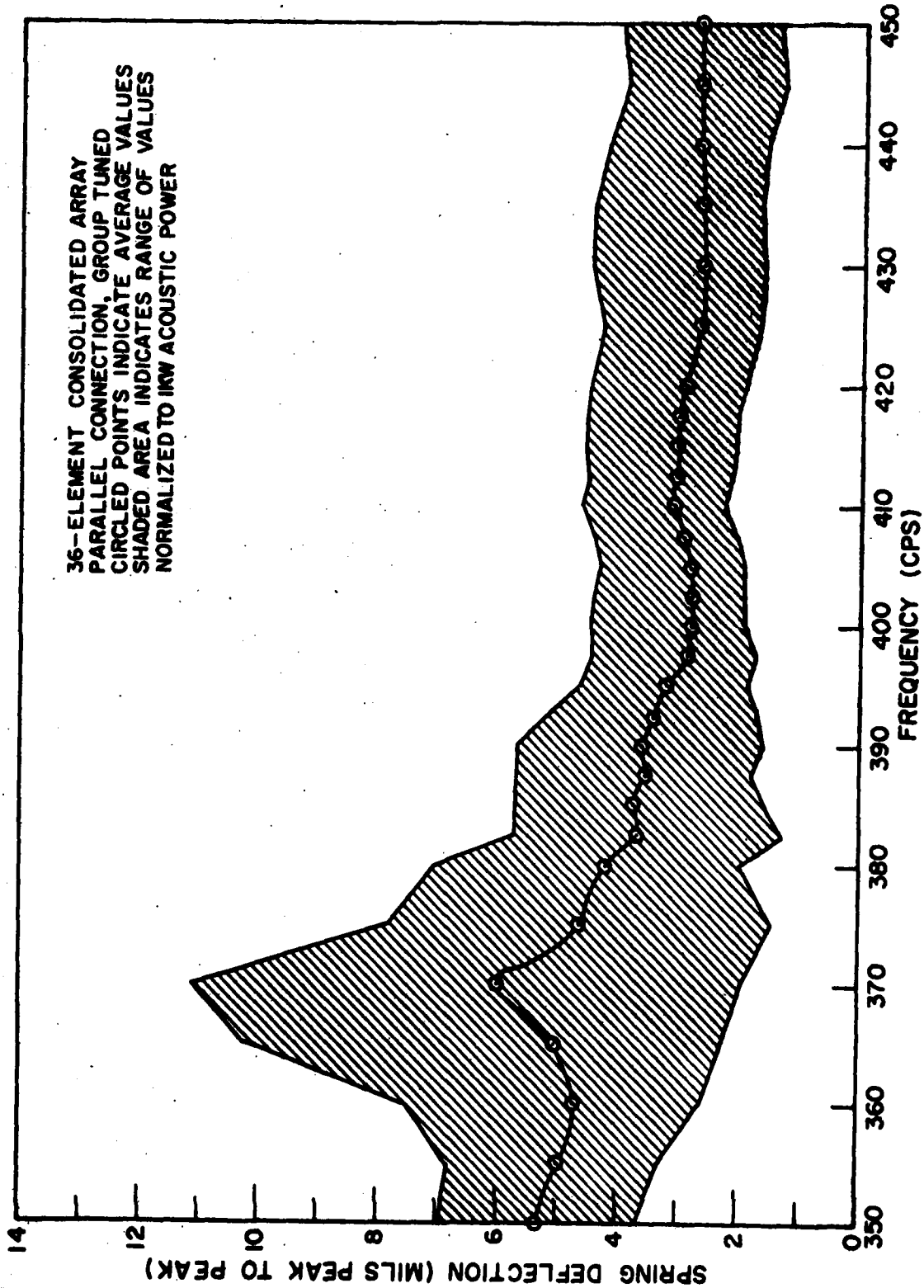

Fig. 76 - Average spring deflections

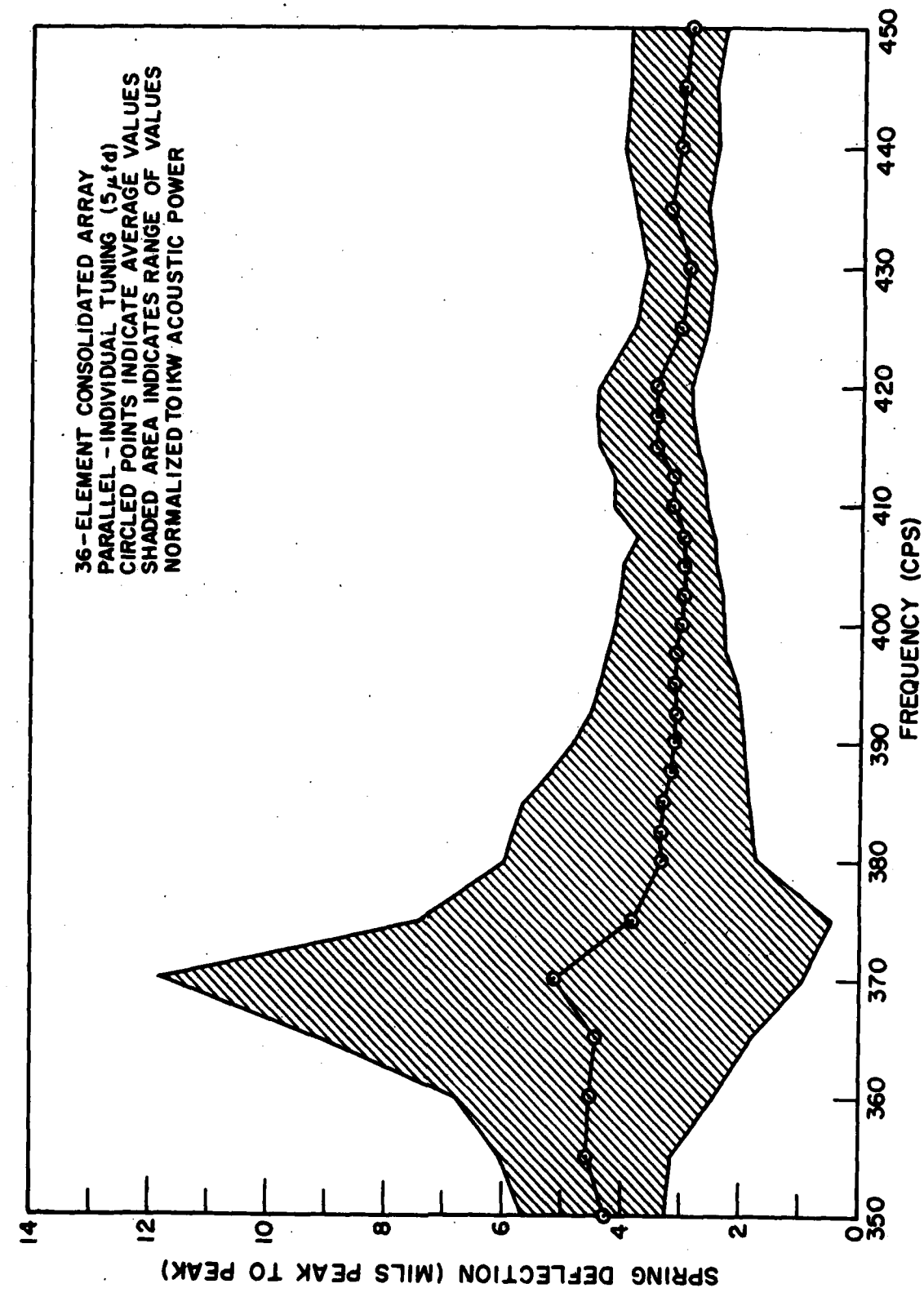

Fig. 77 - Average spring deflections

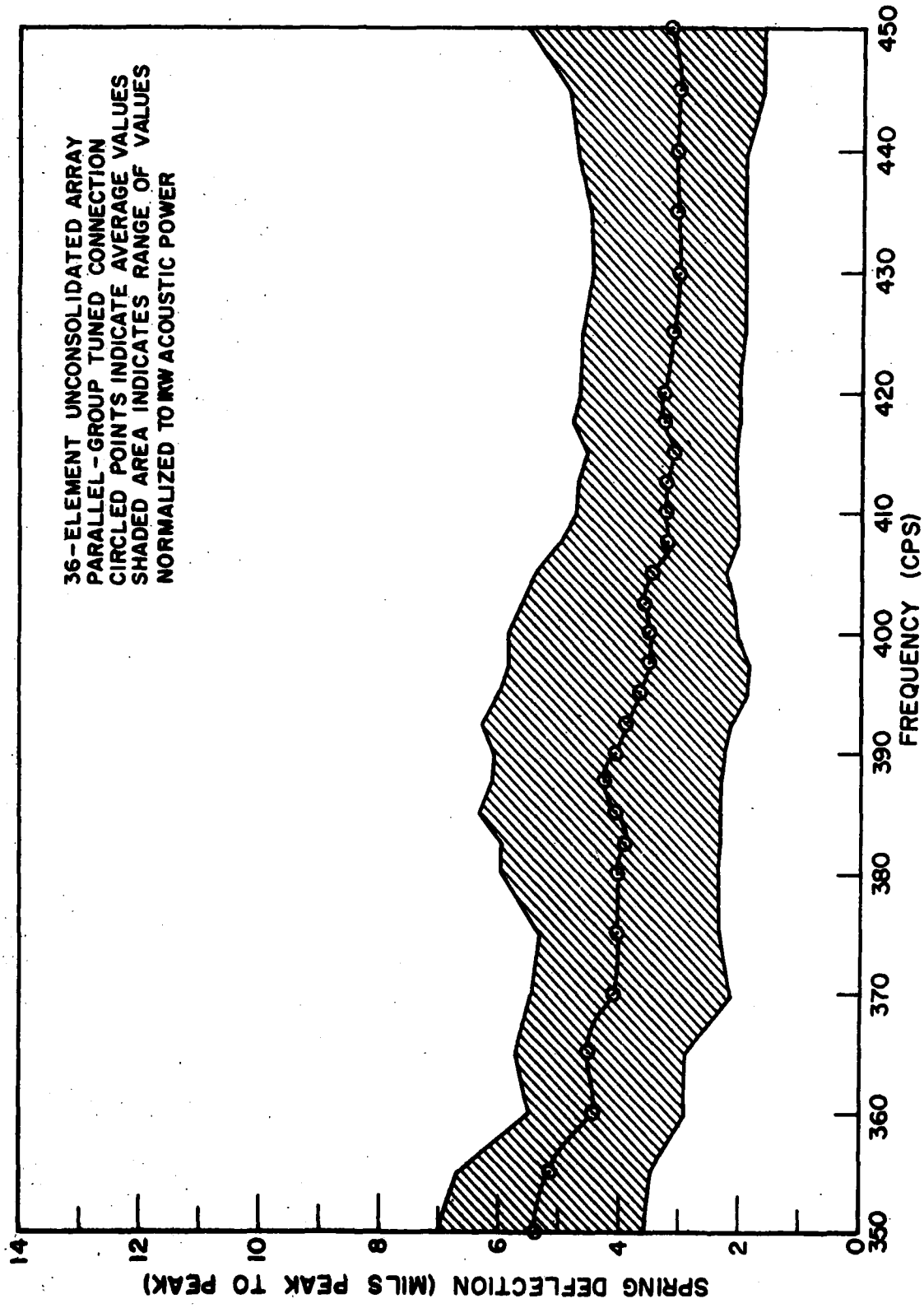

Fig. 78 - Average spring deflections

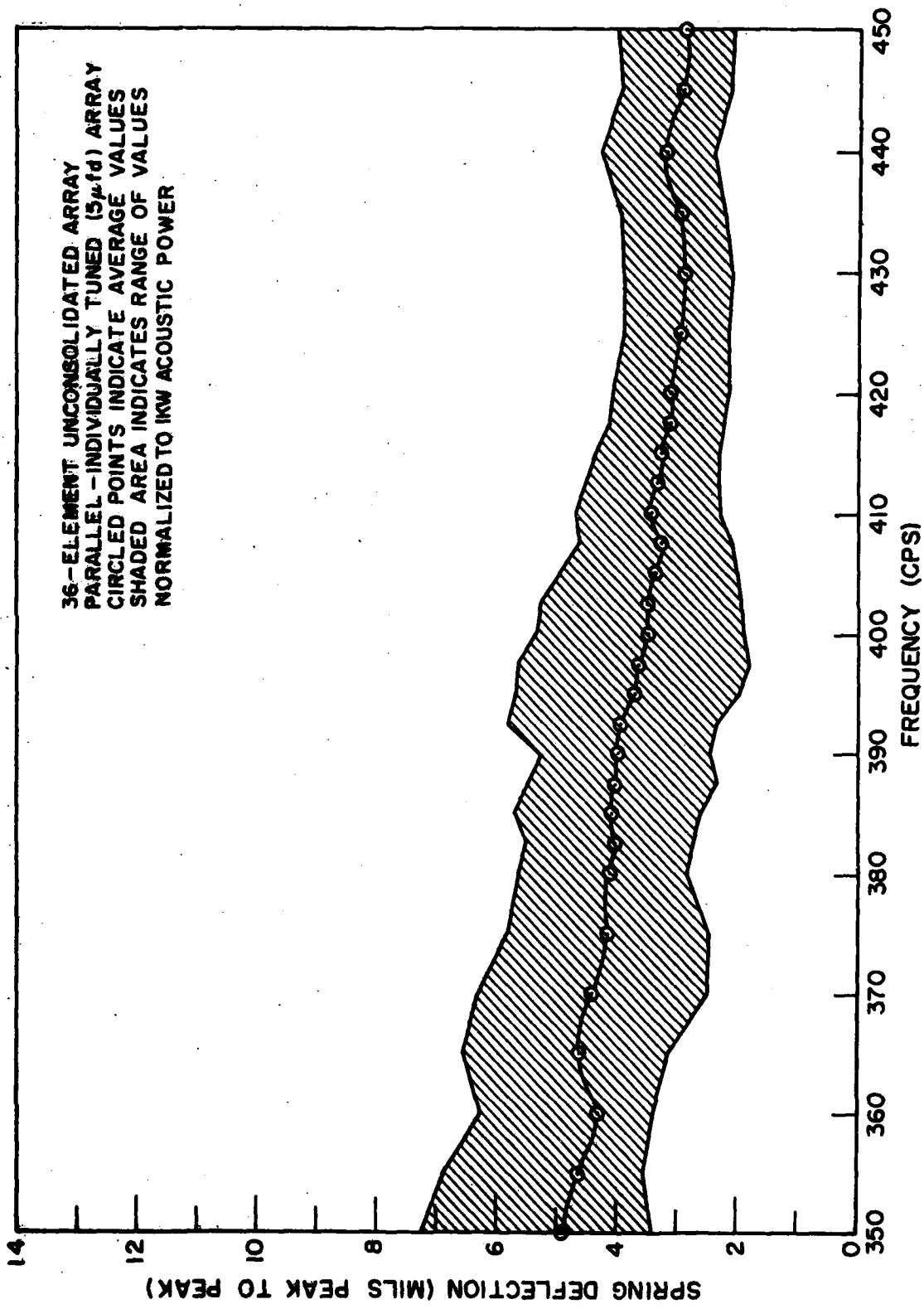

Fig. 79 - Average spring deflections

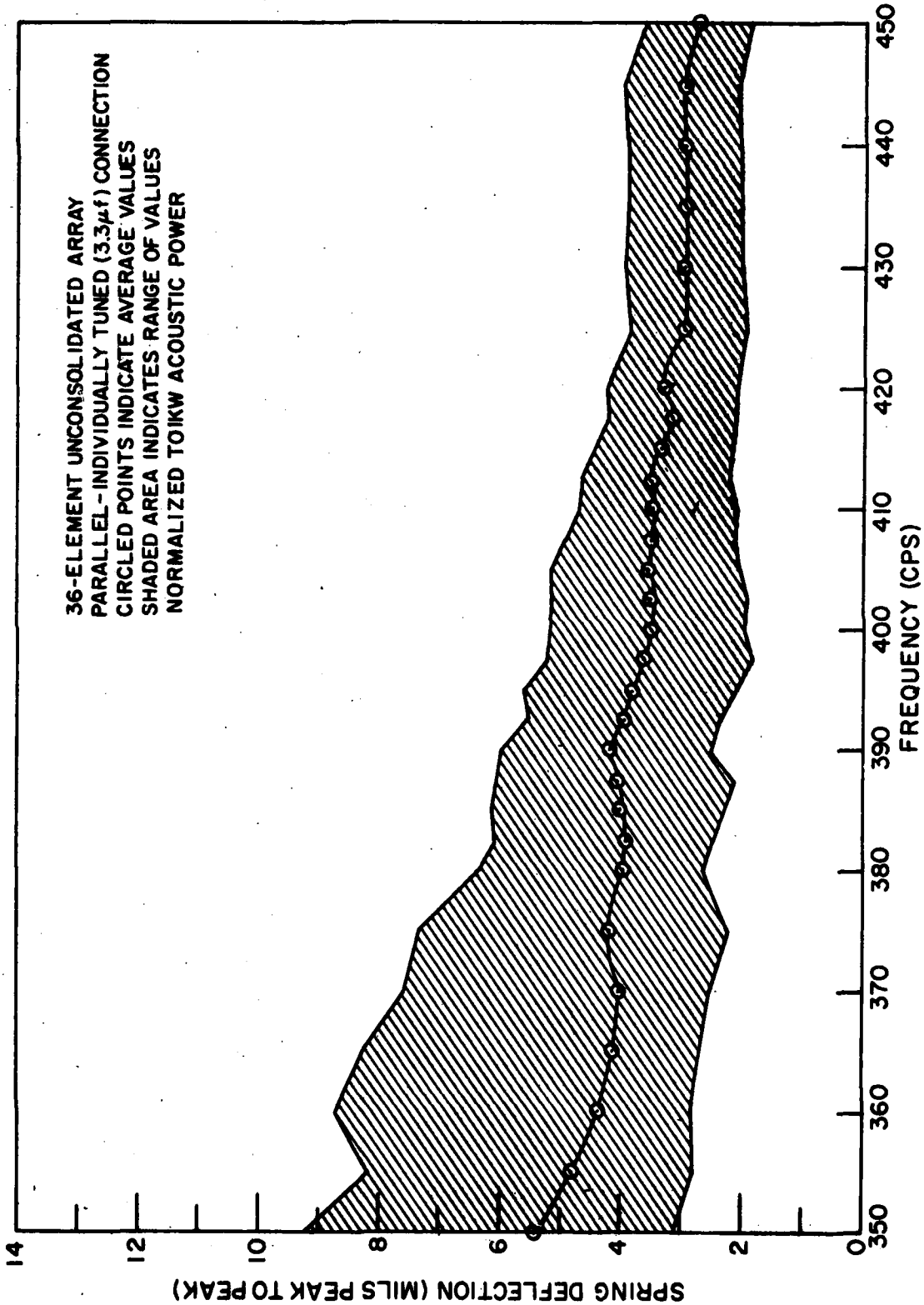

Fig. 80 - Average spring deflections

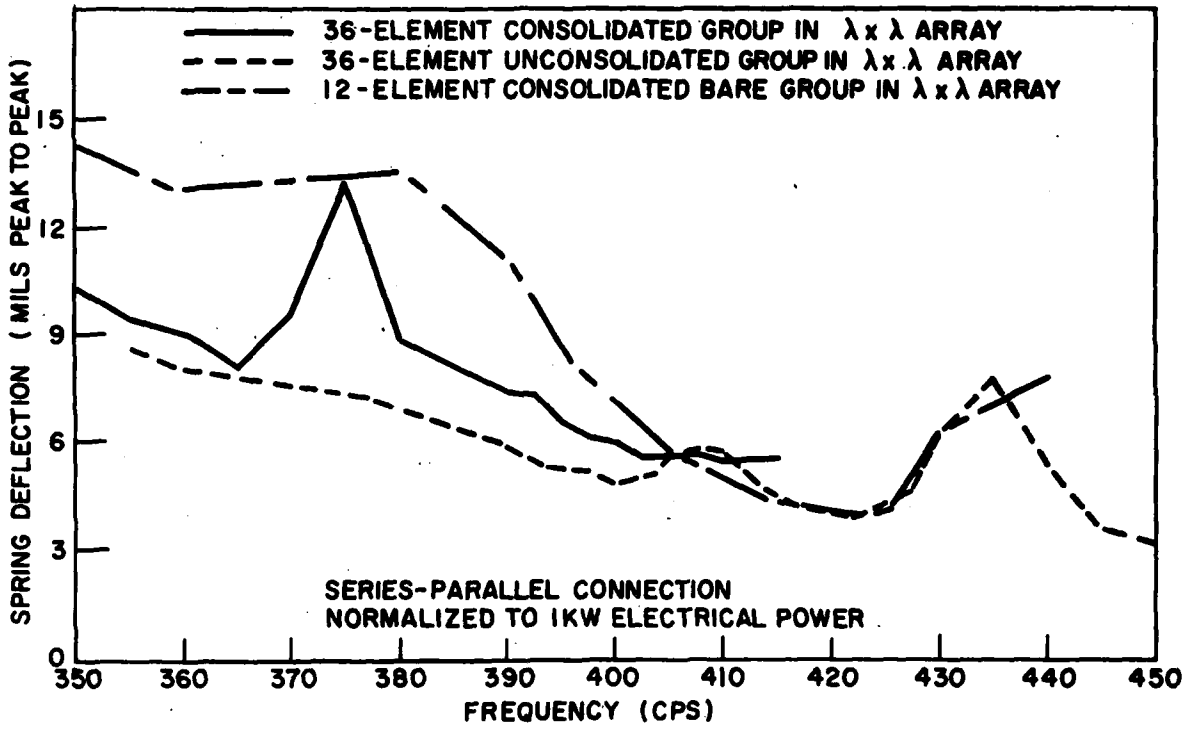

Fig. 81 - Maximum values of spring deflection

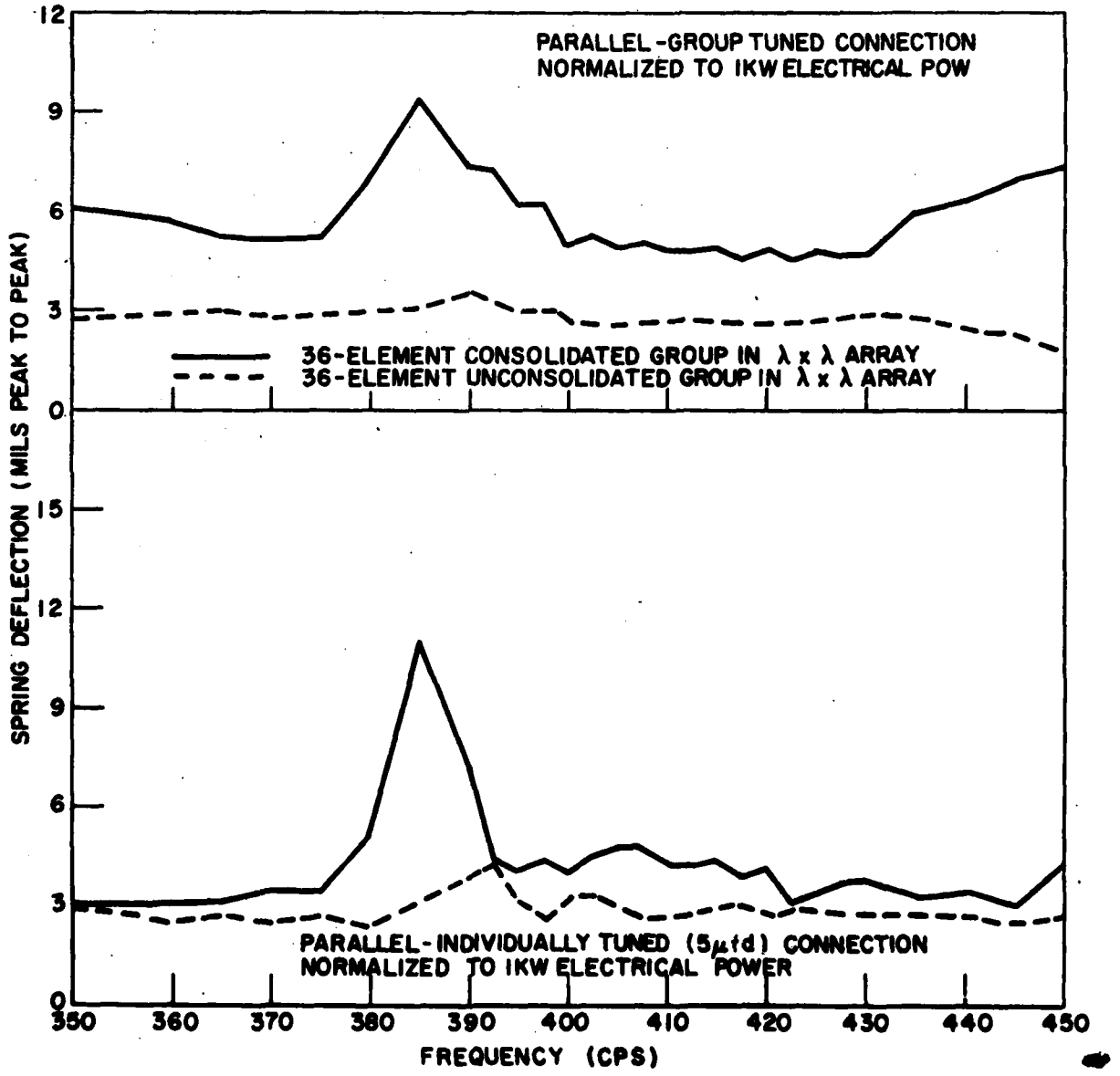

Fig. 82 - Maximum values of spring deflection

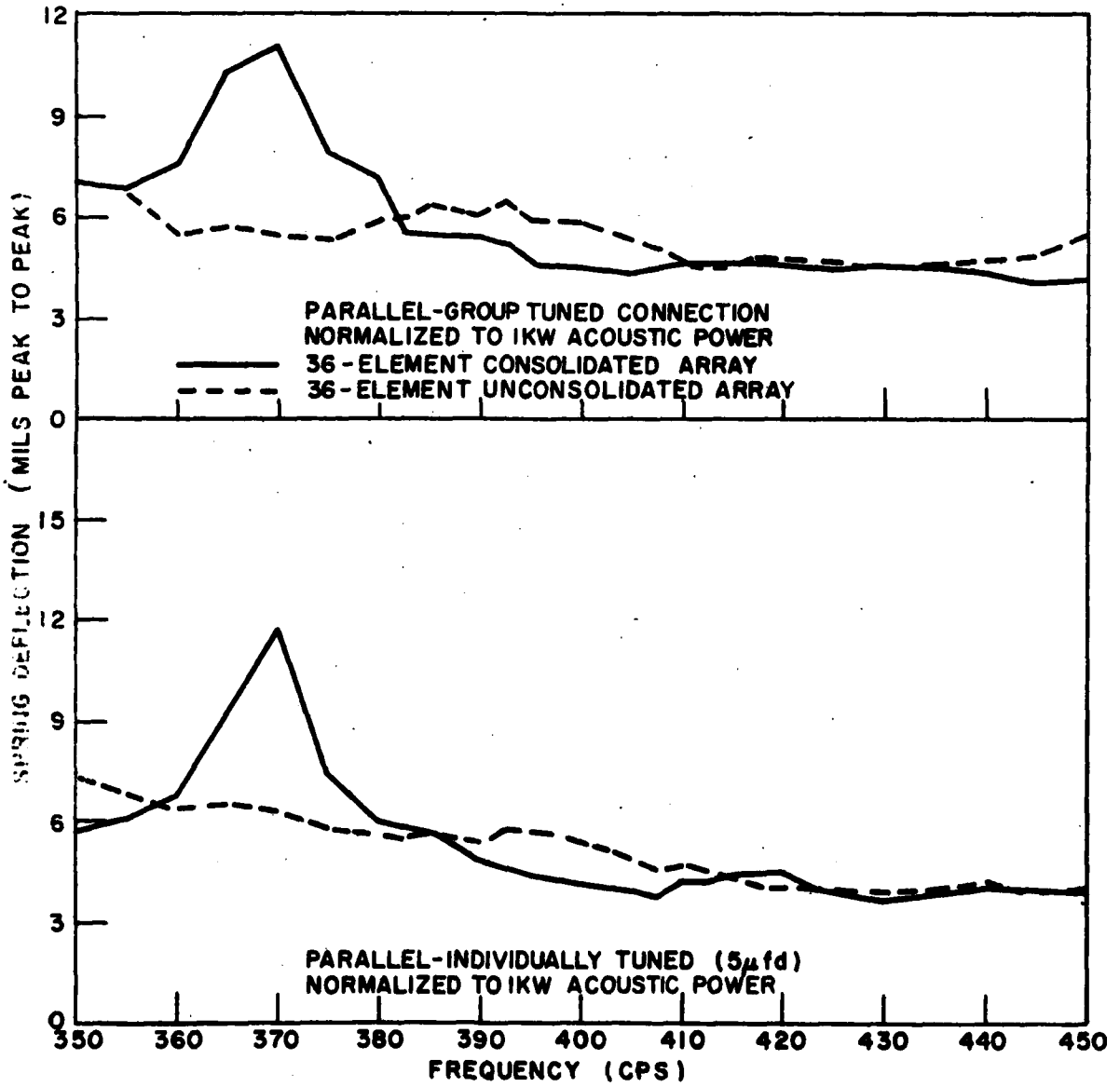

Fig. 83 - Maximum values of spring deflection

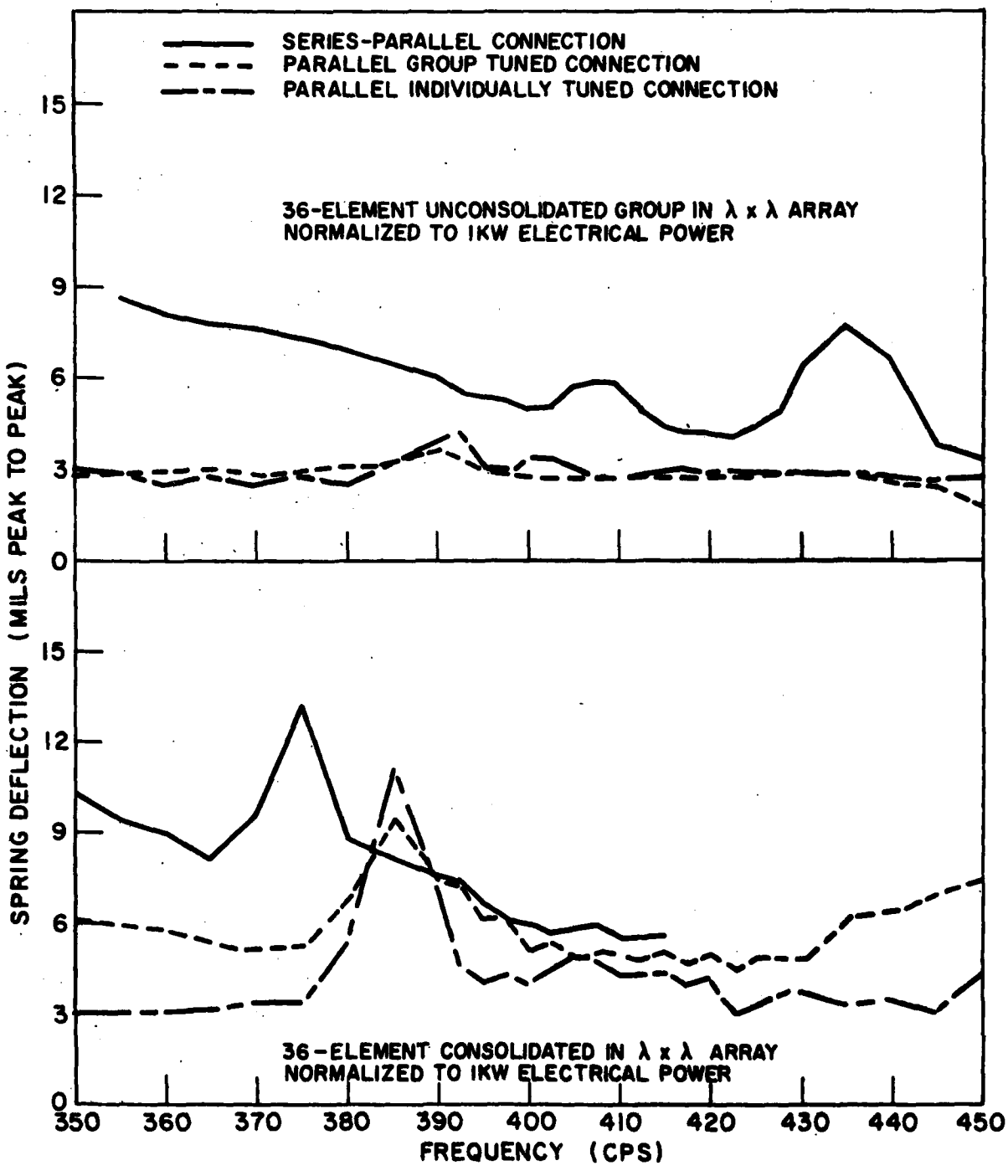

Fig. 84 - Maximum values of spring deflection

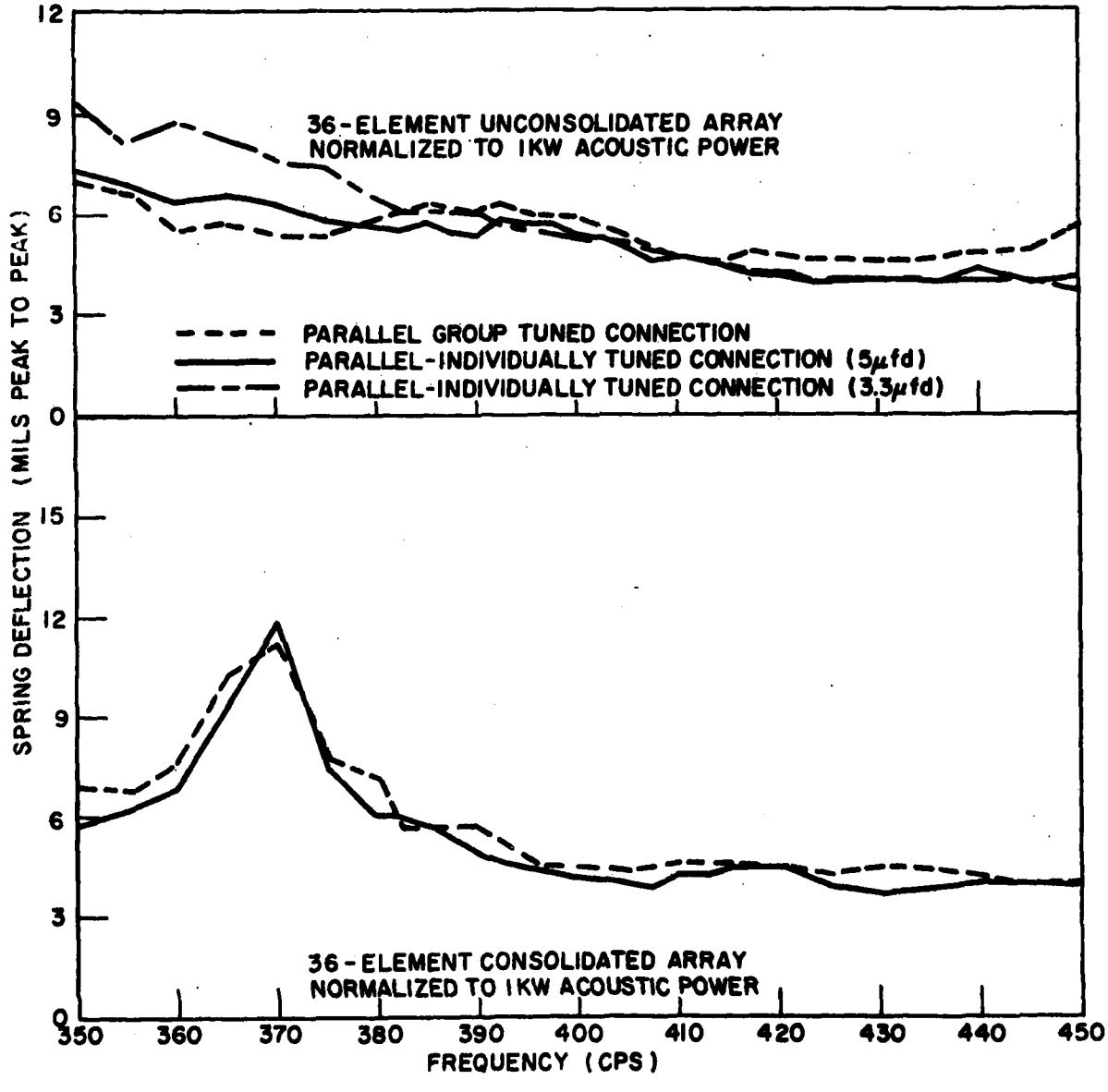

Fig. 85 - Maximum values of spring deflection

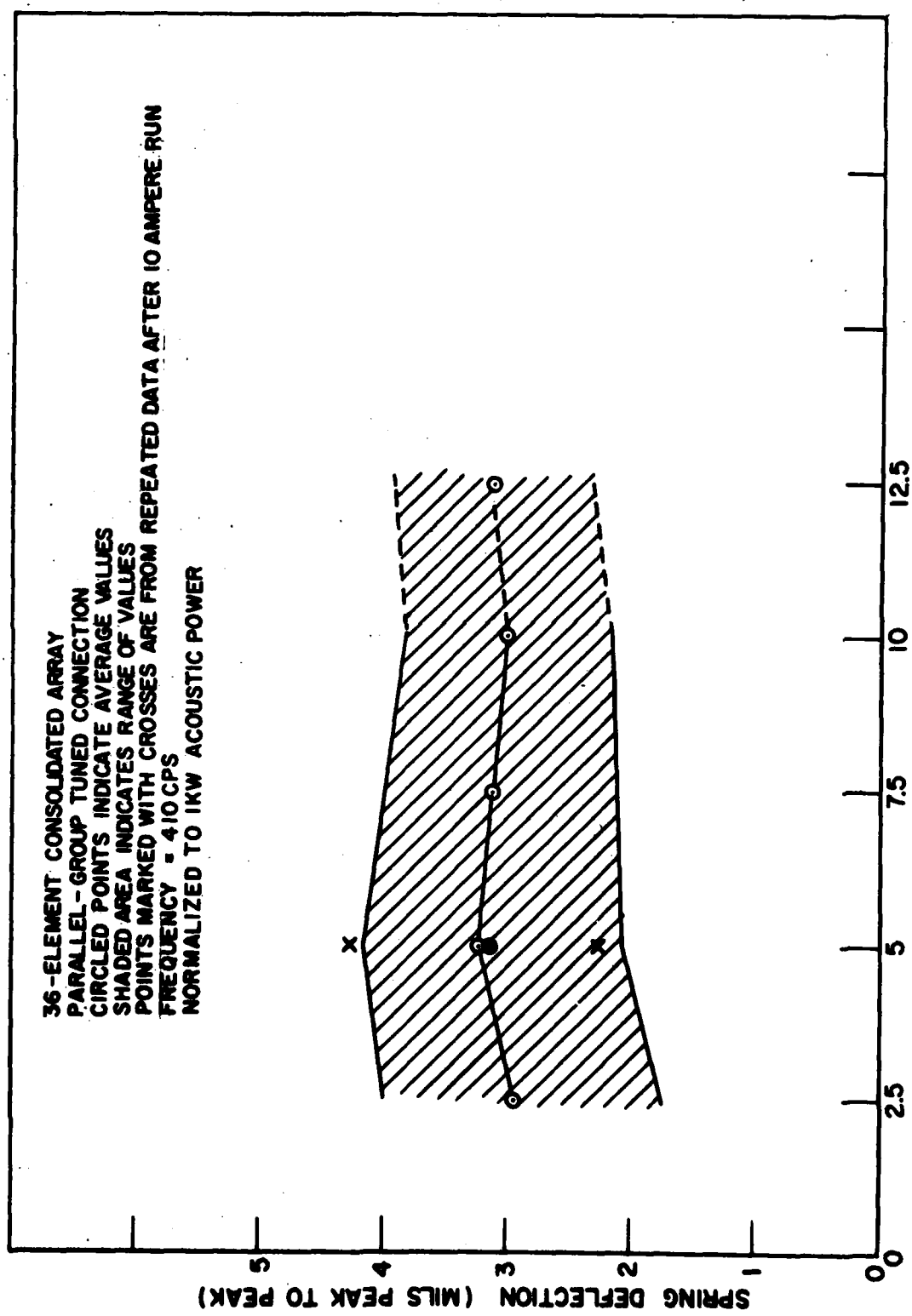

Fig. 86 - Dependence of spring deflection on operating power level

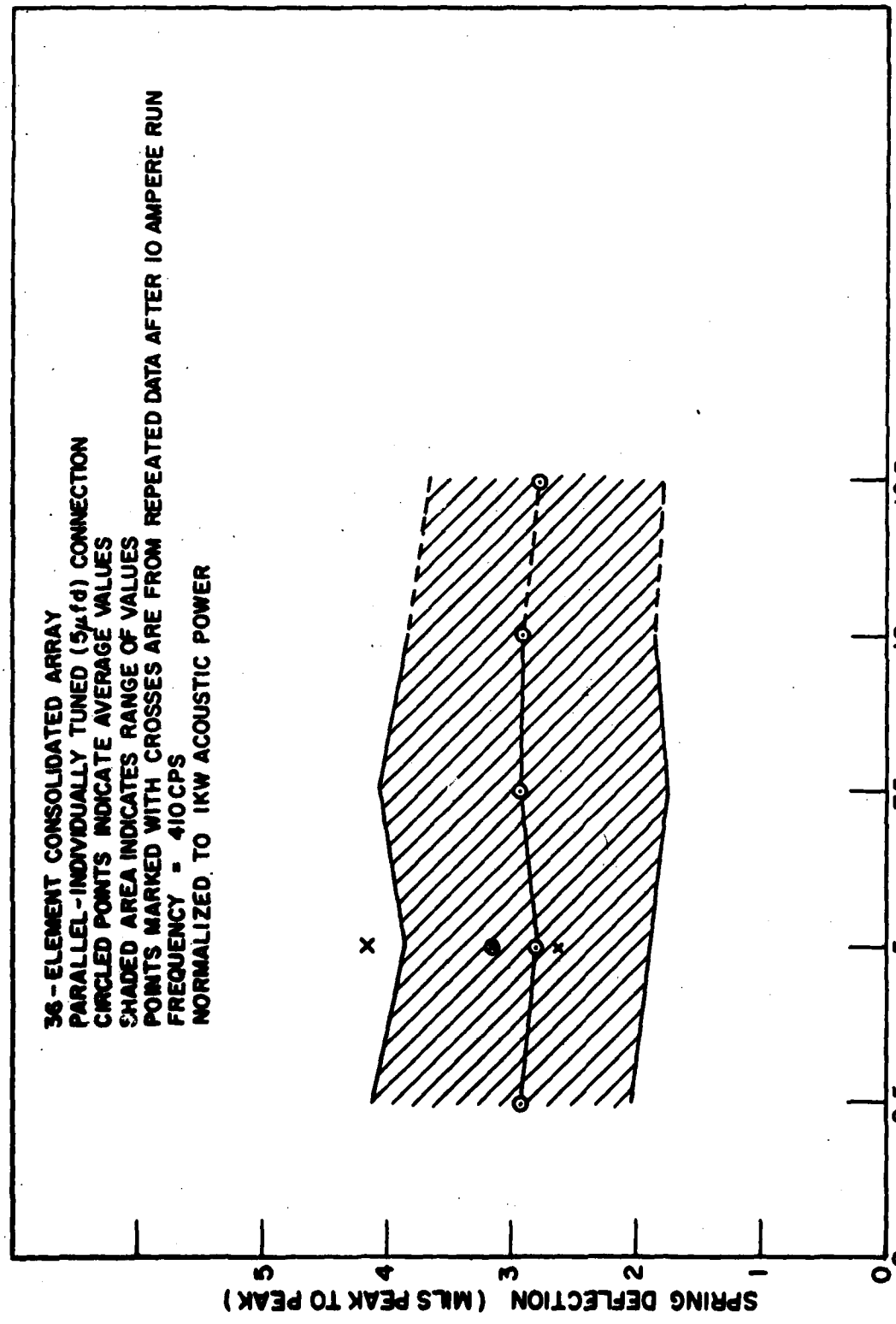

Fig. 87 - Dependence of spring deflection on operating power level

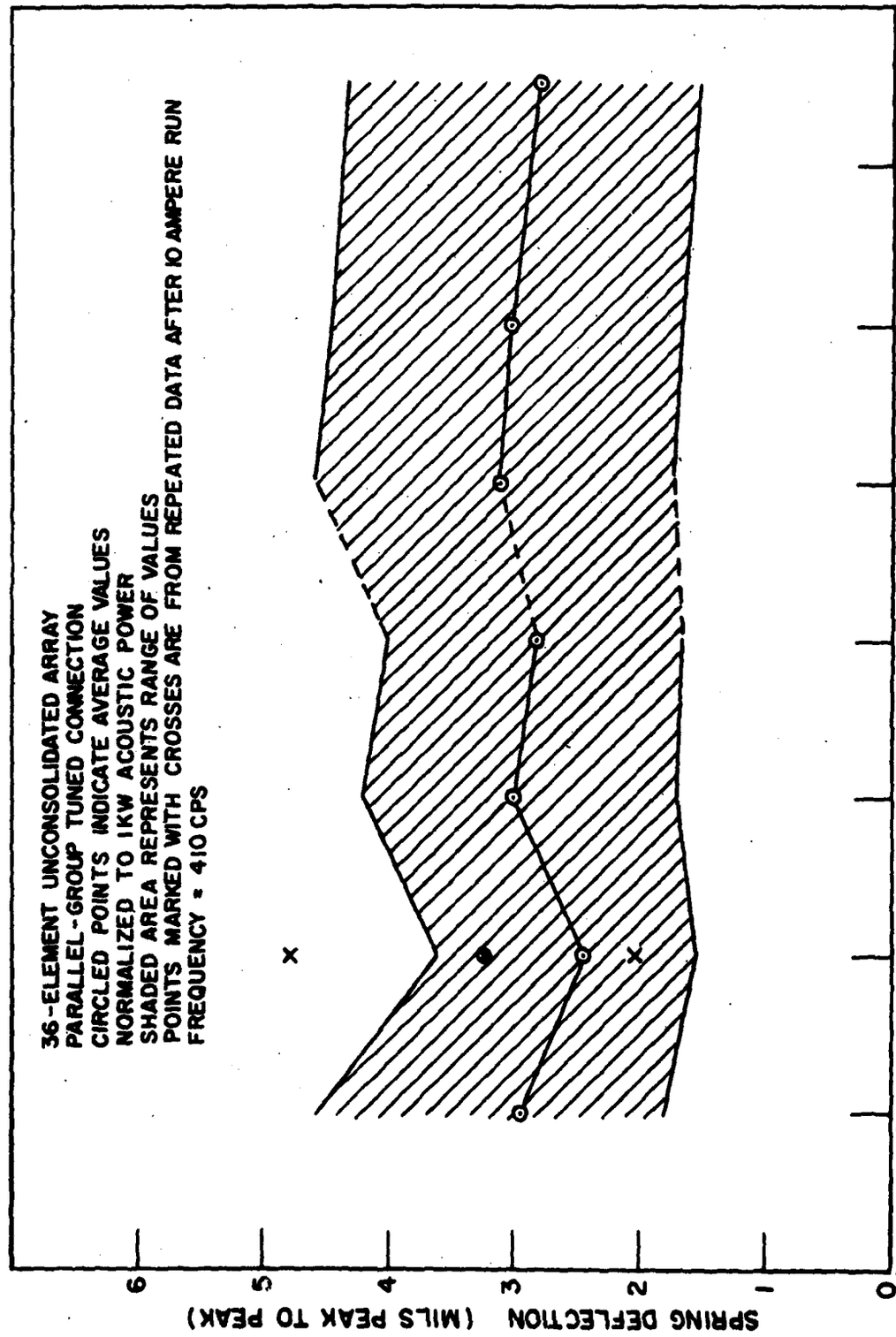

Fig. 88 - Dependence of spring deflection on operating power level

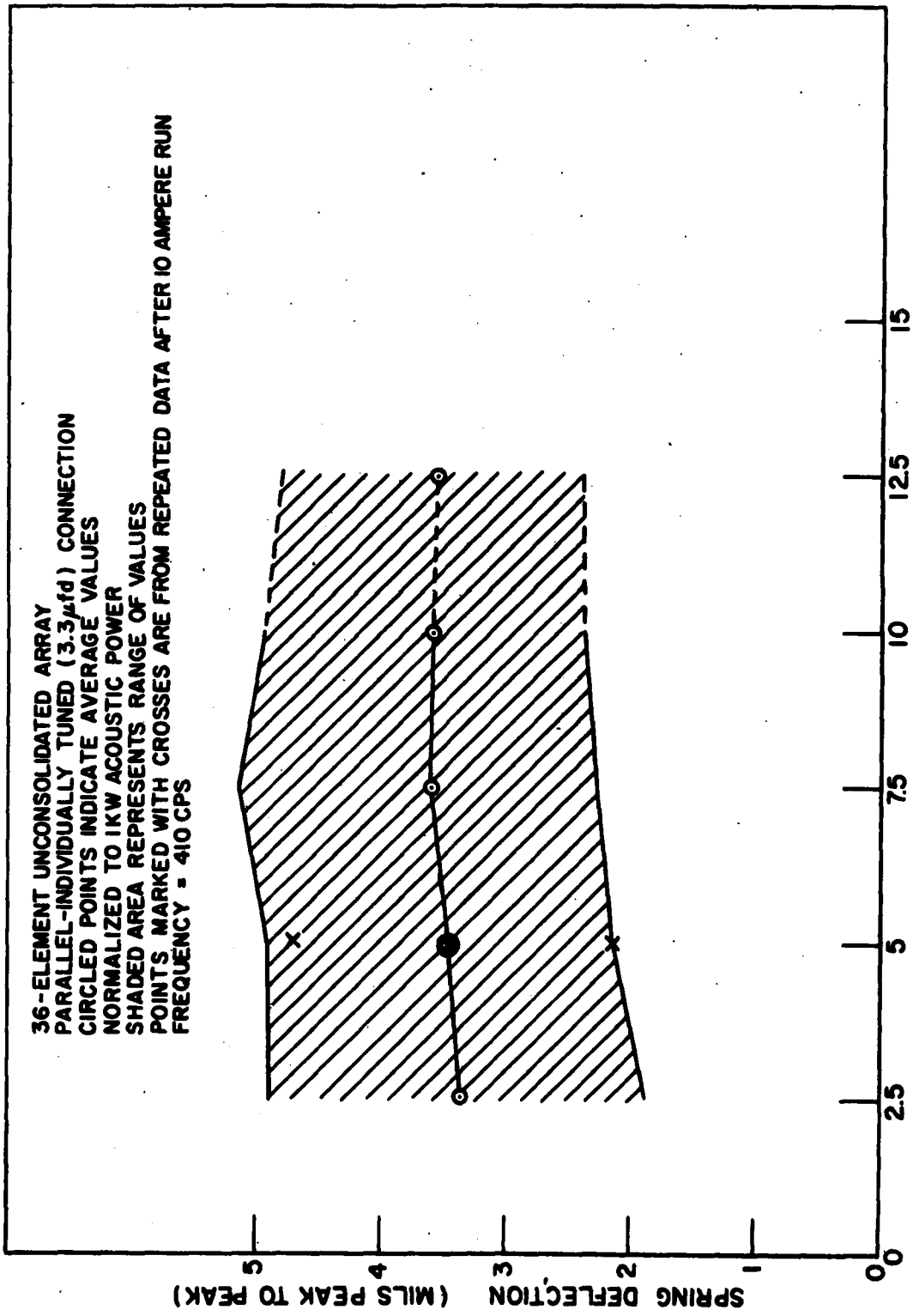

Fig. 89 - Dependence of spring deflection on operating power level

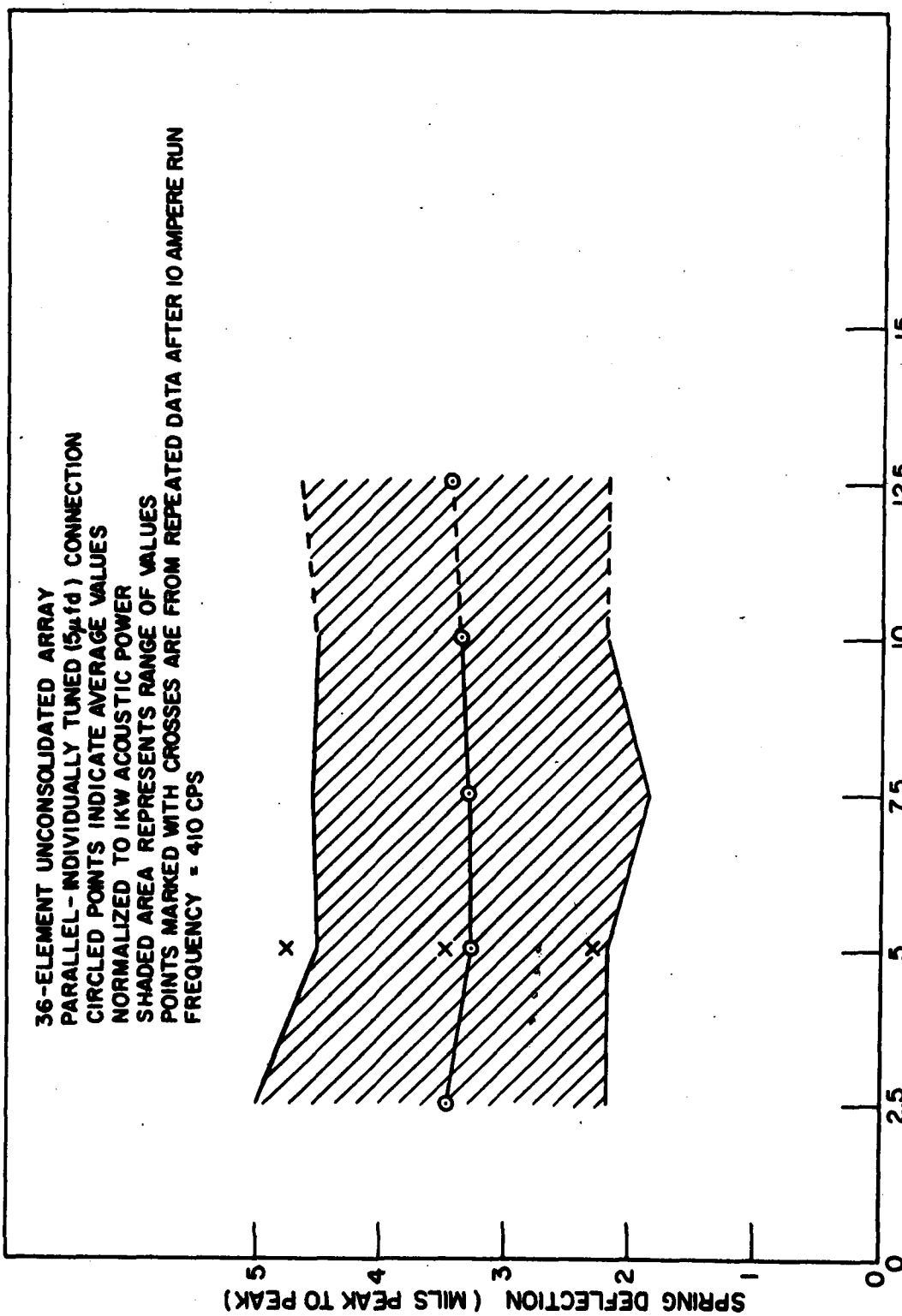

Fig. 90 - Dependence of spring deflection on operating power level

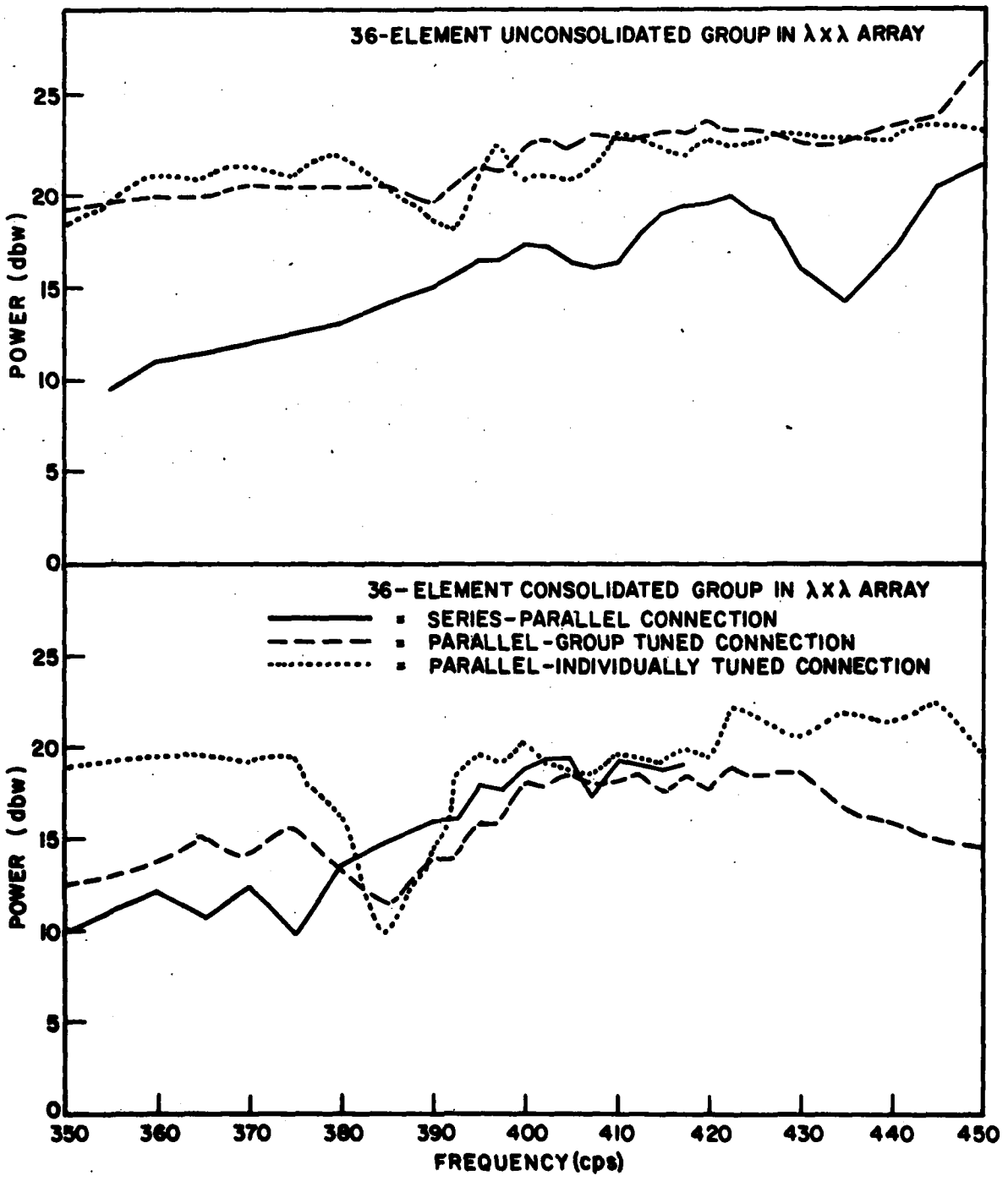

Fig. 91 - Acoustic power per element with array limited to a maximum spring deflection of ten mils peak to peak

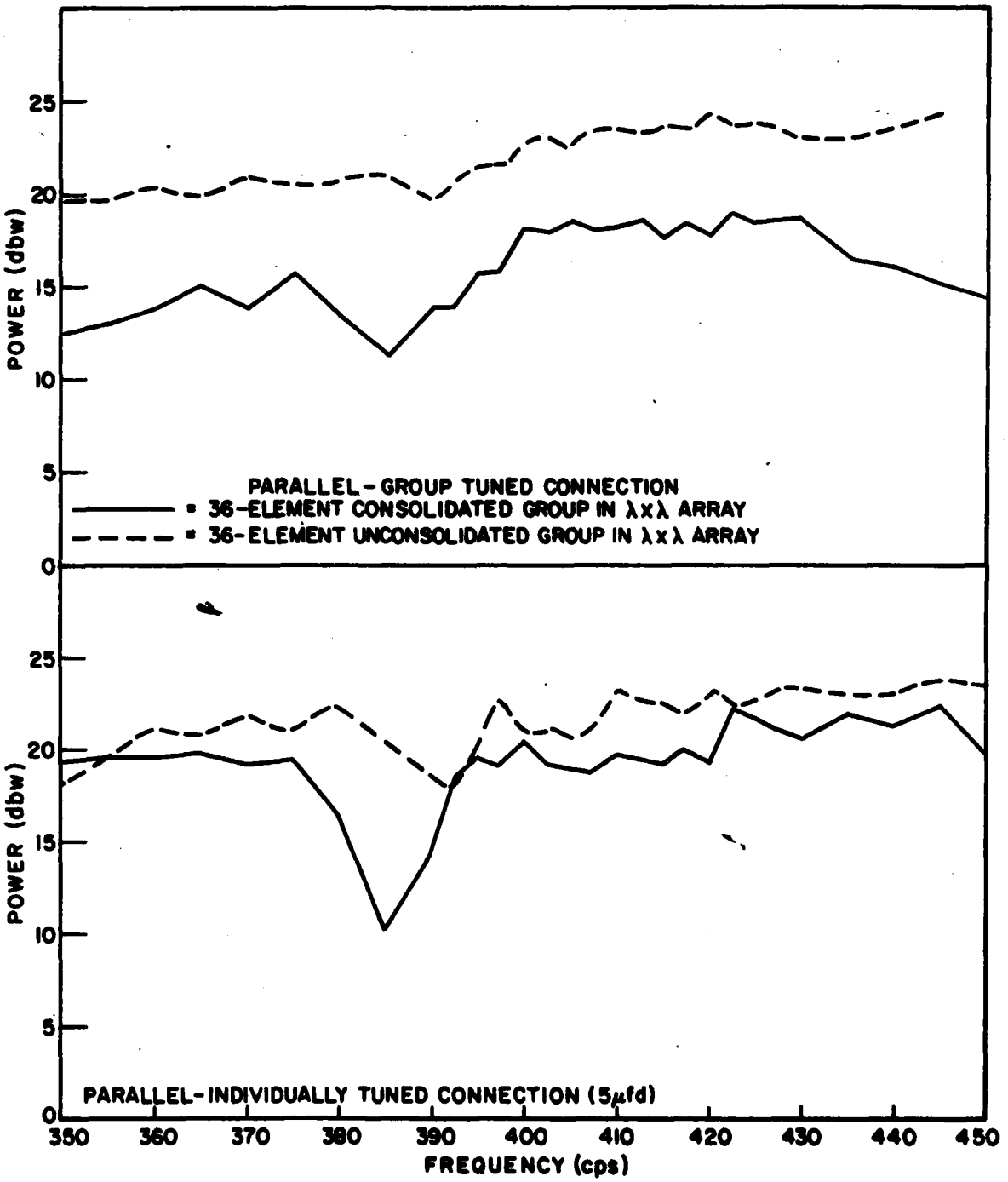

Fig. 92 - Acoustic power per element with array limited to a maximum spring deflection of ten mils peak to peak

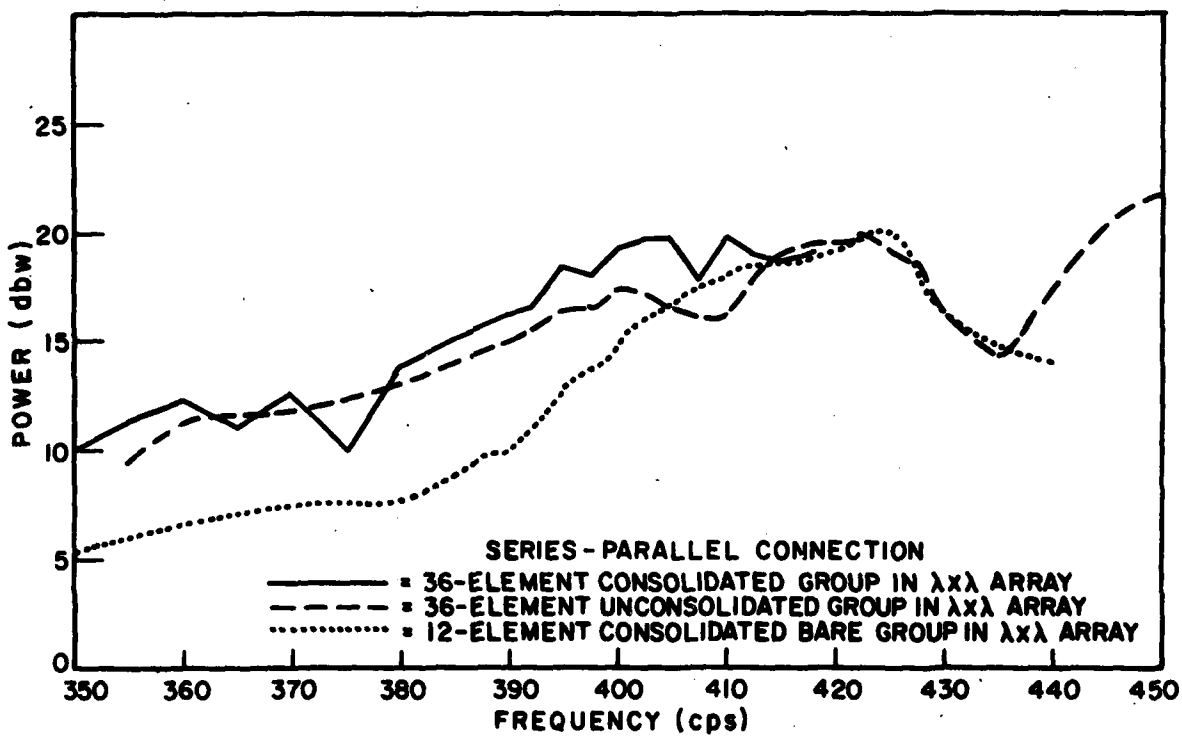

Fig. 93 - Acoustic power per element with array limited to a maximum spring deflection of ten mils peak to peak

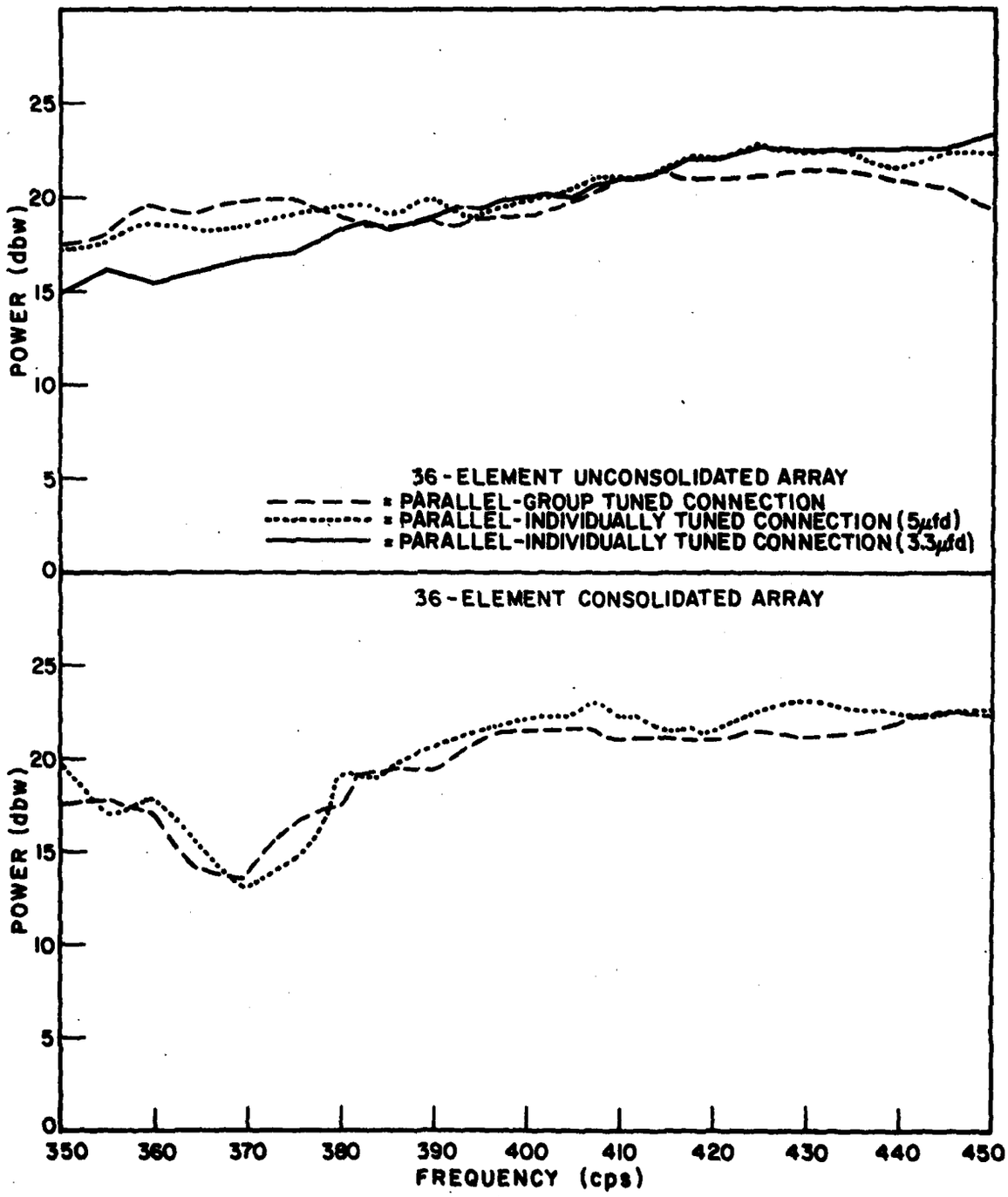

Fig. 94 - Acoustic power per element with array limited to a maximum spring deflection of ten mils peak to peak

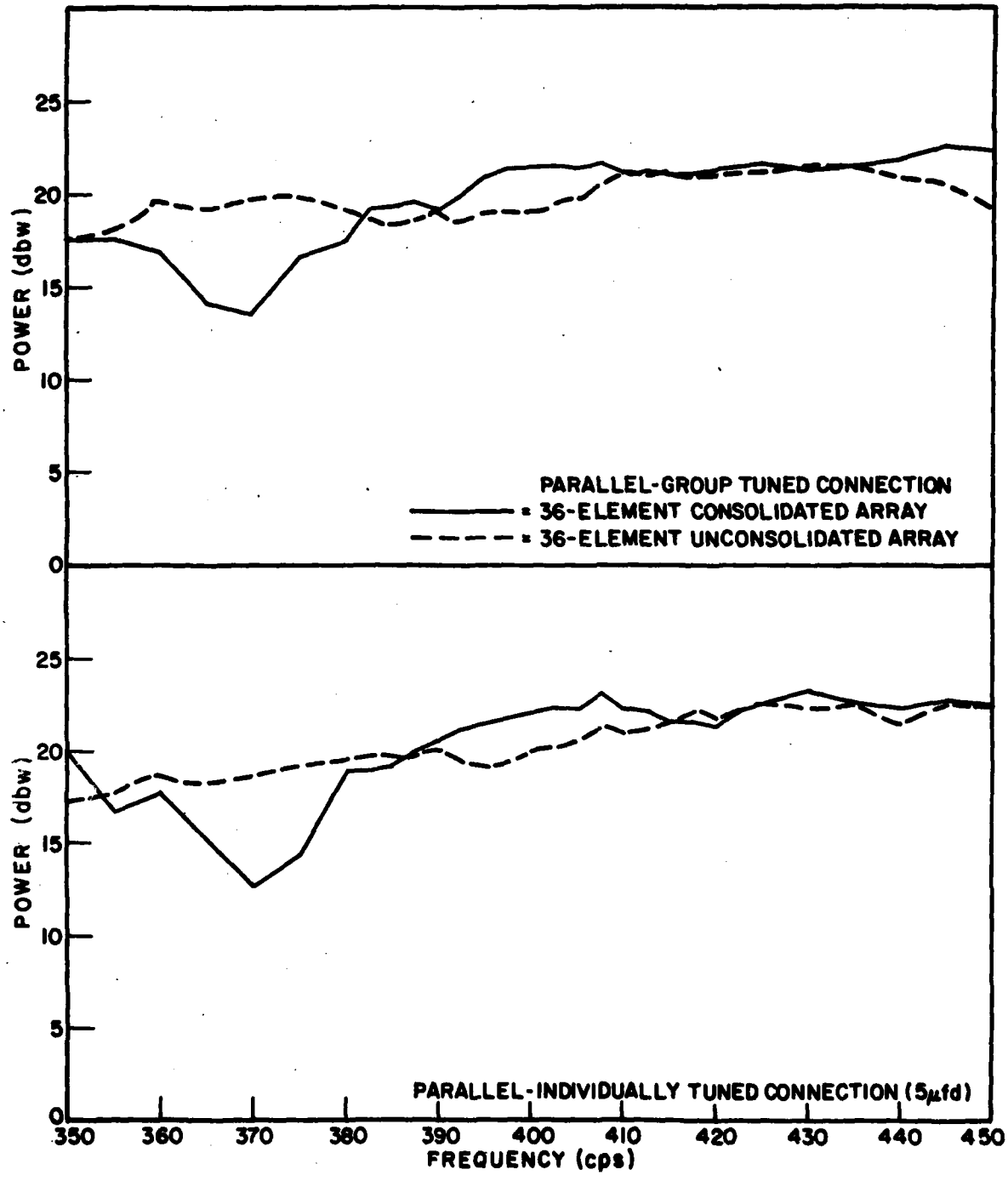

Fig. 95 - Acoustic power per element with array limited to a maximum spring deflection of ten mils peak to peak

CONFIDENTIAL

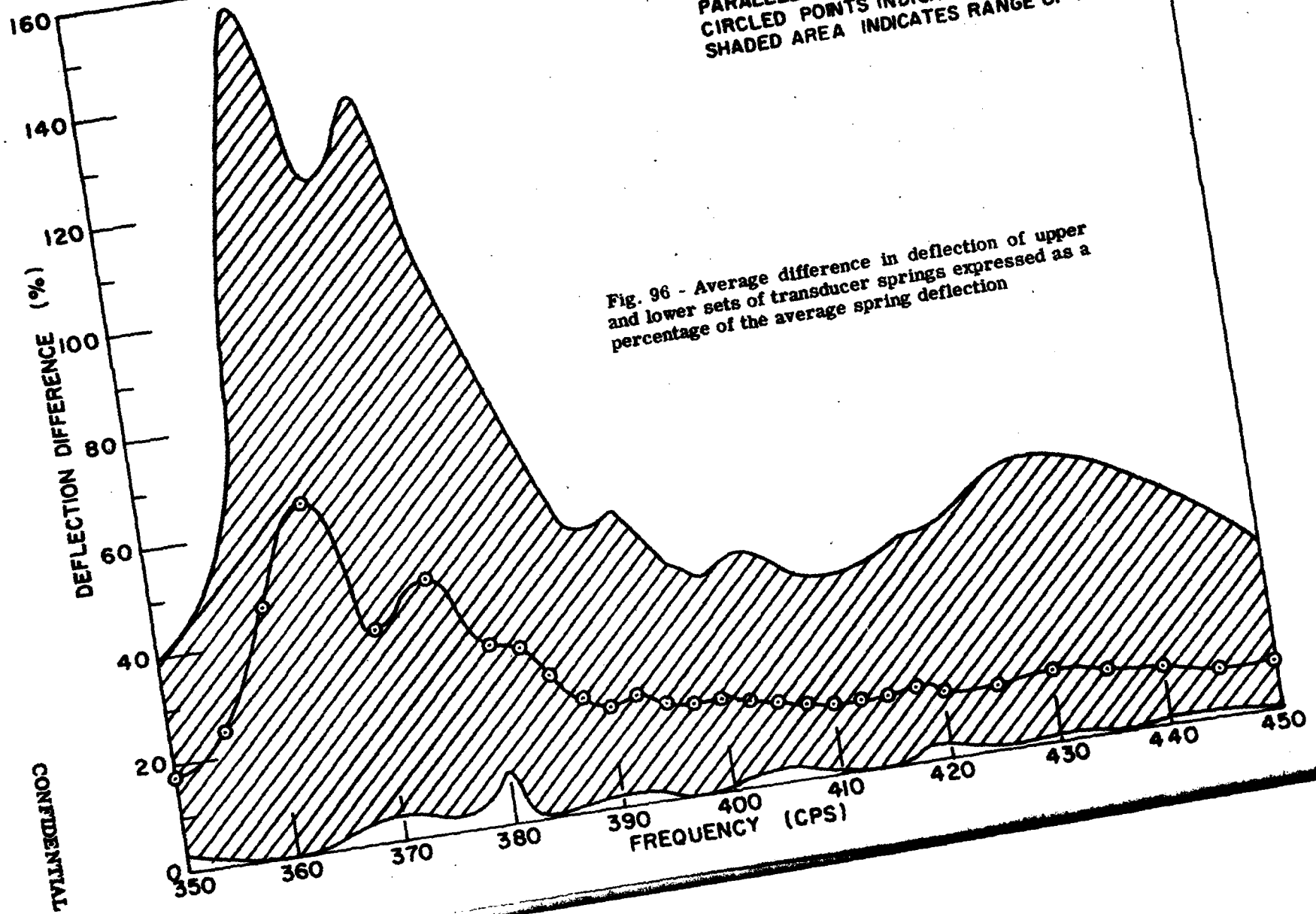

Fig. 96 - Average difference in deflection of upper and lower sets of transducer springs expressed as a percentage of the average spring deflection

CONFIDENTIAL

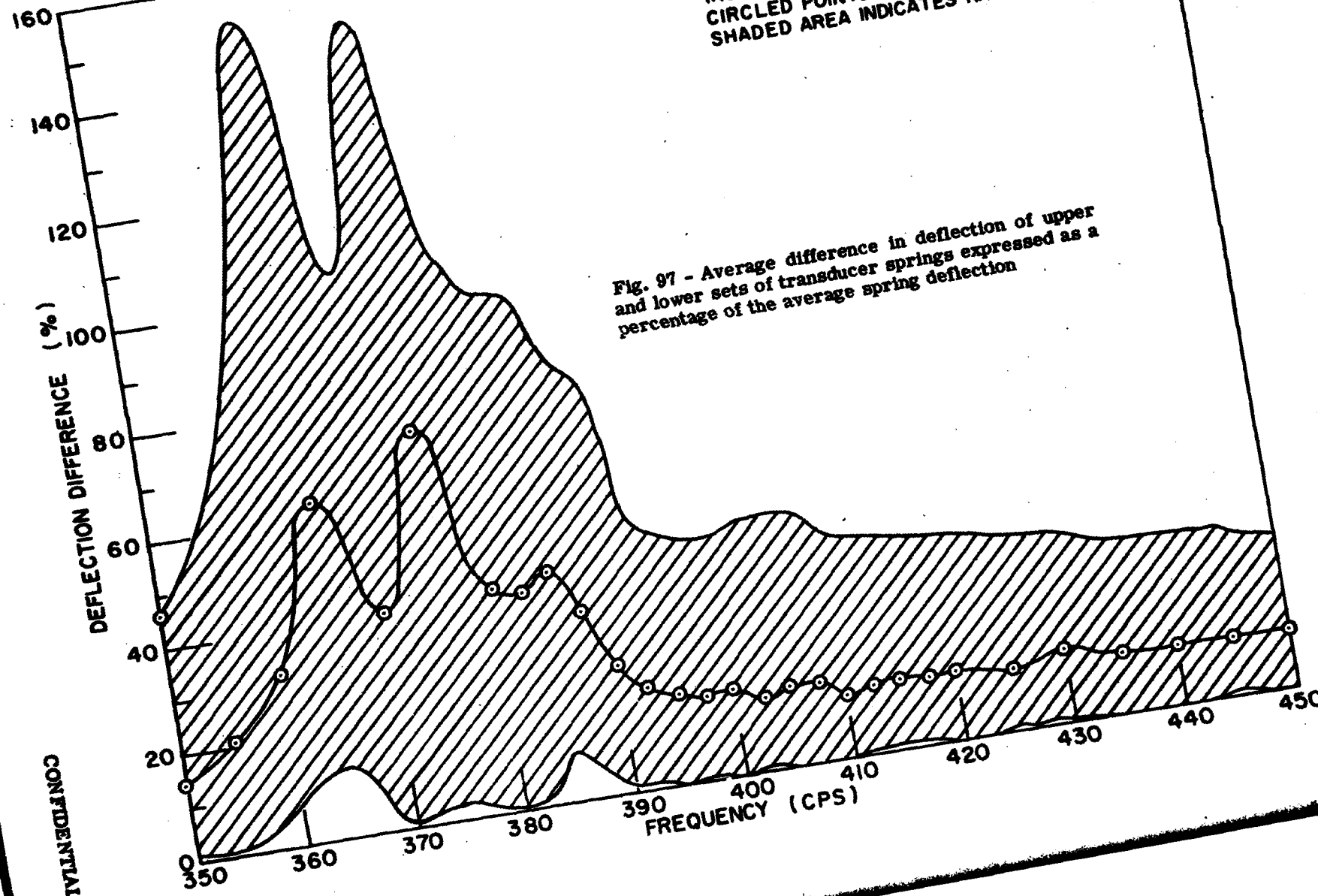

Fig. 97 - Average difference in deflection of upper and lower sets of transducer springs expressed as a percentage of the average spring deflection

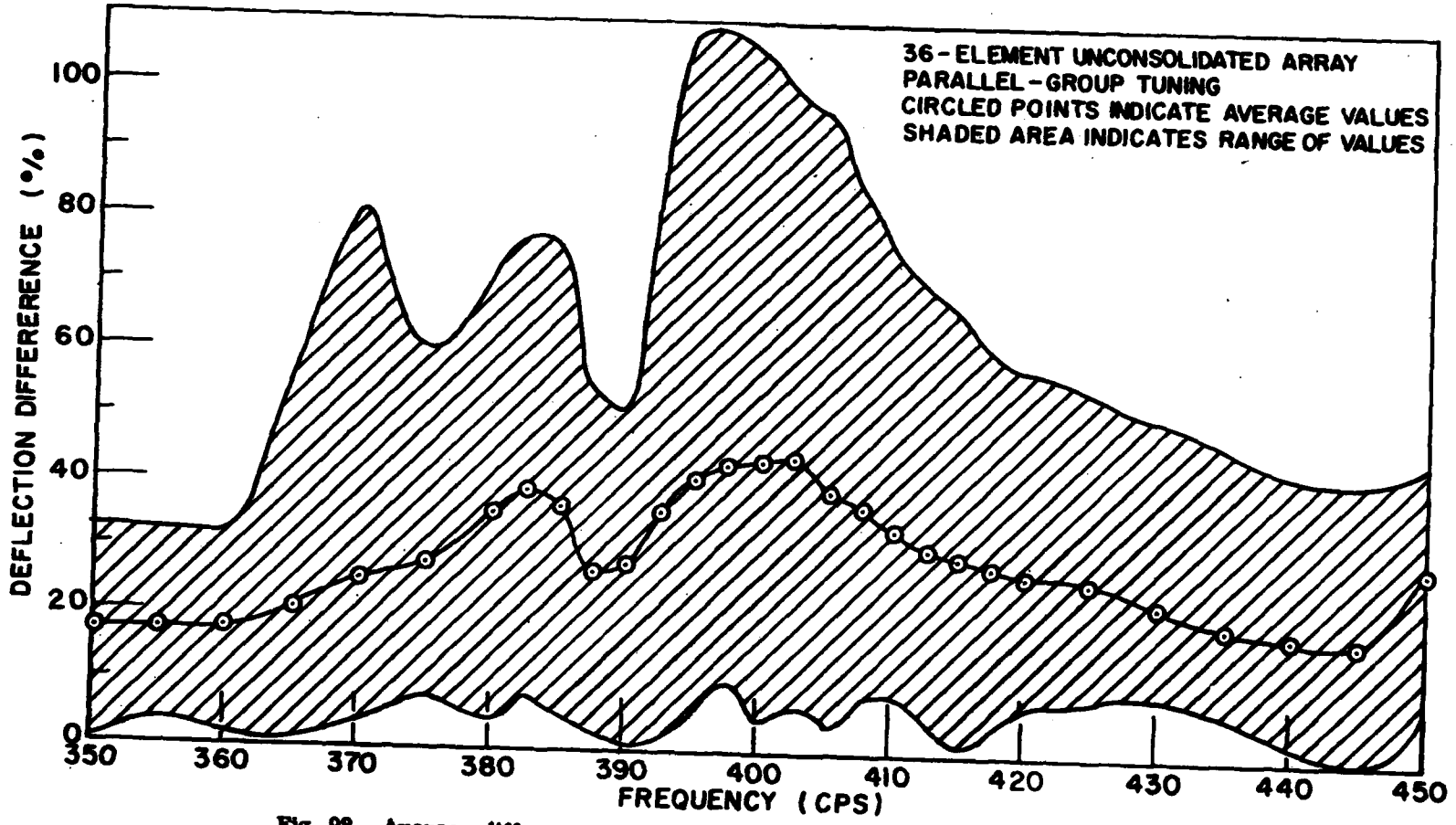

Fig. 98 - Average difference in deflection of upper and lower sets of transducer springs expressed as a percentage of the average spring deflection

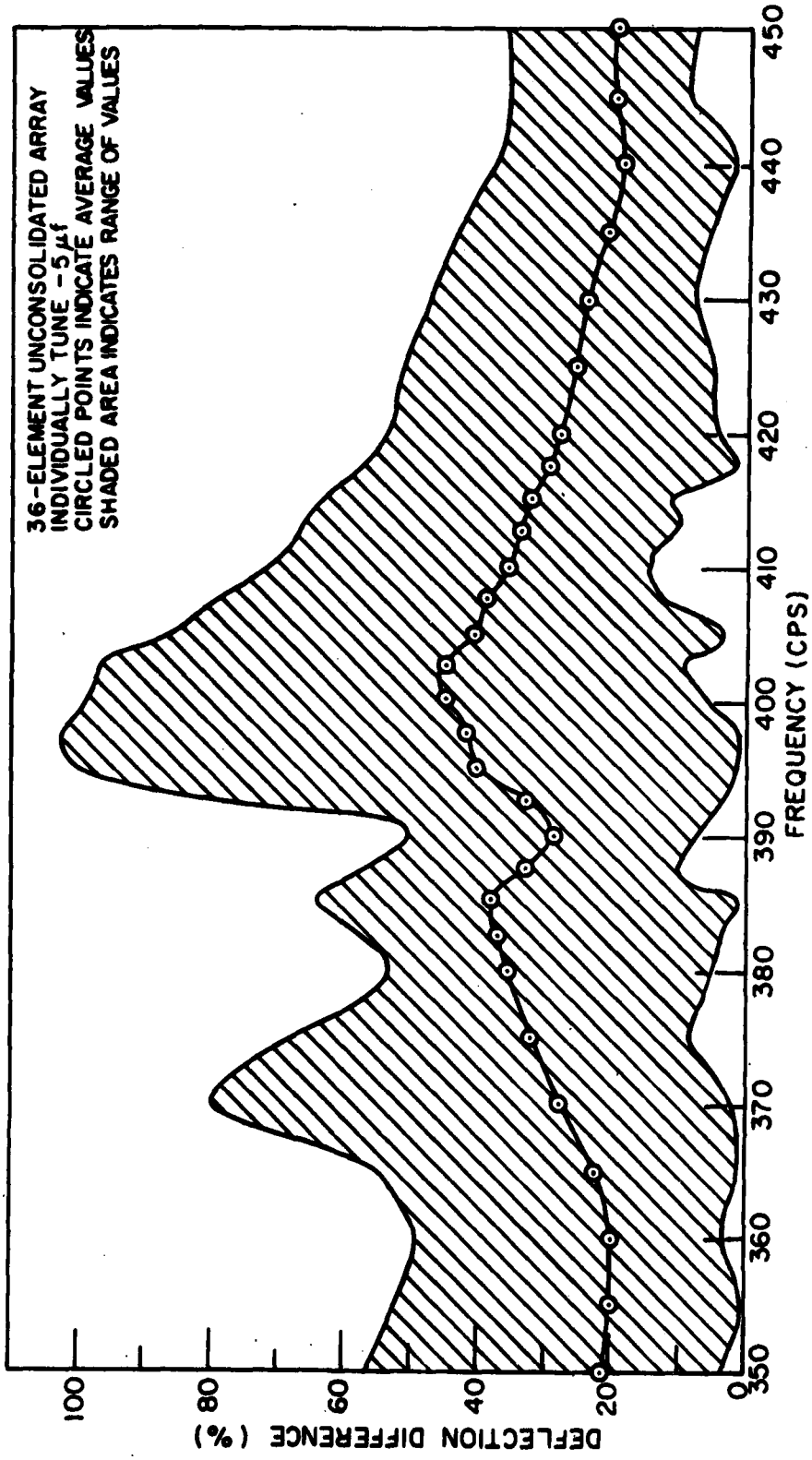

Fig. 99 - Average difference in deflection of upper and lower sets of transducer springs expressed as a percentage of the average spring deflection

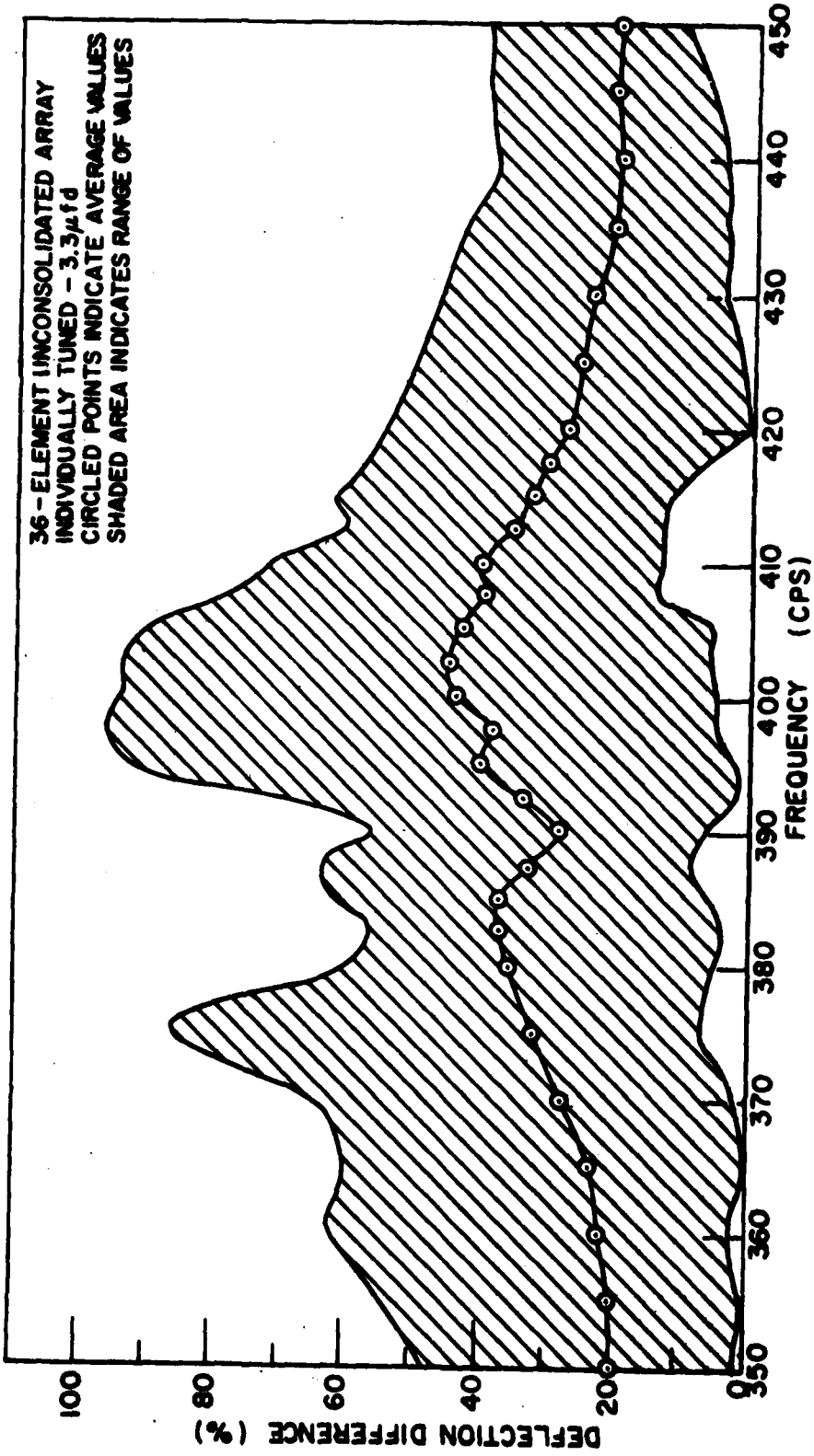

Fig. 100 - Average difference in deflection of upper and lower sets of transducer springs expressed as a percentage of the average spring deflection

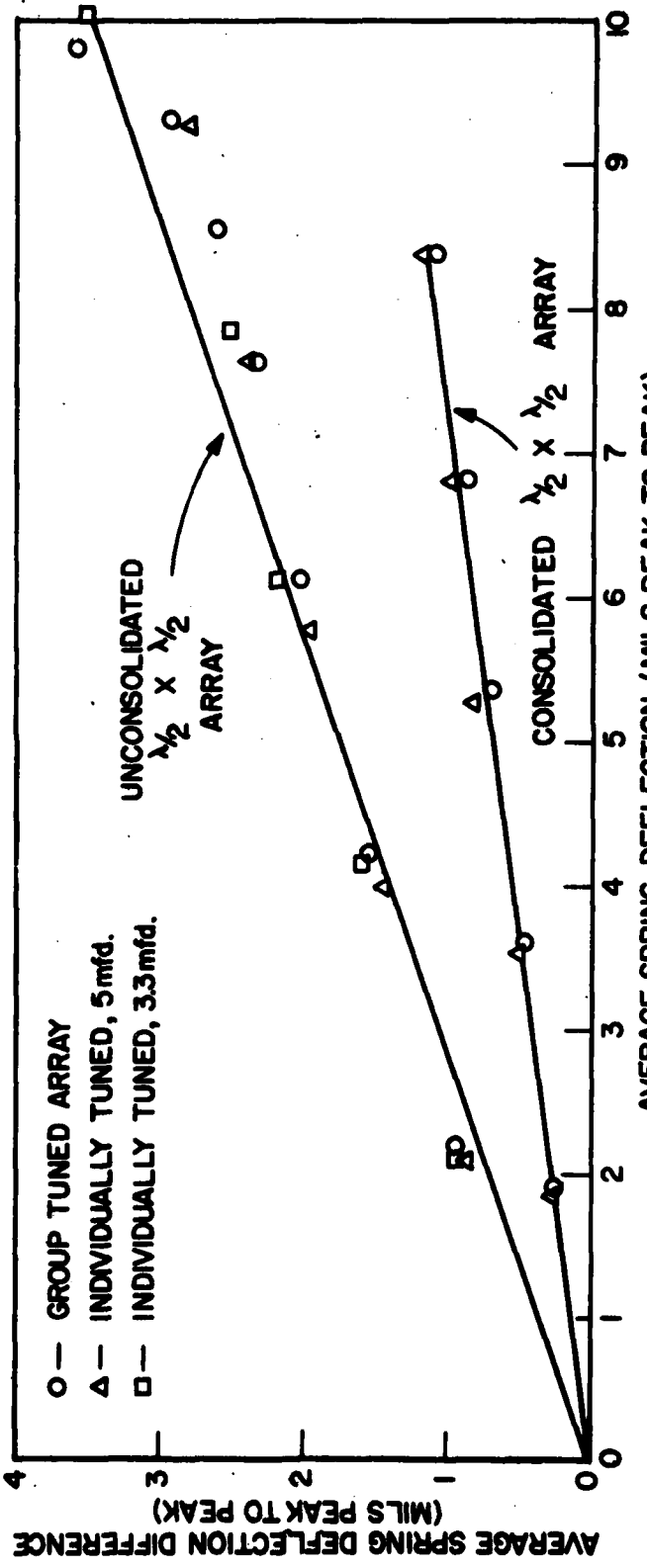

Fig. 101 - Relationship of spring deflection difference to spring deflection magnitude for $\lambda/2 \times \lambda/2$ array at 410 cycles per second

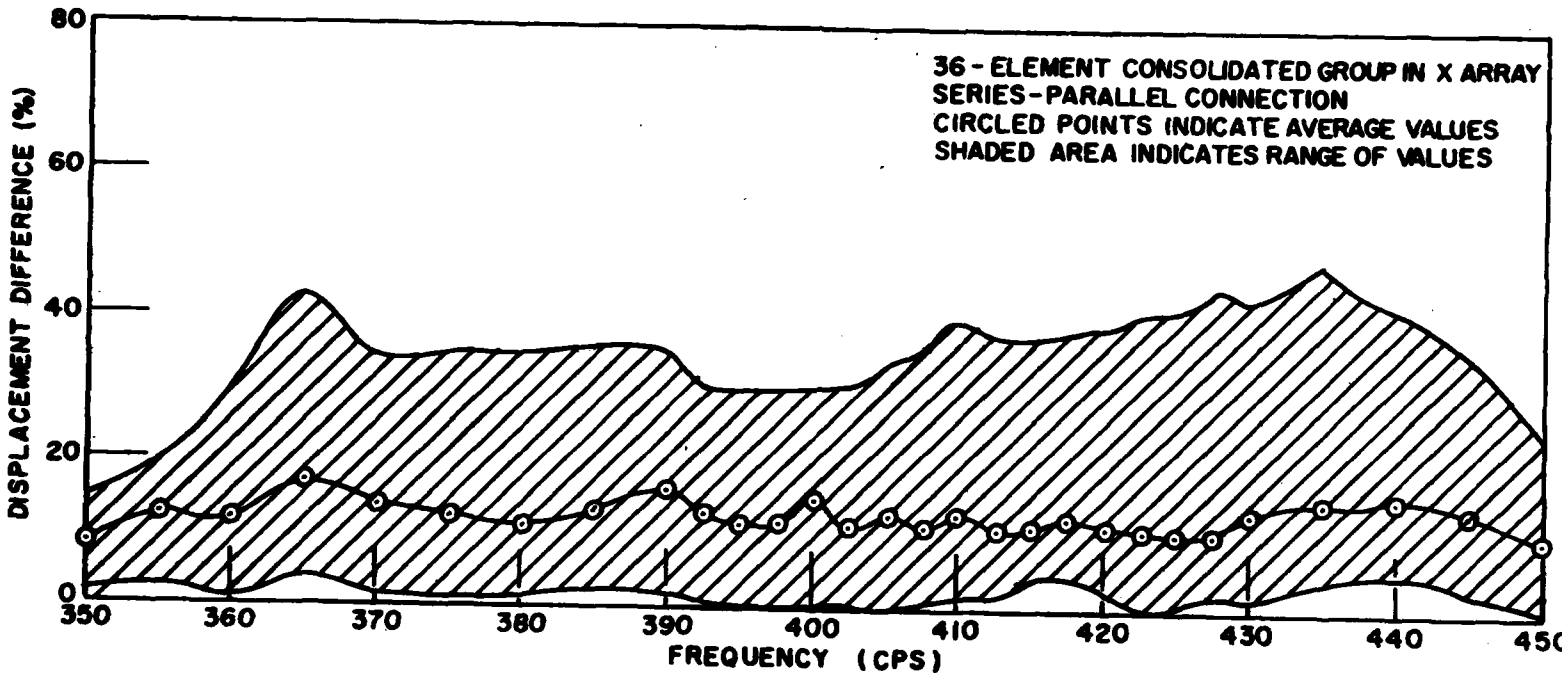

Fig. 102 - Average difference in displacement of center and lower edge of transducer element faces expressed as a percentage of average displacement

UNCLASSIFIED

UNCLASSIFIED

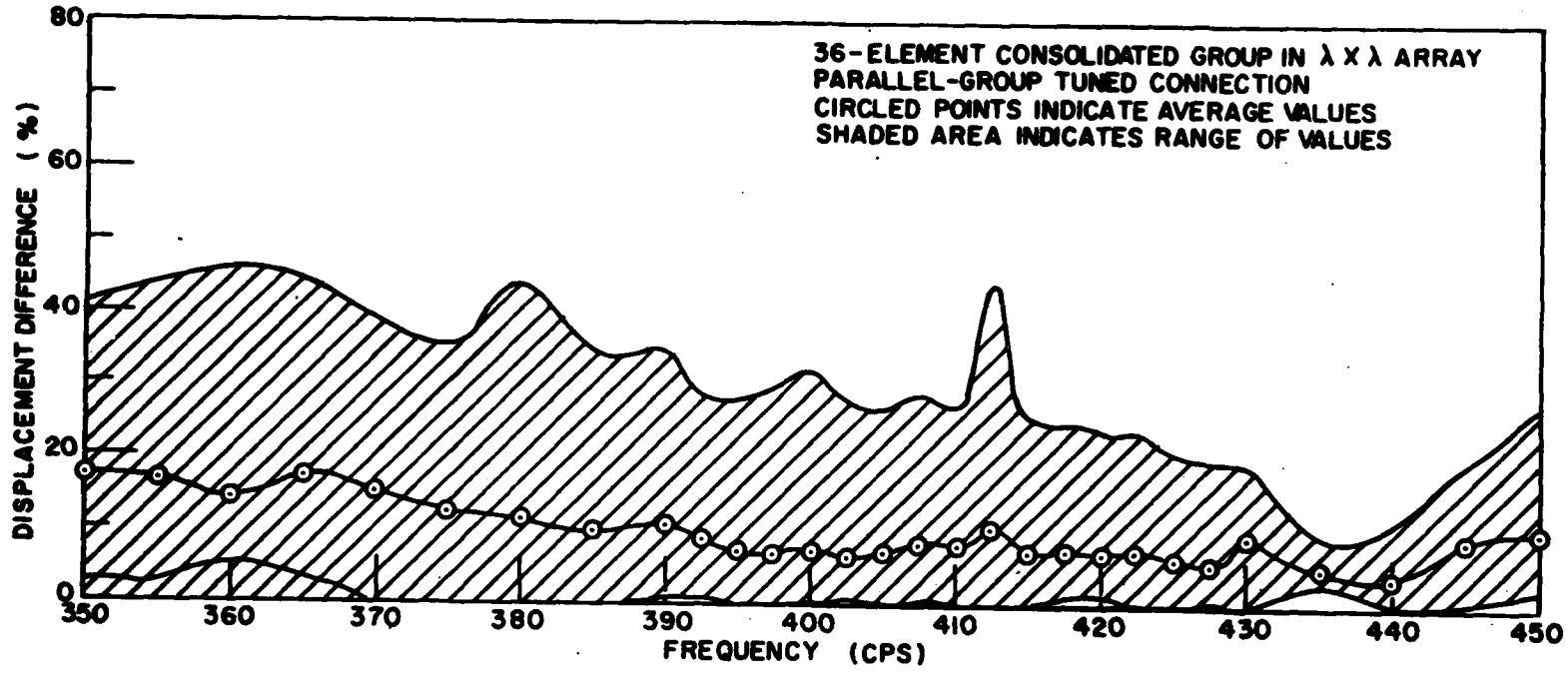

Fig. 103 - Average difference in displacement of center and lower edge of transducer element faces expressed as a percentage of average displacement

UNCLASSIFIED
UNCLASSIFIED